Technical Report No. 157
4951-4-F

EXPERIMENTAL SIGNAL AND ERROR DATA FROM TROPOSCATTER DIGITAL COMMUNICATION LINK

by

M. P. Ristenbatt
E. P. Gould

COOLEY ELECTRONICS LABORATORY

Department of Electrical Engineering
The University of Michigan
Ann Arbor, Michigan

Contract No. DA-36-039 sc-89168
U. S. Army Electronics Materiel Agency
Fort Monmouth, New Jersey

November 1964

ACKNOWLEDGMENTS

The authors gratefully acknowledge the work of Mr. Alan Collins, who did all of the computer programming for the data analysis. Credit is due Mr. Irvin Kullback and his associates at the Radio Relay Branch of USAEL for the operation of the link during these tests, and for supplying technical and calibration information about the link. Finally, we wish to acknowledge the contribution of Mr. Kenneth Haines, who is responsible for the equal gain diversity analysis depicted in Appendix D.

TABLE OF CONTENTS

LIST OF ILLUSTRATIONS

LIST OF ILLUSTRATIONS (Cont.)

LIST OF TABLES

1. INTRODUCTION

Due to the ever increasing demand for communication of digital information, troposcatter is being tested with digital signals at increasingly higher bit rates. As is well known, a troposcatter link provides a reliable link for distances between 50 and about 500 miles. Although a troposcatter link requires relatively high power, its transmission is generally more persistent and reliable than that of an ionospheric reflection link (Ref. 1).

In considering any digital communication system it is convenient to determine two related but separate issues: (1) the probability of error assuming that the system is synchronized, and (2) the effect of the channel conditions on synchronization. Much of the classical theory dealing with the probability of error assumes that the system is synchronized. There are two levels of synchronization: (1) the bit synchronization and (2) the frame synchronization. Under poor channel circumstances the frame synchronization is the more difficult problem. If frame synchronization is temporarily lost, the search procedure necessary to re-establish frame sync amounts to an error extension of the original channel errors.

This error extension caused by frame sync "search" has been a source of difficulty during attempts to operate a time division multiplexed PCM train over an experimental troposcatter link (Ref. 2). It was therefore decided to make a detailed study of the error run characteristics of the experimental troposcatter link. A primary objective of this study is to ascertain the timing circuit requirements for successful handling of the frame sync (and bit sync) situation during signal fades. An additional immediate motive is to contribute whatever possible to understanding the causes of the errors on a typical high data-rate troposcatter link. For both of these reasons, then, experimental data were taken on the Tobyhanna, Pennsylvania-to-Fort Monmouth, New Jersey link.

The reported data are the first of a series of data which will be taken during the coming year. Results of present data have already led to improvement of the error detection part of the link and to improvement of the calibration procedures for the tests. Thus the present data are somewhat preliminary since various sources of measurement error will be

improved in the remaining data. However, these preliminary data are sufficiently accurate to indicate the essential phenomena on the link. Various issues which are presently uncertain will be settled later by studying the entire set of data.

In addition to the preliminary description of the data, this report will provide a detailed description of the data acquisition method used. Basically this method entails the recording of the data directly on a digital tape for immediate access to the digital computer. In addition, the signal and error data are interlocked on the tape for any desired computer analysis. The computer programs which were written to analyze these data are also described in this report. (See Appendix B.) The general techniques used in these programs may be useful for other similar computer analysis projects.

First, we will describe the historical background of troposcatter links. We will then proceed with a description of the link, a description of the data acquisition equipment, and finally a presentation of the experimental results. Wherever possible, the experimental results will be compared briefly to available applicable theory.

It should be noted that the appendices play an especially important role in this report. Appendix A describes in detail the equipment arrangement and characteristics which were provided and implemented by our laboratory. Appendix B contains a description of the computer programs used to analyze the data. Appendix C contains additional data curves which are referred to in the main text. Appendix D contains a theoretical derivation for the probability of a fade length, given diversity combining, exceeding a given value in a given observation time. Prior to the availability of experimental data, this theoretical prediction was used to estimate the frame timing requirements on a digital scatter link. An additional description of this work may be found in Section 5.

2. BACKGROUND

Historically, troposcatter links have been involved largely with analog modulations. A number of operational troposcatter links use analog modulations which typically are either FM modulation or single sideband (SSB). Although much is known about the use of the troposcatter link for analog signals (Refs. 3 and 4), relatively little information is available on the behavior of troposcatter links for digital signals.

A recent study of digital troposcatter is reported in Ref. 5. A primary issue in this work is to account for the selective fading, in addition to the flat Rayleigh fading, at the higher bit rates.

When digital communication links are tested, the signal measurements and the probability of error (P_E) measurements are often made separately because the signal data occur continuously while the error data occur only sporadically (and infrequently). However, in order to analyze the causes of the particular error behavior, it is necessary to interlock the signal and the error data. Data interlock was accomplished here by directly multiplexing the signal and error data on a digital tape. This interlock permits investigating the relation between the particular signal behavior and error behavior. The digital tape containing the multiplexed signals is taken directly to a digital computer without any intermediate signal processing.

The experimental results discussed in this report were taken from the experimental digital troposcatter link which is operated by the Radio Relay Branch of USAEL. The link has a bit rate of 576,000 bits per second and uses binary FM at a radio frequency of 4.8 kMc with space (dual) diversity. The data recorded consisted of multiplexing an amplitude sample from each of the two diversity receivers, an amplitude sample from the combined signal, and a sample indicating the instantaneous probability of error. These four signals were directly recorded on a digital tape and then analyzed on a digital computer.

The link being studied is unique in that it has the relatively high bit rate of 576,000 bits per second. Also, the RF frequency of 4.8 kMc is relatively high for tropo. In

addition, the direct digital recording of the multiplexed data represents a modern data processing facility in which the signal and error data remain time related.

The objective of this report is to present the results of this first series of tests and to describe briefly the manner in which these data were recorded and analyzed. It is hoped that these results will be of interest to anyone studying the use of troposcatter links for digital communications. Although every link is somewhat unique, certain basic phenomena can be expected to occur on any similar link.

The following discussion describes first the link and then the data facility. The experimental results are then considered in terms of: (1) the probability of error, (2) the single channel RF signal distributions, (3) the single channel fade curves, (4) the combined signal fade curve, and (5) the error run data.

3. DESCRIPTION OF LINK

The link is operated between Tobyhanna, Pennsylvania and the Hexagon at Fort Monmouth, New Jersey by the U. S. Army Electronics Laboratory. The total distance is about 100 miles. The signal for these tests is a repetitive 1010-train at 576,000 bits per second. Binary frequency modulation is used with a peak-to-peak deviation of 750 kc. Dual space diversity combining is accomplished with an equal gain predetection diversity combiner. The antennas are spaced 40 feet or 200 wavelengths apart (center-to-center) and consist of 15-foot parabolic dishes. The transmitter power is 1 kilowatt with an RF frequency of 4.8 kMc. The bandwidth of the modulated signal is about 1.1 megacycles. A profile chart of this particular link is shown in Fig. 1 (furnished by the Radio Relay Branch of USAEL). As noted, the transmitter site is on a mountain at an altitude of 2210 feet above sea level. The receiver is on the roof of the Hexagon Building at Fort Monmouth, at an altitude of 168 feet above sea level. There are two major obstructions in the path occurring at heights of 2000 and 1500 feet. The antenna beams are set so as to graze these obstructions for maximum received signal, which resulted in about one-half the beam above the obstruction and one-half below (Ref. 6). The scattering angle is estimated to be 0.674 degrees.

According to the Radio Relay Branch the path loss on this link exceeds the predicted path loss figure (Ref. 6). This causes the link operation to be unsatisfactory at the poorer times in the year (winter).

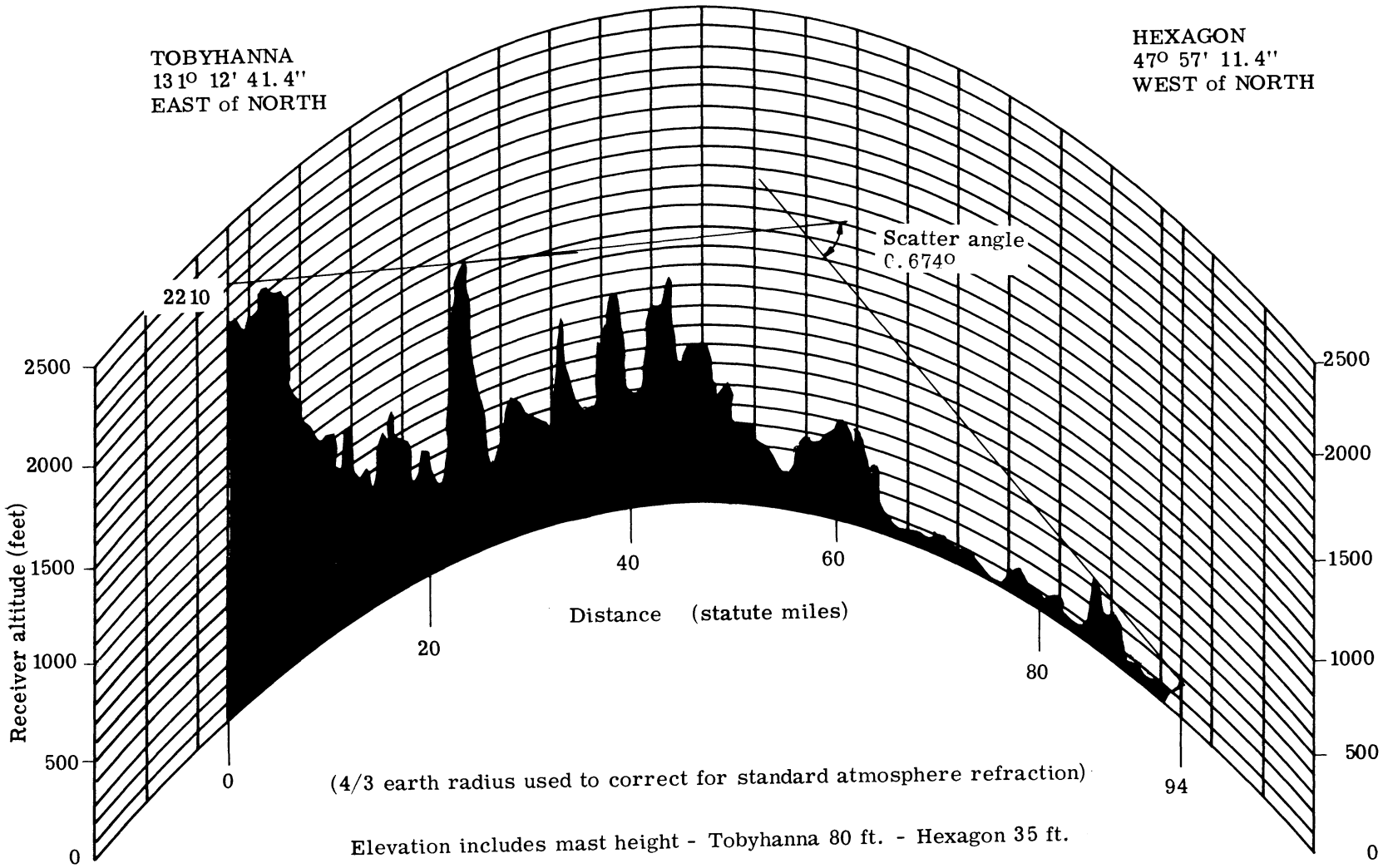

Fig. 1. Profile chart.

4. DESCRIPTION OF DATA ACQUISITION EQUIPMENT

Figure 2 is a block diagram of the equipment used to acquire the data described below. The troposcatter link receiver detects the alternating 1010-modulation pattern with an FM discriminator and produces a (PCM) video signal. This video signal is sent to an error detection system supplied by USAEL and built by RCA (Ref. 7). The continuous signal strength measurements are obtained directly from the receiver by first using a log-linear amplifier (at IF) for a suitable compression characteristic and then detecting the output. The "combined" signal strength, measured by a linear amplifier, is obtained directly at the output of the combiner before entering the AGC amplifier.

The remaining operations of frame error counting, timing, and multiplexing these four signals were performed with Cooley Electronics Laboratory equipment. The basic timing is established by our digital recording rate of 41, 142 characters per second, with 6 lateral bits per character. We quantized each of the four signals into 64 levels (6 bit), and sampled each signal about 10, 285 samples per second.

Measurement of the three signal strength was achieved simply by sampling at the correct time. For the error measurement, we counted the errors during a "frame" corresponding to a sample time. At a 576, 000-signal bit rate, a frame time of about 0. 1 millisecond (10. 285 samples/second) specified 56 bits per frame. The error count within such contiguous frames was obtained by forming a shift-register counter, and feeding a D-A converter (labeled Frame Error Counter in Fig. 2).

In some of the tests the dual diversity was not used; only two signals were multiplexed--the signal strength and the frame error count. Consequently, the sample rate was increased to 20, 571 samples per second, and the frame size reduced to 28 bits.

The timing for all these operations represented a sizable problem. The sampling times had to be coordinated with the frame error counting and resetting. The timing equipment and the frame error counting system was formed with commercial digital data blocks.

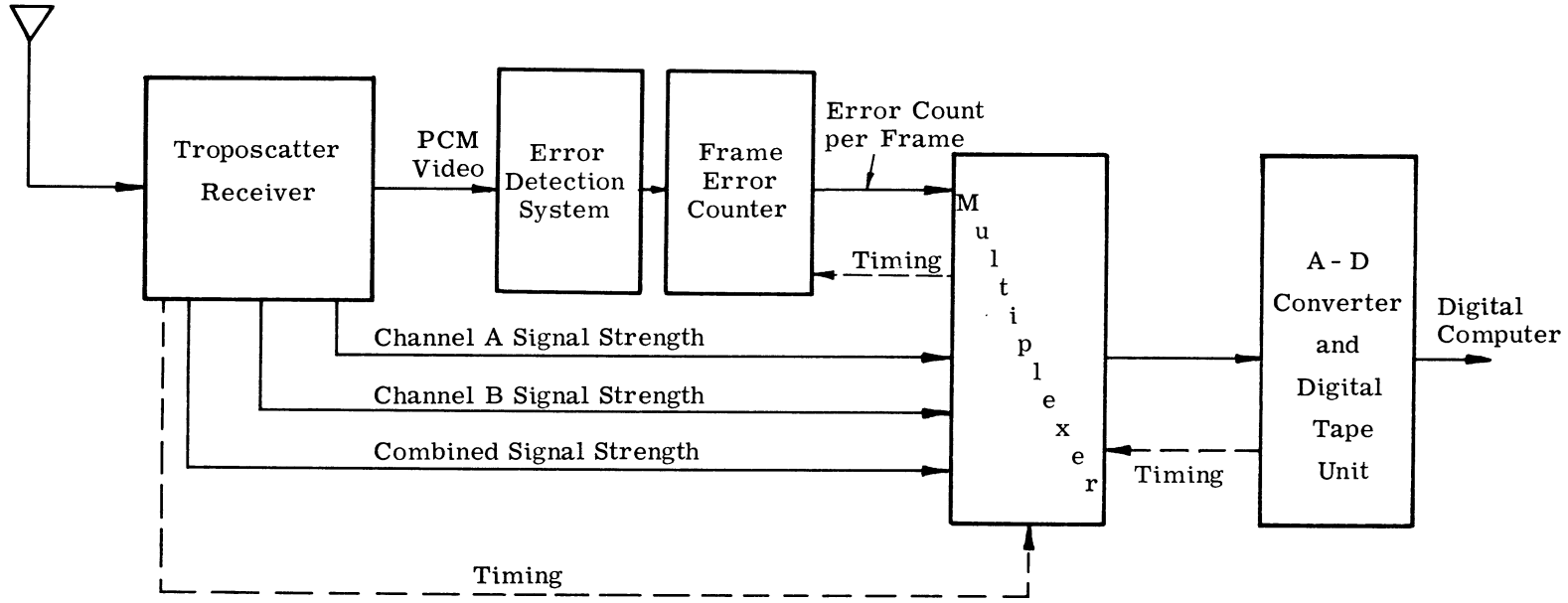

Fig. 2. Block diagram of data acquisition equipment.

The multiplexer-A/D converter (with their internal timing) was accomplished with equipment built to our specifications by Raytheon Company. The digital tape unit is an IBM 729 II. This multiplexer, an A-D converter-tape recorder combination, is a recently acquired facility which we use to interface between various physical experiments and the digital computer.

As mentioned, the timing and frame error counting system represents a sizable problem in interfacing the receiver and error detection circuit on the one side, and the multiplexer-A/D converter-tape unit on the other side. This entire complex was devised at this laboratory, and represents a typical instrumentation which must be accomplished when using the A-D converter and digital tape unit with real-time physical experiments.

With the use of this direct recording technique, we are able to retain the time relation between instantaneous signal behavior and short-term error behavior. Also this direct-access-to-computer method avoids some of the operational problems associated with usual data processing systems.

4. 1 Timing Considerations

It is sometimes desirable to have a record of whether each particular transmitted bit is received correctly or is in error. This is not possible in real time since the bit rate of the troposcatter link is 576 kilobits per second, while the maximum tape writing speed of the A-D/tape unit is only 41. 667 kc. For this reason, it is necessary to divide the data into "frames" of bits and gather information only on the number of bit errors that occur in a particular frame.

In the four (data)-channel situation one is restricted to a character rate of 10, 417 (41, 667/4) with 6 bits per signal. Grouping the bits into 56 bit frames yields a character rate of 576 kc/56 or 10, 285 characters (samples) per second per signal for a total of 41, 142 characters per second. Although slightly different from the standard IBM clock rate, this bit rate is within the reading tolerance of the IBM unit.

For the two (data)-channel case, where the number of errors per frame is recorded along with the signal strength of the only input channel, the frame size is 28 bits per frame. Further, it is possible to record only the number of bits in error per frame; then the frame size is reduced to the smallest frame size (14 bits) possible with this equipment.

4.2 Auxiliary Signals

As noted above, auxiliary information is recorded on the behavior of the tropo-scatter link at the time of the frame error count. With the link operating in a dual-diversity mode, the input signal strength of each input channel and the signal strength of the combined signal are recorded to provide the most useful auxiliary data. In the single channel mode the most useful auxiliary data are provided by recording the signal strength of the only operating channel.

The signal strength measurements were taken at test points within the tropo-scatter receiver. Figure 3 is a block diagram showing the points at which the test signals were taken. The signals which are tapped from the mixer preamplifier output are put through a log-linear amplifier which compresses (or compands) the output axis of the voltage. This is required on the single channel signals since there is a wide variation in the signal strength during the fading.

The combined signal output is taken from the output of the phase combiner as shown in Fig. 3. This test signal is put through an IF amplifier and then detected.

Using calibration curves for the outputs of the log-linear amplifiers, we can relate the signal strength to the analog sample value which is sampled by the multiplexer of Fig. 2. The only remaining processing needed on these signals is a variable gain analog amplifier which adjusts the signals so that they use the total range of the A-D converter.

4.3 Frame Error Counter

Since all measured auxiliary signals could be placed directly into the multiplexer of the A-D/tape equipment, we decided to process the number of errors per frame such that it also could be placed directly into a channel of the multiplexer. A method was devised that would convert the number of incoming bit error pulses per frame to an analog voltage level directly proportional to the number of bit errors per frame.

The way in which the error count is formed, and the timing with which this error count is sampled along with the other signals are indicated in Fig. 4 which shows the interface equipment between the tropo receiver and the multiplexer. From the tropo receiver

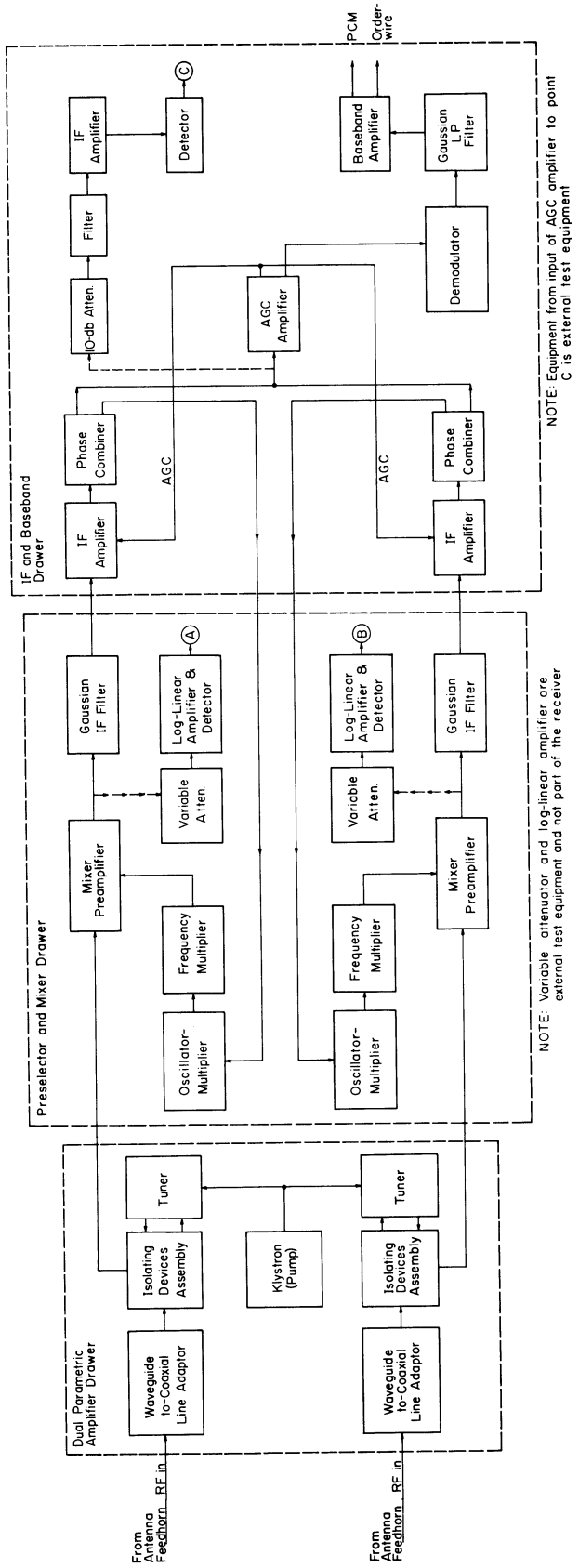

Fig. 3. Block diagram of troposcatter diversity receiver.

we obtain the three outputs for the amplitude samples of the three signals. In addition, the two error signals from the receiver are:

1) an indication a bit error has occurred,
2) a clock signal which indicates when a bit has arrived.

The occurrence of a bit error is indicated by a positive pulse output at a test point on the terminal equipment. A basic 288-kc positive pulse clock with a one-one correspondence with every two incoming data bits is provided by a second test point of the terminal equipment. The basic idea behind processing these two signals to form an analog waveform whose height is proportional to the number of bit errors per frame is as follows:

1) The 288-kc clock pulses are counted down in a special flip-flop count-down circuit. This circuit puts out pulses corresponding to each frame (whether 14, 28, or 56 bits) and a basic clock pulse of 41, 142 kc to drive the A-D/tape unit. The pulses corresponding to each frame are used to transfer data to a flip-flop buffer and to reset the bit error counter.
2) The bit error pulses are counted in a basic flip-flop counter. This counter has the provision that it can be reset by a frame pulse in 0. 5 microsecond so that no bit error pulses are dropped at the end of a frame. At the end of each frame the contents of each stage of the counter are read out into a flip-flop buffer. The contents of this buffer are automatically transferred to a D-A unit which converts the input bits to a voltage level proportional to the number of errors counted in the frame.

The proper transfer of bits necessitates the use of delays of the proper magnitude, as indicated by the timing diagram in Fig. 4. A more detailed discussion of this circuitry is contained in Appendix A.

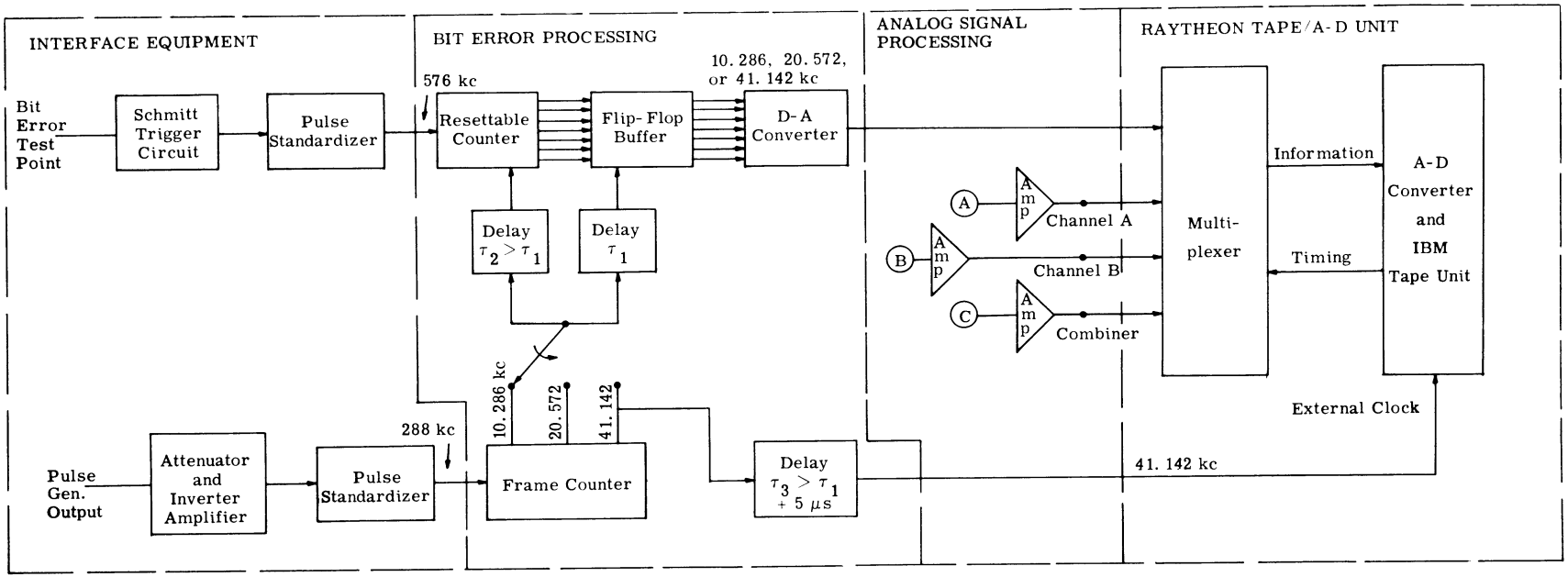

NOTE: The D-A and multiplexer timing is independent of the resettable counter because of the flip-flop buffer. The criterion on the delay τ_3 is determined by the amount the auxiliary analog signals are sampled in time behind the actual bit error per frame count.

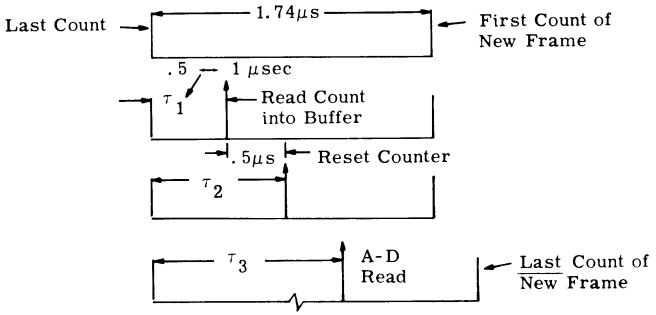

Timing Diagram

Fig. 4. Timing system and frame error counter.

5. EXPERIMENTAL RESULTS

We will discuss the experimental results in terms of the following categories: (1) the over-all results, (2) the P_E versus signal level, (3) distribution of the diversity receiver signals, (4) distribution of the diversity receiver fade levels, and (5) the error run data. In each case the results will be compared to available theory.

5. 1 Over-all Considerations

The data consist of three test tapes, each of which consisted of a 5. 75-minute sample of troposcatter data recorded in the early afternoon of Friday, April 10, 1964. More data had been recorded but various equipment difficulties prevented successful analysis. Consequently the data can be considered as single "test samples" for the link. The method used is appropriate only for relatively short, but detailed, data tests. If long tests are run the computer costs may become prohibitive.

Table I shows the over-all characteristics of the data. The normal link operation consists of using the dual diversity and the parametric amplifiers (Tape No. TPO/4). A single channel test was run to test the improvement provided by the diversity (Tape No. TPO/3). Finally, the parametric amplifiers were turned off (with diversity) to ascertain the link operation at a lower signal-to-noise curve. The over-all P_E and the mean signal level for these three data runs are shown in the table.

An item which is important for these data (and for this link) is the presence of airplanes in the path. The data were taken early Friday afternoon which probably is a time of maximum airplane traffic. The estimated percentage time of airplane interference is shown in Table I. The possible role of this airplane-type fading will be considered in interpreting the data from this test.

Figure 5 shows two samples of a single-channel signal strength and resulting error behavior. Figure 5(a) indicates a relatively normal, slowly varying fade which, near the bottom, causes a substantial error run. The upper trace is the signal strength and vertical spikes from the lower trace indicate number of errors within a frame. Figure 5(b)

Table I. Gross characteristics of data.

Code Name	Description	Over-all P_E (10% Accuracy)	Approximate Mean Signal Level (dbm)	db (of mean) Above FM Threshold	Estimated % Time Airplane Interference
TPO/4	Dual Diversity Parametrics On (Normal Operation)	3.43×10^{-5}	-82	20	28
TPO/3	Single Channel Parametrics On	4.7×10^{-3}	-84	15	17
TPO/2	Dual Diversity Parametrics Off	1.5×10^{-4}	-82	12	2

indicates the action typical of an airplane in the path. The signal strength is quite periodic and undergoes deep fades. At the bottom of these fades, of course, error runs appear, as indicated by the vertical spikes from the baseline.

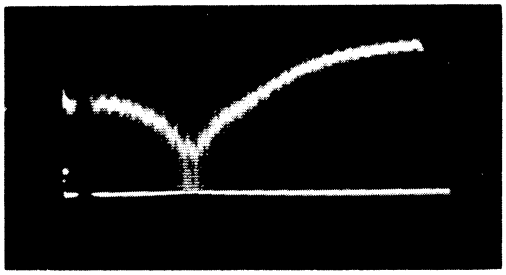

Fig. 5(a). Normal fading of the signal.

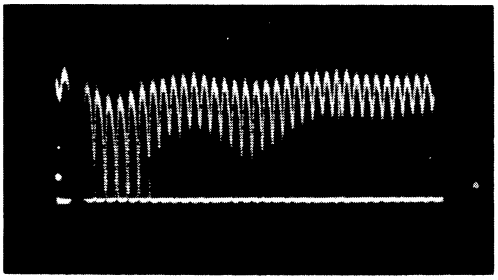

Fig. 5(b). The effects of an airplane on signal strength.

Since this was the first attempt to collect data with this particular method, there were some problems with calibration, both in error count and in signal strength. Also, as will be seen below, the link exhibits some (relatively few in the data here) spurious errors due to transients in the receiver. We believe that the data, except for the number of fades, are at least within 10 percent accuracy throughout. This is quite sufficient accuracy for the nature of the data being dealt with.

We will now describe the various results for these three data runs.

5.2 P_E Versus Signal Level

Figure 6 shows the P_E versus signal level for the three cases noted above. The P_E here refers to the number of bits which were in error (at the given signal level) divided by the total number of bits during which the signal was at that level. [1]

It is seen that TPO/2 and TPO/3 give quite similar results at the higher error region; in the lower P_E region the TPO/2 does better by about 2 db than does the TPO/3. As expected, this verifies that dual diversity is more important than the parametric amplifiers. The placement of the error curve for TPO/4 (normal operation) is somewhat uncertain because we did not have sufficient information to take account of the fact that the combiner output is the result of the combining after an AGC action is performed. However the estimated position is as shown in the figure. For comparison we drew the theoretical diversity curve based on the single channel TPO/3 results. One would not obtain all this improvement unless the channels were independent and the combiner worked perfectly.

It is of interest to note the over-all performance of this P_E with respect to a theoretical prediction. For this calculation we have made the assumption that the carrier-to-noise ratio at FM threshold is 10 db (Ref. 7). This value is based on defining the peak noise as that voltage level which is exceeded about 1 percent of the time. With this assumption, and using the mean signal levels, we obtain the P_E for various assumed receiver action (see Table II). The single-channel coherent FSK results were obtained by using the equation (Refs. 4 and 8):

$$P_{E,1} \approx \frac{1}{2\,\overline{S/N}} \tag{1}$$

where:

$P_{E,1}$ = single channel P_E

$\overline{S/N}$ = mean S/N.

[1] During publication of this report, it was learned that spurious errors in the link are being incurred by transients coming from the thermostatic control of the two crystal ovens. This accounts for the points appearing at the bottom right of Fig. 6 which, in each case, depart significantly from the consistent data points at lower signal values.

The equal gain diversity improvement (Ref. 4) over single channel is taken to be:

$$P_{E,2} = 3 P_{E,1}^2 \tag{2}$$

where:

$P_{E,2} = P_E$ when equal gain diversity is used.

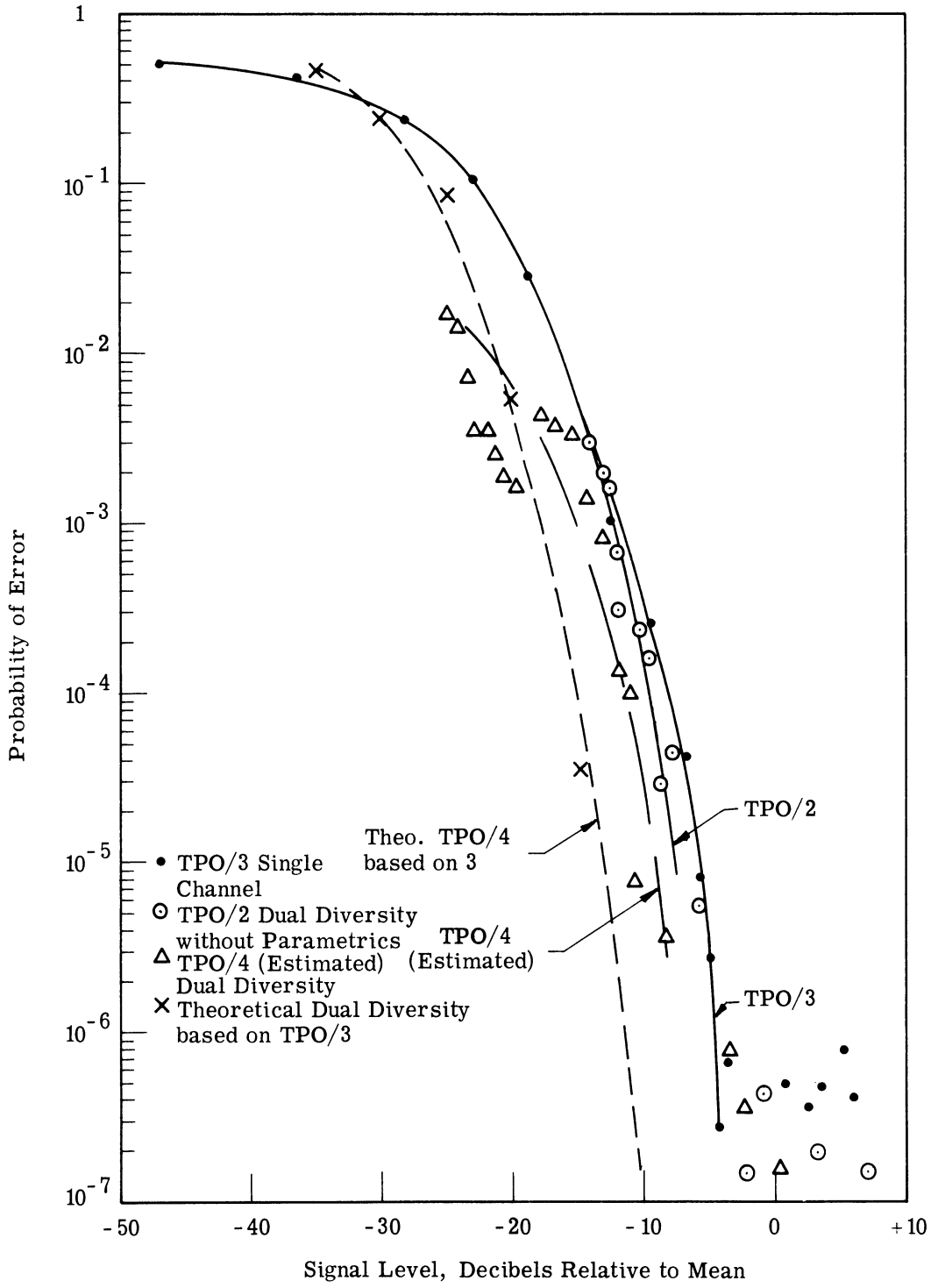

Fig. 6. Comparison of P_E vs. signal level.

The resulting values for coherent FSK are shown in Table II.

For the incoherent FSK theoretical case the equation used for the single channel P_E was (Ref. 4):

$$P_{E,1} = \frac{1}{(\overline{S/N} + 2)} \tag{3}$$

If the diversity relation of Eq. 2 is applied to the incoherent case, the values in Table II[2] are achieved.

Table II. P_E comparison to theory.

Code Name	Description	Experimental FM P_E	Theoretical Incoherent FSK - P_E	Theoretical Coherent FSK - P_E
TPO/4	Dual Diversity Parametric On	0.343×10^{-4}	0.3×10^{-5}	0.075×10^{-5}
TPO/3	Single Channel Parametric On	0.47×10^{-2}	0.3×10^{-2}	0.15×10^{-2}
TPO/2	Dual Diversity Parametric Off	0.15×10^{-3}	0.12×10^{-3}	0.03×10^{-3}

We see that the dual diversity experimental P_E, for this short sample, is approximately a factor of 10 above the incoherent FSK case. Note that the single-channel experimental case and the dual diversity without parametrics is approximately equal to the incoherent FSK case. One factor here is that the experimental correlation between the two channels (for TPO/4) was 0.588. This high value is probably due to the large amount of airplane interference. Consequently, the entire diversity effect is not achieved on TPO/4. However, the experimental correlation for TPO/2 with only 2 percent airplane interference was only 0.0006, indicating the diversity effect was achieved. Thus the system appears to approximate the performance of an incoherent FSK system.

It is of interest to compare the bit error probability versus signal level with the respective frame error count for each signal level. A "frame error" is defined as any case where there is one or more errors per frame. Figure 7 shows the bit error and frame error probabilities versus signal level for TPO/2; Fig. 8 for TPO/3 and Fig. 9 for TPO/4.

[2]The spurious errors mentioned in the footnote on p. 16 inflate the experimental P_E slightly. However, since the spurious error rate is in the 10^{-7} range, they do not greatly affect the error rates here.

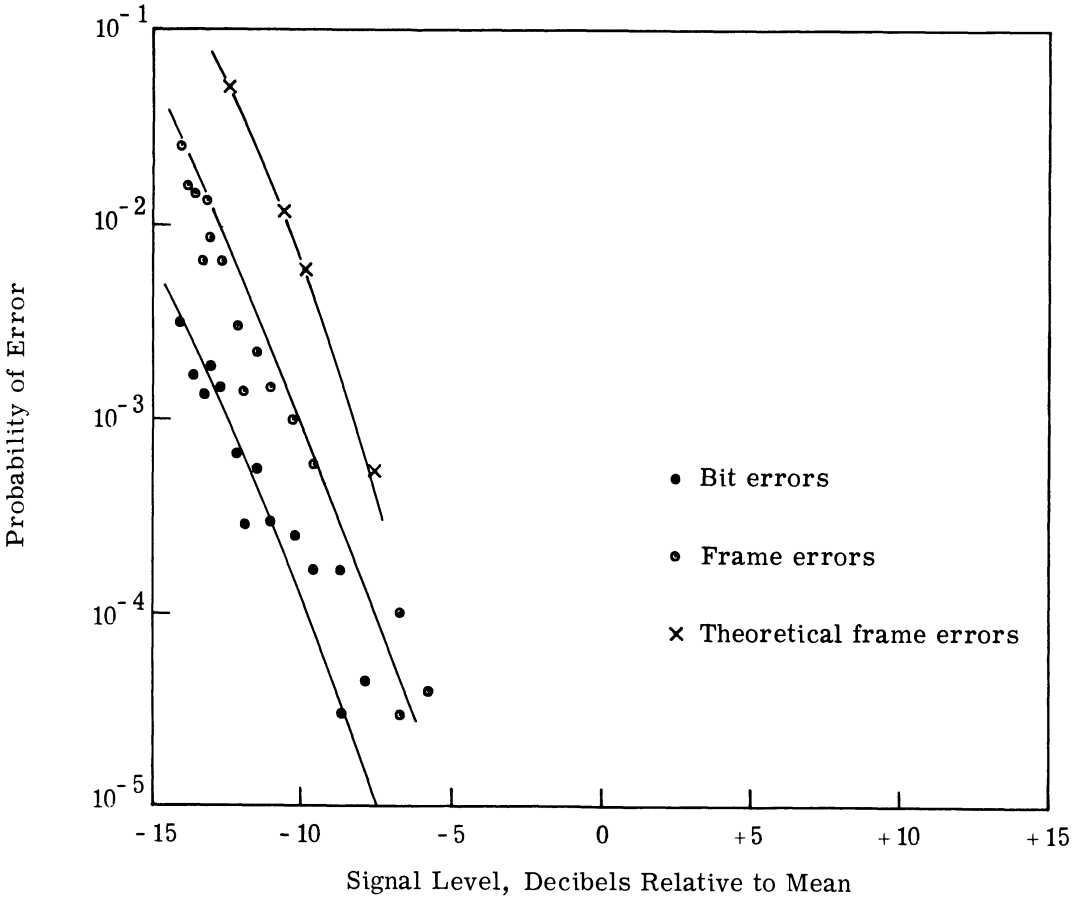

Fig. 7. Probability of bit errors and frame errors vs. signal level for tape TPO/2, dual diversity with parametric amplifiers off.

In addition the theoretical frame error based on the particular bit error probability is plotted versus signal level for each of these curves. The theoretical frame error probability is derived by using the individual bit error in a binomial equation which assumes Bernoulli trials. It may be seen that the theoretical frame error always lies above the experimental frame error count. The differences between the frame error count and the theoretical frame error probability may be partially due to the signal varying sufficiently fast during a frame so that the P_E varies slightly during a frame. The binomial equation assumes that it remains constant. In addition, the dual diversity cases of Fig. 7 and Fig. 9 are subject to some error from the fact that an AGC operation is performed on the signals before they are combined. The spurious errors can be seen at the lower right of both Fig. 8 and Fig. 9. Figure 7, if extended, would also show spurious errors.

In conclusion, it appears that the P_E results are the right order of magnitude and the data appear consistent.

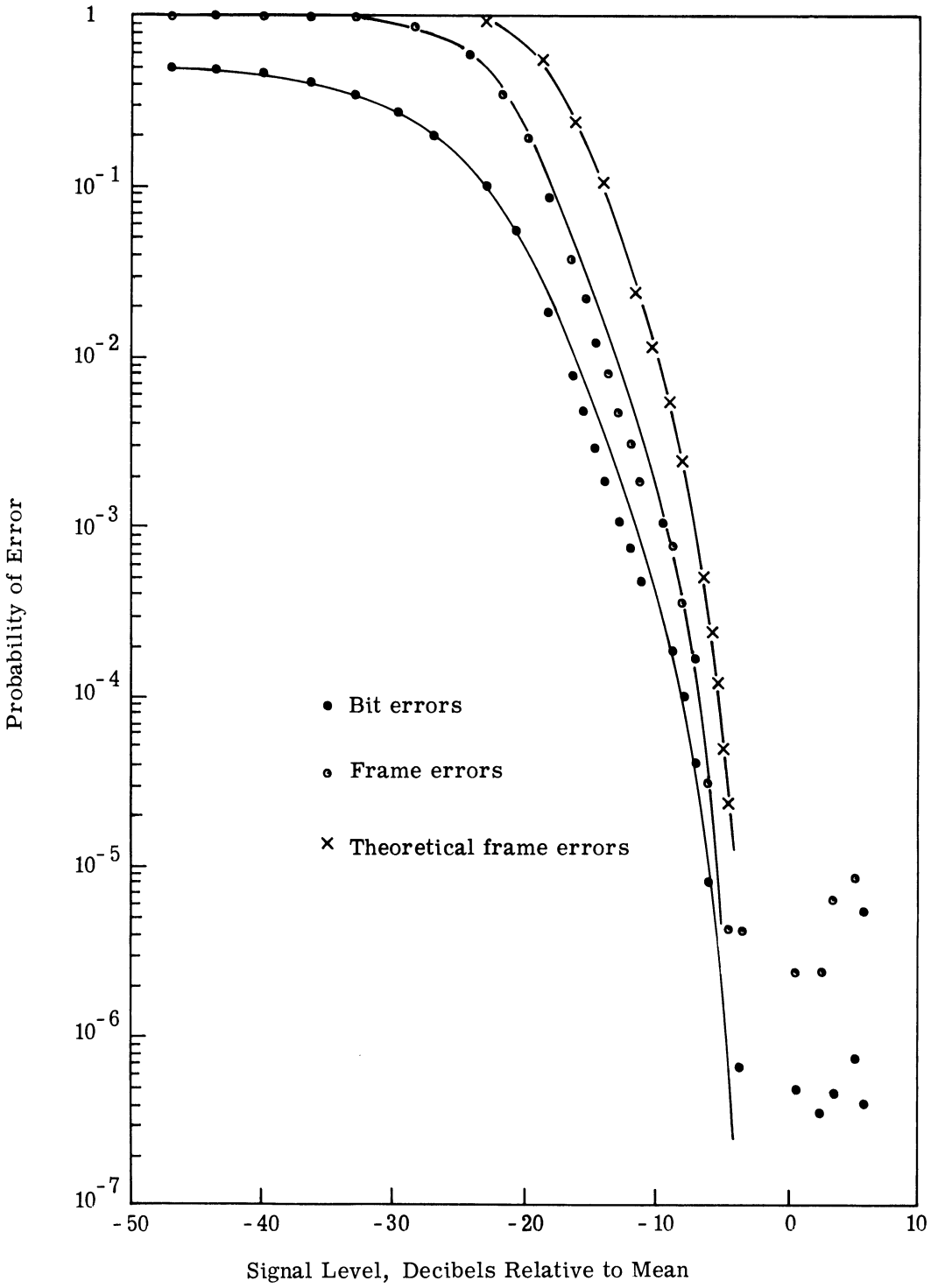

Fig. 8. Probability of bit errors and frame errors vs. signal level for tape TPO/3, single channel with parametric amplifier on; mean signal strength = -84. 4 dbm.

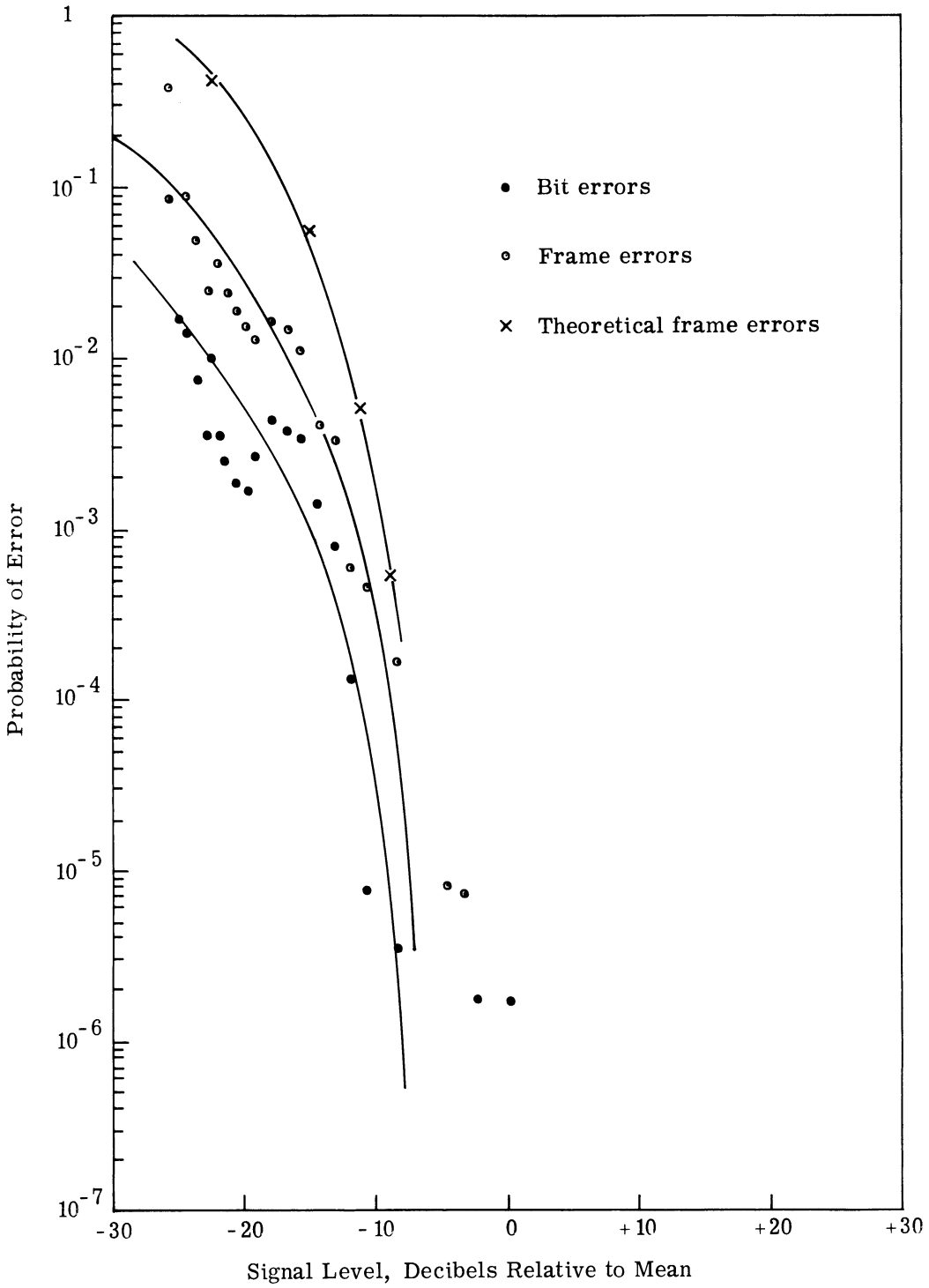

Fig. 9. Probability of bit errors and frame errors vs. signal level for tape TPO/4, dual diversity with parametric amplifiers on.

5.3 Distribution of Signal Levels

Figure 10 shows the cumulative distribution of signal levels for the individual channels of the diversity test (TPO/4), and for the single channel test (TPO/3). Also shown in Fig. 10 is the theoretical (flat fading) Rayleigh curve. The ordinate in this curve is the probability that the amplitude is less than the abscissa.

Figure 11 shows the similar curves for TPO/2 (diversity without parametrics) along with the theoretical Rayleigh curve.

The experimental curves tend to rise above the theoretical ones near the bottom (right); this means that the Rayleigh density is skewed to the left. Thus there are more lower values than would be true in a theoretical Rayleigh case.

Examination of Figs. 10 and 11 reveals that Channel B consistently shows more of this action of rising near the bottom than does Channel A. This phenomenon is sufficiently consistent to cause us to believe that Channel B was behaving somewhat differently than Channel A, or the calibration for Channel B was not as accurate as that for Channel A. A legitimate reason for these curves rising near the bottom would be the selective fading that is present with the wide bandwidth modulation here. In addition, it must be remembered that tape TPO/4 has a relatively high percentage of airplane fading which could be expected to effect distributions of this type.

As another way of depicting the results in Figs. 10 and 11 above, Fig. 12 shows the amplitude density curve for the TPO/3 case. Also plotted is the theoretical Rayleigh density curve. It is seen how this skewness to the left of this density curve results in the particular behavior on the cumulative curve shown in Fig. 10. Still another representation would be to plot straightforwardly the cumulative distribution of the same type as the density in Fig. 12. Figure 13 shows the corresponding cumulative curve for the curve of Fig. 12 (TPO/3). In both Figs. 12 and 13, the experimental curve is normalized by the observed standard deviation and compared with a theoretical Rayleigh probability function with a standard deviation of unity. Here the effect of the skewness is directly seen as the experimental curve lying to the left of the theoretical one.

Other curves similar to Fig. 13 for the various runs are shown in Appendix C-1. Appendix C shows additional data which are not included in the main text.

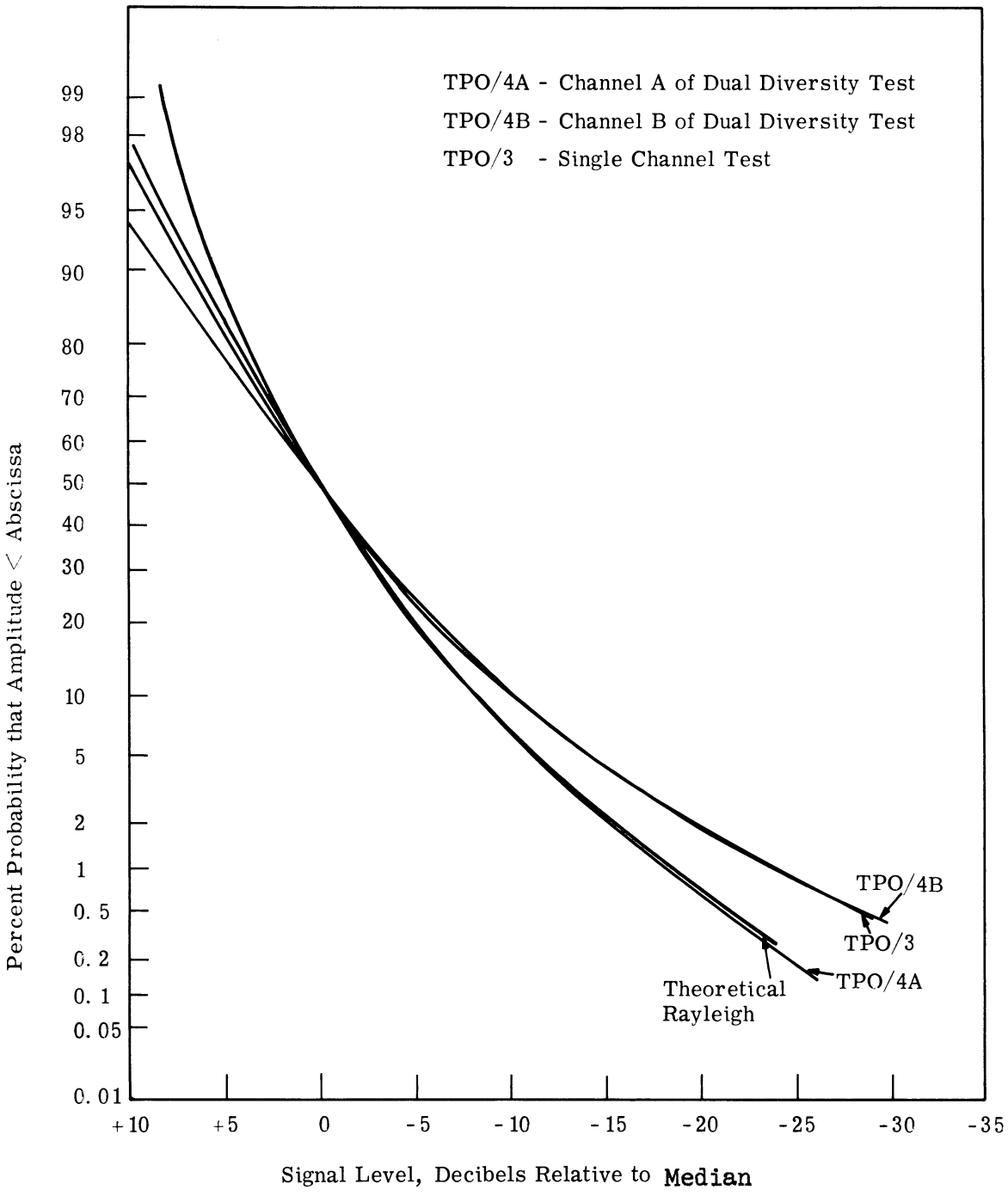

Fig. 10. Comparison of data to Rayleigh distribution.

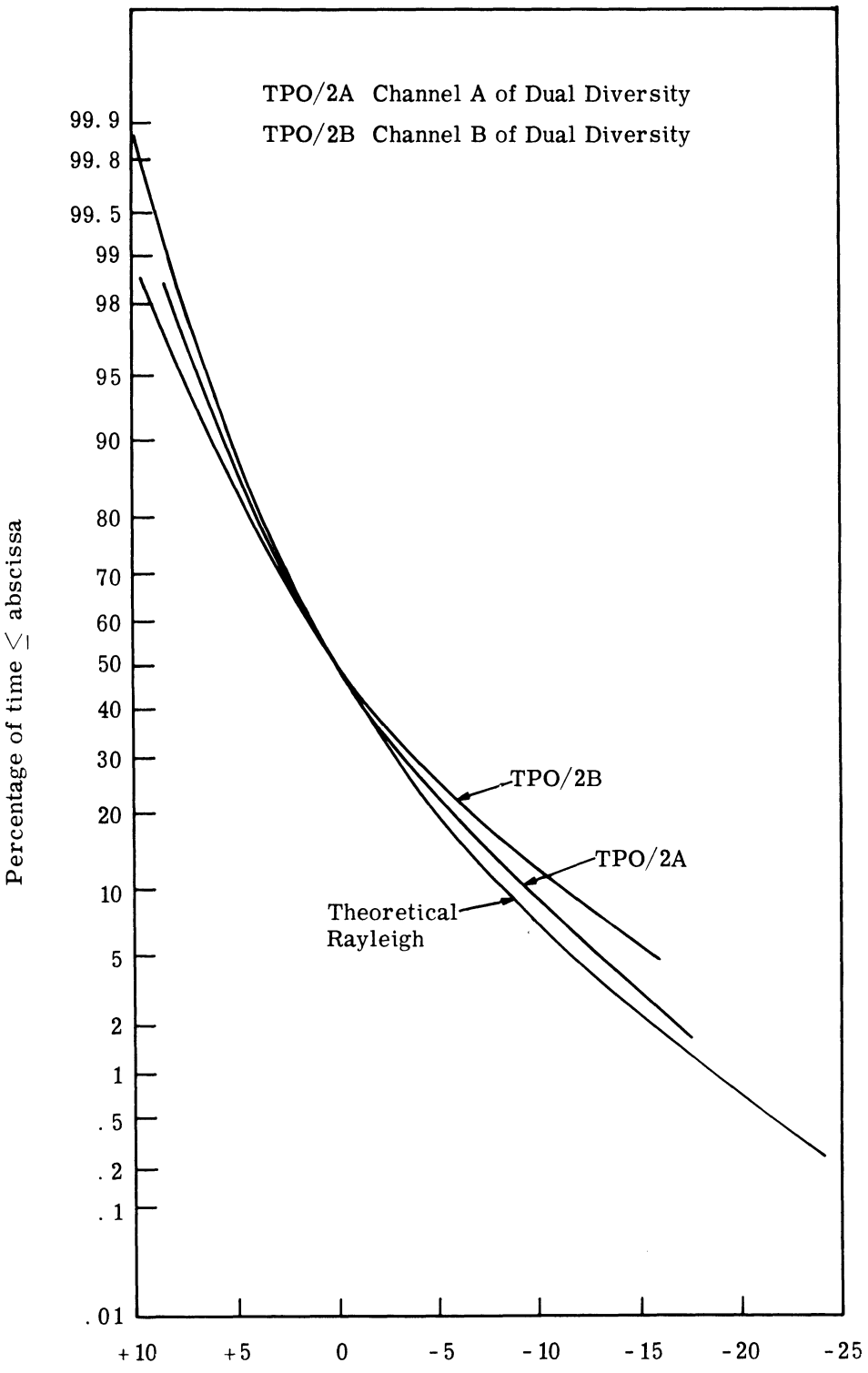

Fig. 11. Comparison of TPO/2 to Rayleigh distribution.

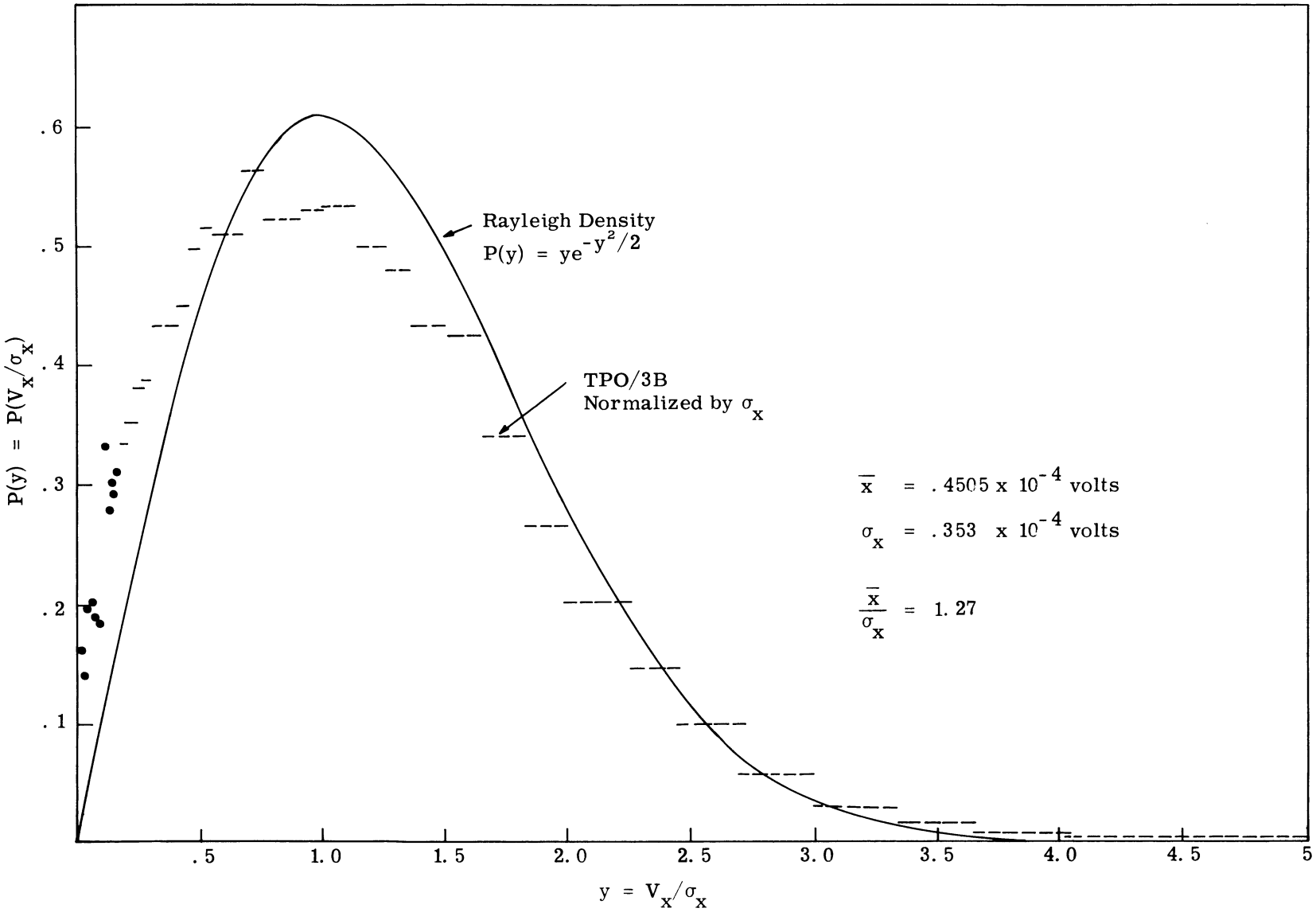

Fig. 12. Comparison of tape TPO/3B to a Rayleigh density curve.

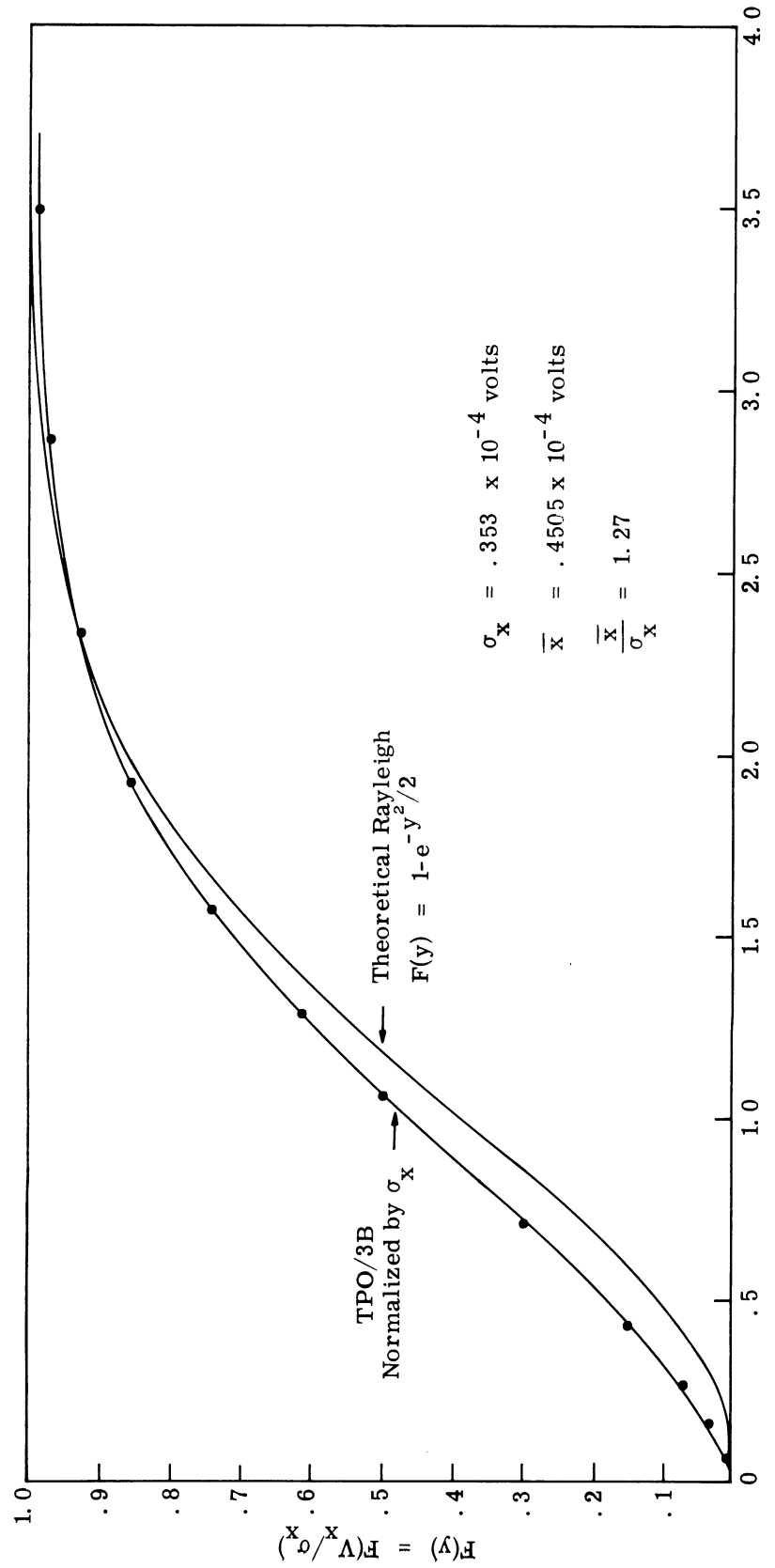

Fig. 13. Comparison of TPO/3B to Rayleigh cumulative distribution.

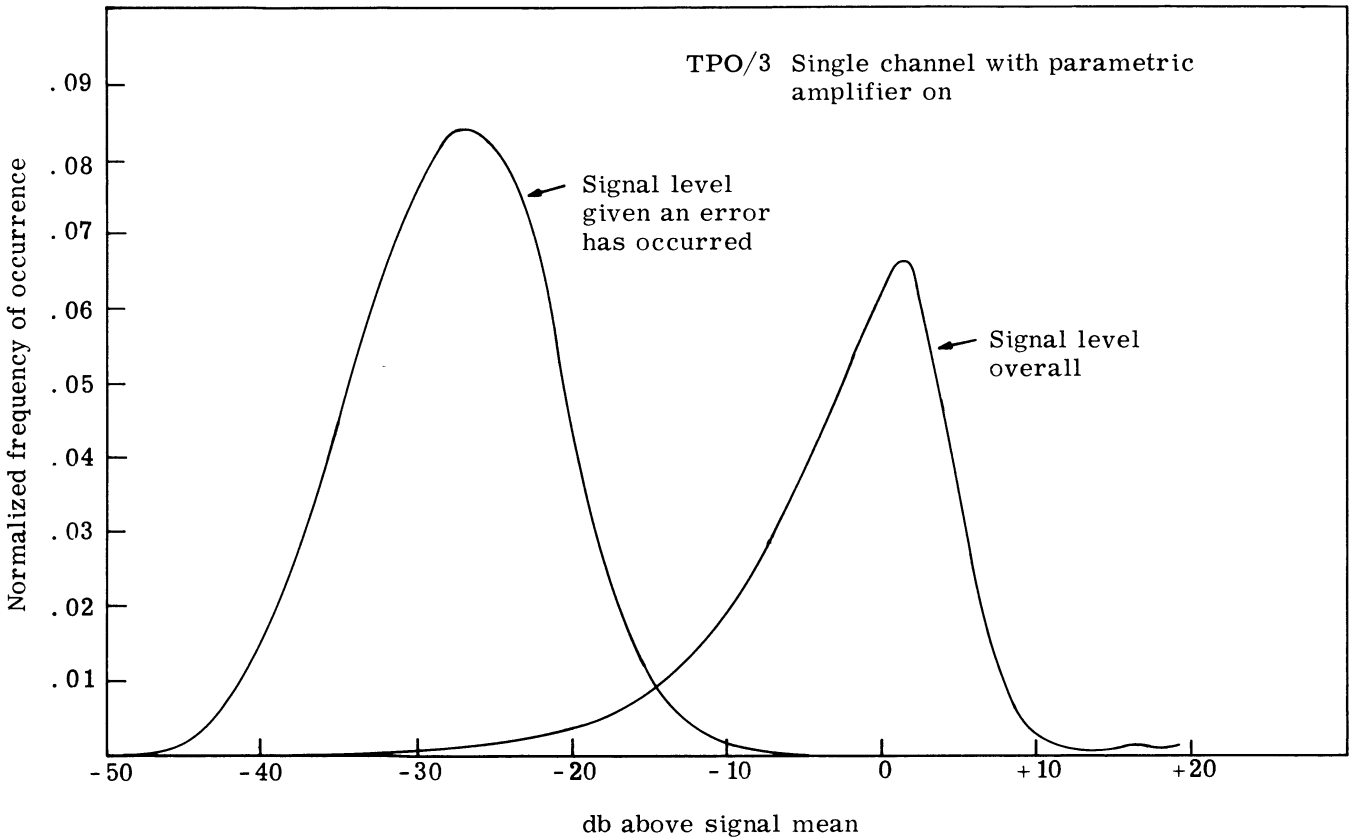

Fig. 14. Frequency distribution of signal over-all and signal given an error has occurred.

Another interesting way to depict signal distribution is shown in Fig. 14. This plot shows the difference between the distribution of the signal, given that frame errors occurred, and the distribution of the over-all signal. The distribution for the signal level, given that an error has occurred, is analogous to a "noise alone" case in signal detectability theory, while the over-all signal level distribution is analogous to the signal-plus-noise curve. For the TPO/3 case it is seen that the mode of the signal with errors curve occurs at about 27 db below the mean. Note that these curves are normalized by different quantities and so it is the relative position of the curves and not their respective heights that is of importance.

In conclusion, the distributions are essentially Rayleigh but increase from Rayleigh at the low values.

5.4 Single Channel Fade Behavior

The fraction of time spent in a "fade" for Channels 4A and 4B is shown in Fig. 15.[3] These curves were taken for a threshold setting of about 21 db below the mean. The data are consistent in that both curves have the same form. The fact that Channel 4B is higher than 4A is again attributed to the inaccurate calibration for Channel B.

Note that the fade data resulted from a wideband transmission, and not a single frequency transmission, such as in Ref. 3. The data here are comprised of two distinct phenomena: (1) a low-frequency, slowly varying fade phenomena, and (2) a hash or ripple superimposed on this low-frequency phenomena. This hash appears to have some legitimate components due to selective fading and link perturbations and some illegitimate components, such as 60-cycle ripple. This hash controls the fade data for short fade lengths because the computer analysis is quite sensitive. Consequently we are applying a precise analysis to data which has some jitter on it.

The longer fade data are more reliable since the hash perturbs this only slightly. Therefore, in order to interpret these fade data we will try and separate the long range from

[3] A comment on the abscissa scale on Figs. 15-20 is needed. The axis was originally plotted in "frames." The number of frames was multiplied by 0.0973 millisecond per frame to obtain the present abscissa for the diversity cases.

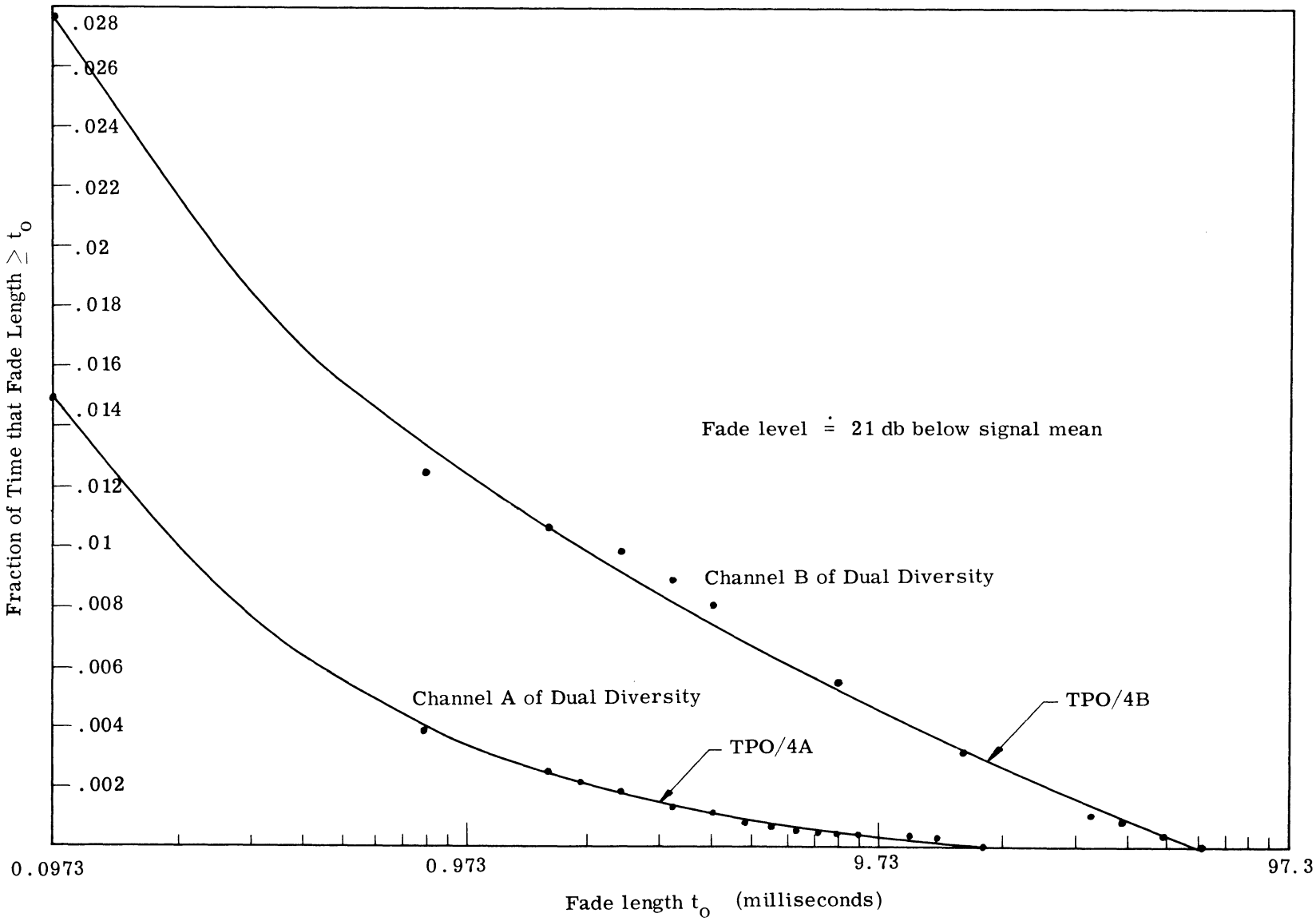

Fig. 15. Fraction of time below fade levels for single channel signals.

the short range. It is of interest to compare the single channel fading bandwidth to that of flat Rayleigh fading.

An indication of f_b is to use the theoretical values derived in Refs. 3 and 10. We will apply Eq. 25 of Ref. 3 to estimate the bandwidth via this means. Equation 25 of that reference is repeated below in Eq. 5. This analysis assumes the spectrum of the flat Rayleigh process is a Gaussian curve with standard deviation σ,

$$N(E) = (8\pi \ell n 2)^{\frac{1}{2}} \sigma \left(\frac{E}{E_m}\right) e^{(-\ell n 2)\left(\frac{E}{E_m}\right)^2} \tag{5}$$

where:

$N(E)$ = number of crossings at level E

E_m = mean value

σ = standard deviation of Gaussian power spectrum.

Table III shows partial results obtained using Eq. 5 with the troposcatter data. A more complete discussion and table of results are presented in Appendix C-2. The N(E) is calculated by using Eq. 5 for a particular threshold level. The equivalent flat power spectrum is given by f_b. The method of calculation of f_b is indicated in Appendix C-2. The quantities f_b' are closer estimates of the true fading bandwidths. A further discussion of f_b' is given later.

Table III. Experimental fading bandwidths.

Channel	N(E)	Experimental Crossings per Second	f_b	f_b'
TPO/2A	0.324 σ	23.1	14.2	1.71
TPO/4A	0.361 σ	18.2	10.05	1.32
TPO/2B	0.260 σ	37.0	28.5	1.92
TPO/4B	0.247 σ	25.2	20.3	2.1

It is seen that the fading bandwidth using all the data is estimated to be of the order of 20 cps or less. This number is undoubtedly inflated by the high-frequency hash. As is well known this rate is much faster than would be predicted by solely flat Rayleigh fading. Some of the

increase may be due to selective fading and such factors as moisture in the common volume. A part, however, is due to such undesired factors as 60-cycle ripple.

In a simulation of a flat Rayleigh fading process (Ref. 9) it has been found that the rate of fading crossings should theoretically be exponentially related to the fading length. We plotted the experimental fade occurrence versus fade length and found that the rate does vary exponentially for fade lengths greater than 2.0 milliseconds. If we extrapolate this exponential behavior to the low region (which ignores the increase in the number of shorter fades) and then find the total number of fades, the above equation yields a fade bandwidth of about 2 cps as indicated by the various f_b'. Note that eliminating the increase in the number of short fades decreases the total number of fades by about a factor of ten.

Consequently, if we ignore the hash the apparent fade rate is on the order of a few cycles per second. If we include the hash, a fade rate of the order of 20 cycles per second is obtained. An objective in the next data run will be to ascertain the exact cause of this hash and improve any experimental error contributing to it. As mentioned the possible contributors to this hash are: (1) selective fading, (2) perturbations on the link, (3) receiver malfunction or misadjustment, (4) monitoring malfunction, such as 60-cycle pickup and high-frequency feedthrough.

5.5 Combined Signal Fades and Error Runs

Figure 16 shows the fraction of time that the combined signal faded below its mean (for TPO/2 and TPO/4). Since the combined output is the result of an AGC action (see Fig. 3), there is no simple relation between the combiner level and an error probability. For this reason, we have chosen to relate the combiner signal fades to its own mean (without attempting to estimate the corresponding antenna signal mean). For the fade thresholds chosen, the TPO/2 level is 2.88 db below its mean, while the TPO/4 is 1.56 db below its mean. Combined signal data, like the single channel data, are somewhat inflated by hash. As expected, TPO/2 (without parametrics) experiences a longer fade time than does TPO/4, even though the TPO/4 threshold is higher. Thus these gross curves are consistent with the other data. Also, the behavior of these curves is similar to the error run curves of Fig. 17.

Figure 17 shows a plot of the fraction of time spent in contiguous error runs versus run length. A frame is in error if one or more errors occur within the frame. The

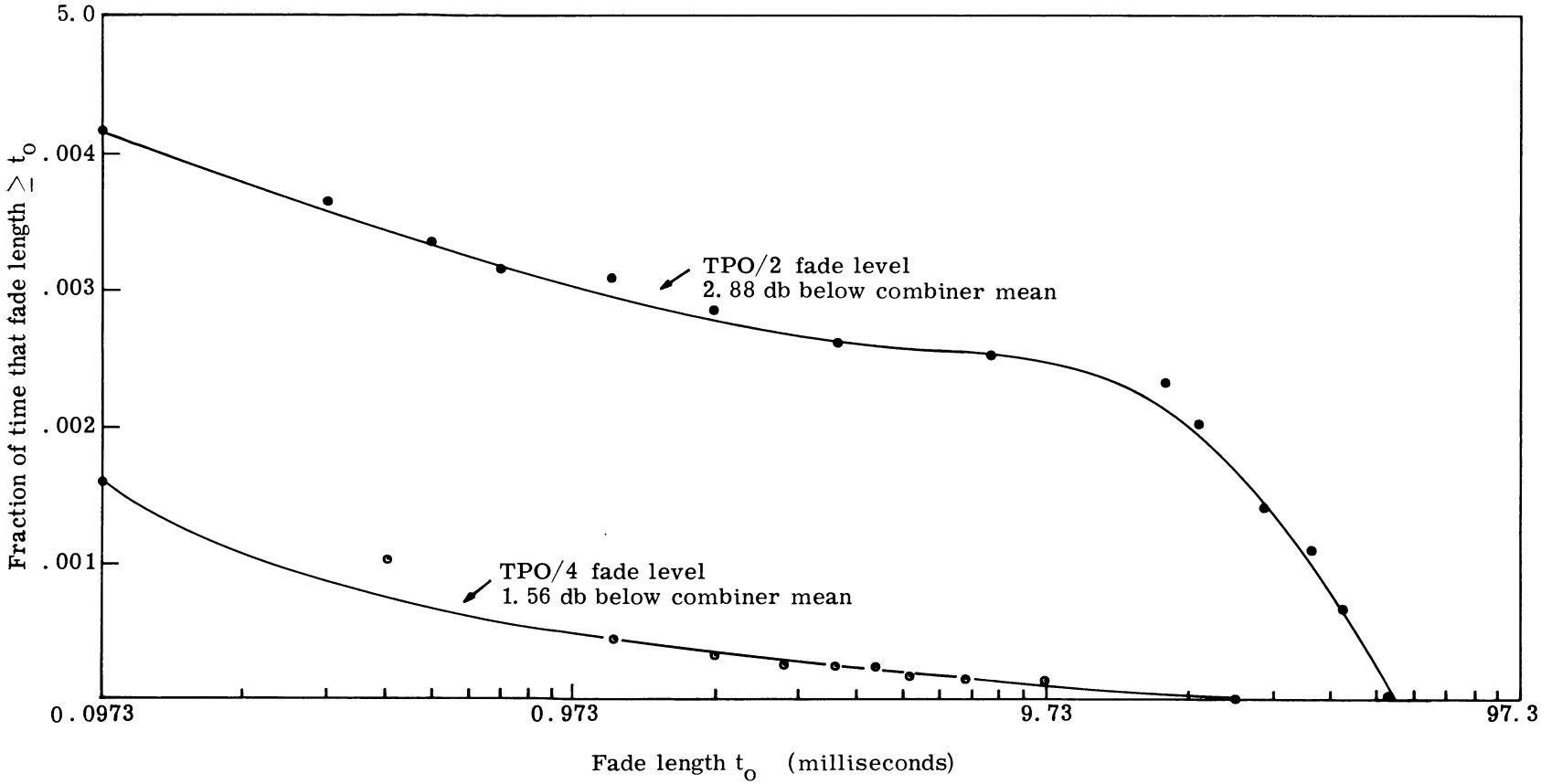

Fig. 16. Fraction of time below fade levels for combined signal.

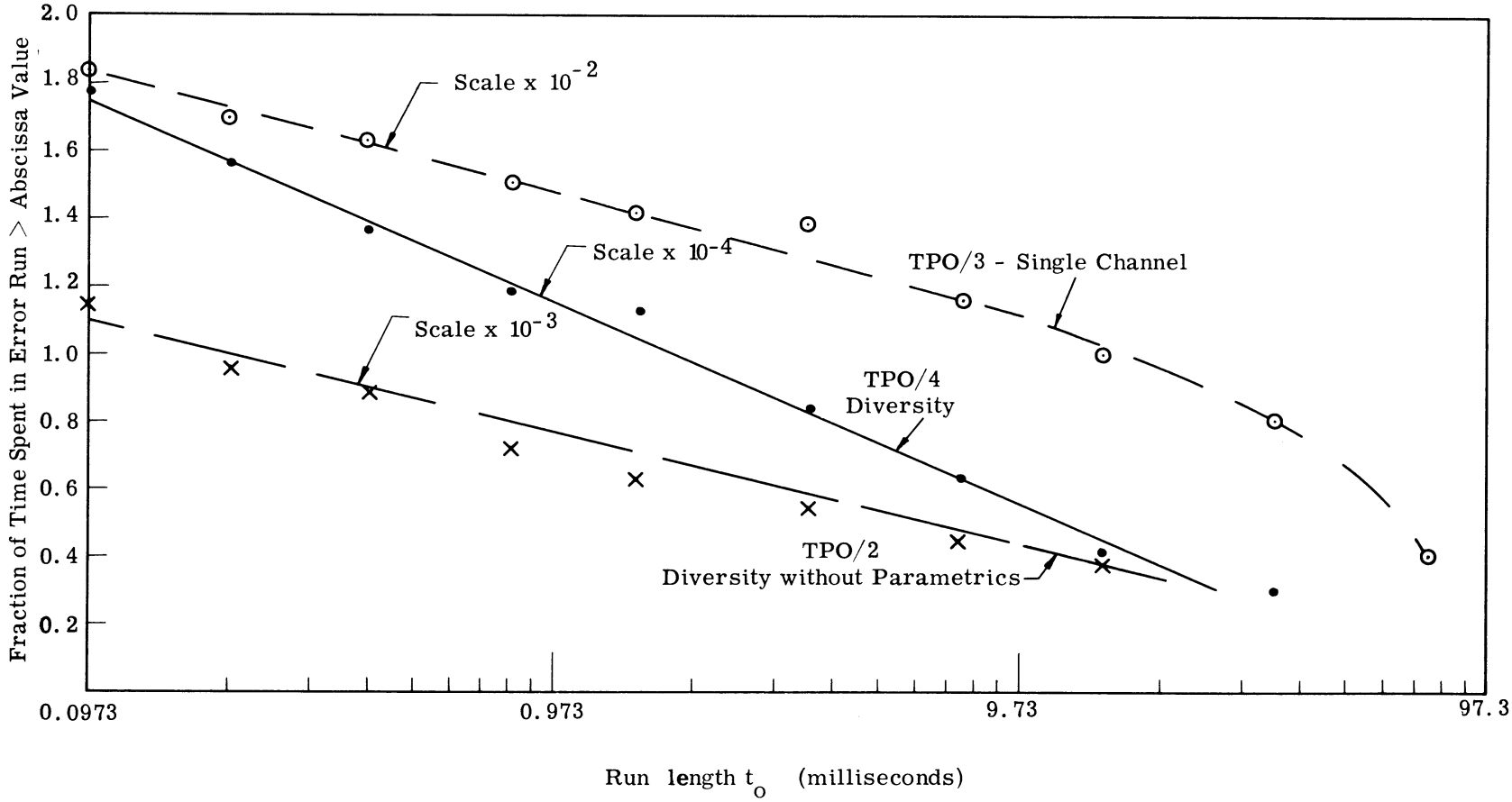

Fig. 17. Fraction of time spent in error runs exceeding run length t_o.

data of Fig. 17 can be considered as the (cumulative) probability of having an error run greater than length t_o. These data correlate reasonably well with the fade data of Fig. 16.

The diversity case has the lowest probability in error run; the diversity without parametrics the next lowest, and the single channel case has the highest probability in error run. Thus, as expected, the diversity is more influential than is the incorporation of the parametric amplifiers. The TPO/4 case relative to TPO/2 shows the same phenomenon as in Fig. 16; there are relatively more short error runs for the TPO/4 case than for the TPO/2 case. This is probably due to the increased airplane fading in TPO/4.

In conclusion, the curves of Fig. 17 indicate the probability of incurring error runs under conditions similar to those experienced during these data runs. [4]

It is interesting to note the pictoral action of the three signal channels and the resultant error behavior. Figure 18 shows three signal strengths plotted and the error length indicated by departures from the baseline. The phenomenon shown is a direct airplane effect. It is seen that the two single channel signals are quite well correlated during most of this time. When the two signals go into a fade situation, the AGC signal experiences a rise. (In all other reported data, the third signal is the combined signal, which moves in the same direction as the individual signals. The AGC signal was taken on an earlier recording whose data are not reported.) When the AGC signal rises, the corresponding error burst is indicated by the spikes from the baseline. Each of these spikes denotes an error count for the corresponding contiguous frame.

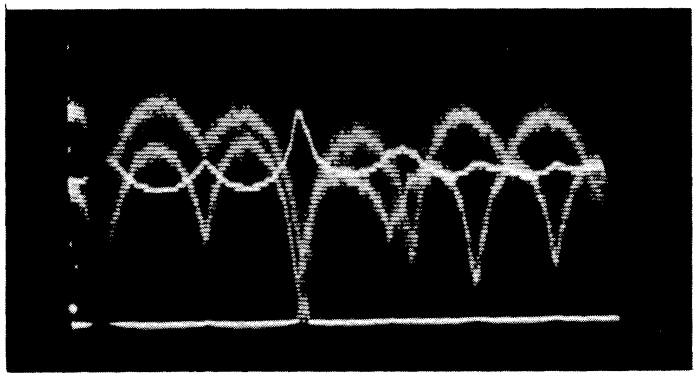

Fig. 18. Multiplexed signals. One-half second full scale.

[4] The spurious errors mentioned on p. 16, at the rate of 10^{-7}, will not seriously affect these error-run curves. The main effect will be to slightly inflate the single frame error-run point.

In addition to looking at the percentage of time spent in fade or error run (or probability of these) it is useful to look at the distributions themselves of the error runs and error-free runs. By using both the error runs and the error-free runs one is looking at the same information, but in a different form, as presented in the time behavior of Fig. 17. Figure 19 below shows the error runs and error-free run distribution for all three cases being reported. First it may be noted that the error run distributions themselves are quite similar, which again reinforces the consistency and credibility of the data. The error-free runs progressively improve as one goes from the single channel with parametrics (TPO/3) on to the diversity case without parametrics (TPO/2) to the normal diversity with parametrics case (TPO/4). [5] Although the error run distribution is quite similar for all the cases, it must be emphasized that the frequency of these error runs does vary among the cases as certified by the different behavior of the error-free runs and as seen in the equivalent information given in Fig. 17.

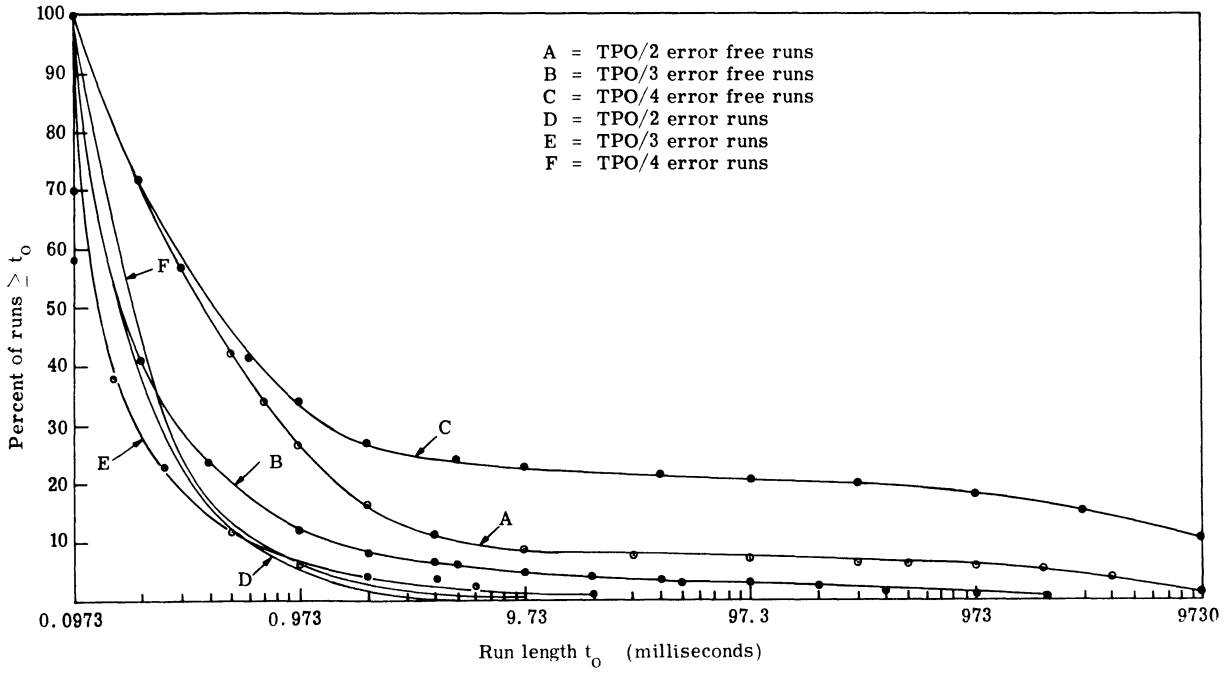

Fig. 19. Distribution of error runs.

Although the curves for TPO/3 go to the 100-percent point on the vertical axis, in actuality the depicted data show that the error run case terminates at 58 percent and the

[5] The major effect of the spurious errors (Footnote 1, p. 16) would be to slightly elevate the shorter error-free runs, while decreasing the very long error-free runs.

error-free case at 70 percent. This means that 42 percent of the TPO/3 error runs and 30 percent of the error-free runs were below 0.0973 millisecond (the minimum frame time for TPO/4 and TPO/2). This is because the frame size in the single channel TPO/3 case is one-half that in the other cases. The smallest value obtainable in the TPO/3 case is 0.0487 millisecond.

When considering smallest frame length, it should be remembered that when the signal is in fade the probability of error is very close to 50 percent. Thus, even though the signal might be in deep fade a run length of one bit is possible, and quite likely. Therefore, the shortest error run length is one bit. We of course are limited to recording the minimum run length of one frame which is 56 bits for the 4 data channel case and 28 bits for the 2 data channel case.

Another aspect that concerns the frame size is given by noting the average errors per frame as a function of run length. Table IV shows the median run length and the average errors per frame as a function of length for both the TPO/2 and TPO/4 cases. Note that in both cases the average errors per frame increase as the run length increases, but the change is not drastic. Additional information concerning the error runs may be found in Appendix C-3 which contains tables showing the error run statistics and the error-free run

Table IV. Average errors per frame versus run length.

Median Run Length in Frames	TPO/2 Avg. Errors per 56 bit Frame	TPO/4 Avg. Errors per 56 bit Frame
1	3.16	5.22
2	4.12	6.33
3.5	5.12	6.9
7.5	5.85	7.6
15	6.50	13.8
35	8.48	18.2
75	8.00	10.65
150	11.30	12.4
350	11.37	---
750	---	---

statistics from the computer. From Table IV it is seen that the number of errors per frame is somewhat higher in the TPO/4 case than the TPO/2 case. However, there are considerably fewer runs in the TPO/4 case. The reason for the values decreasing at the high run lengths of TPO/4 is due to the relatively few data points at these lengths. Also, the increasing length quantization contributes to this inaccuracy.

Along with all the previous data concerning fades and error runs, it is necessary to look at the rate. Table V shows the total number of fades, the average rate of fades, and the average length of fades for fades below a combiner level threshold (see Fig. 16) and the error runs. Note that the fade threshold is 2.88 db below its mean for the TPO/2 case, and 1.56 for the TPO/4 case. Table V indicates that the threshold for the TPO/4 case should be reduced to match the error statistics. Both the number and the average length of fades for the TPO/4 case are higher than the corresponding error behavior. Note that the experimental error runs dropped greatly from TPO/2 to TPO/4. Note also how the rate of fades and error runs drop from TPO/2 to TPO/4, while the average length of each of these increases.

Table V. Comparison of rates of error runs and fade lengths.

	TPO/4	TPO/2
No. of combined fades (from Fig. 16)	618	941
No. of error runs	148	969
Average rate of fades	1.79/sec	2.72/sec
Average rate of error runs	0.427/sec	2.80/sec
Average length of fades	0.88 msec	0.242 msec
Average length of error-runs	0.426 msec	0.390 msec

Also the average fade lengths and error run lengths are comparable and are quite short. This is one of the most important indications in this data and will be investigated closely in the upcoming data. The major question is to ascertain that all of this rapidity is indeed

legitimate link behavior and not partial system malfunction or experimental error.[6]

Selective fading and known link perturbation (such as moisture within the volume) are legitimate sources of extremely rapid activity on the link. The role of selective fading especially will be closely examined in forthcoming data.

In work performed last year (Ref. 8), a theoretical prediction of the probability of encountering fades greater than a given length was made based on simulated flat Rayleigh fading results, and then an extension of the prediction was made for a troposcatter link operating with equal gain diversity. The basic idea was to take the single-channel level crossing results which were reported from a Rayleigh simulation, and then to use these results in a calculation to find the conclusion when diversity is used. One of the first items of work accomplished this year was to perform an improved equal gain diversity calculation. The results and derivation of this calculation are given in Appendix D.

Both the single channel fade results, and consequently the extended diversity results, depend greatly on the fine detail of the spectrum. A gross comparison of the fade probabilities encountered experimentally with those predicted in the theory (of Appendix D) revealed that both the single channel and consequently the equal gain diversity results of the experimental case are much lower than for the theoretical predicted case. This is probably due to the presence of selective fading in addition to the flat Rayleigh fading and possibly a different spectrum for the flat Rayleigh part. The experimental results are more than a factor of 100 beneath those results which would be predicted by that theory. Further study will be required to ascertain the direct reasons for this disparity in the results.

It is useful to discuss the role of the frame size in the data. As seen in both the combined fade signals and the error runs, there appears to be much fast-acting action in this link which requires explanation. This raises the question of whether the frame size of 56 bits for the 4-channel data case is adequate. Any sensible answer depends largely on the objectives. The two primary objectives for error run data for the type under consideration are (1) to ascertain the synchronization requirements for digital systems, and (2) to find the error structure for the possible application of error correcting codes. Clearly, if one wishes to know the error structure for error correcting codes, the frame size must be quite

[6]It has already been found (Footnote 1, p. 16) that part of the error-run rapidity is due to spurious errors.

small since one wishes to know how many times errors are separated by 1, 2, 3, etc. bits. Selection of the criterion for frame size in the case of digital synchronization is not so clear.

The synchronization circuits will depend not only on the length of the error run but also the recovery time between error runs. Consequently, for certain purposes one may wish to group error runs since any synchronization circuit could not recover before the next error run starts. In such a case, it is not sensible to divide the error runs into small segments and to count them separately as separate short runs. Nevertheless, it is quite safe to use the smallest frame size possible because then one can simply group the data into larger frame sizes if necessary.

A good idea of how the error data on this link behave for the 56-bit frame is given by looking at the "run time" portrayal given in Appendix C-3. This shows the length of the consecutive (and alternating) error runs and error-free runs. The X's denote an error run, while the star (*) denotes an error-free run. It will be seen that many times a single error frame occurs, interspersed by error-free runs of varying sizes. By scanning such a chart one can picture the signal conditions. If the error runs are short and are interspersed by short error-free runs, the signal is in a very marginal state.

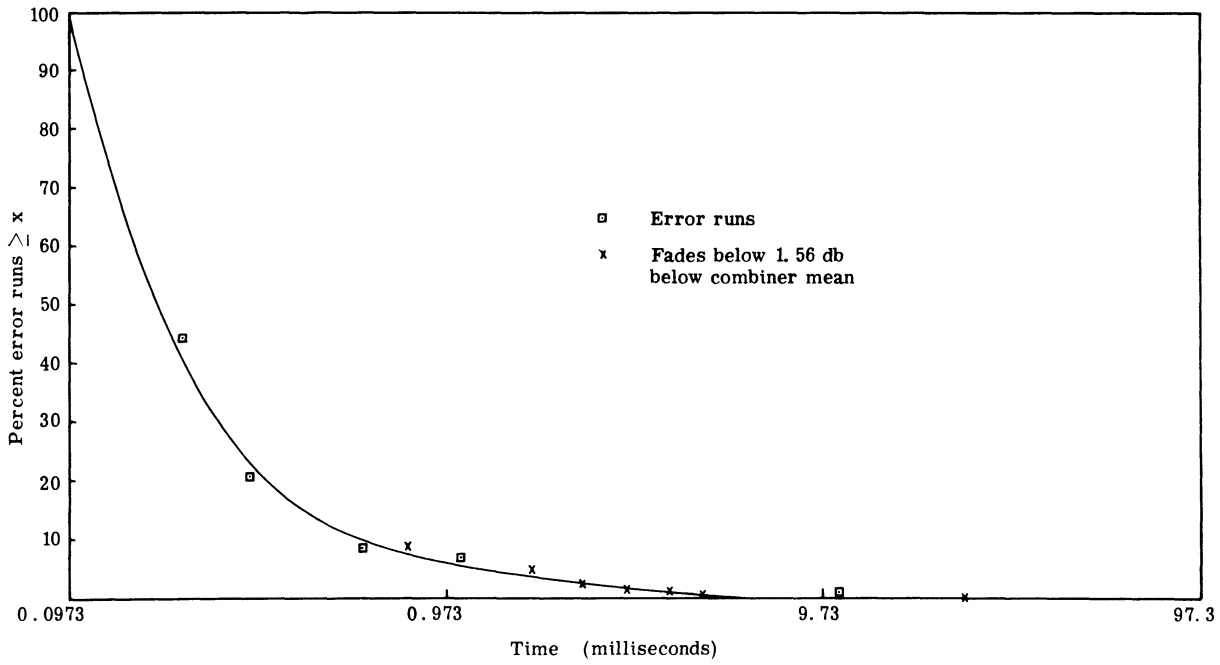

Fig. 20. Comparison of distribution of error run times given an error run and fade length time.

As a final depiction of the error run results, Fig. 20 shows a comparison of the distribution of error runs ("given an error run") and fade length for the TPO/4 tape. A threshold of about 1. 56 db below the combiner mean is compared to the distribution of the error runs. When plotted in this form, the distributions are in excellent agreement.

In conclusion, the curves of Fig. 17 provide the basic information of the amount of time spent in error run versus run length. Such information should be useful in deciding the necessary parameters for digital synchronization circuits. In the other results depicted it has been noted that both the fade activity and the error activity are much more rapid than expected by flat Rayleigh fading. The causes of this will be closely examined in forthcoming data.

A table completely summarizing the data is presented at the end of Appendix C-3.

6. CONCLUSIONS

The data taken represent the preliminary results of a detailed error analysis of a troposcatter link. The purpose of this detailed analysis is to permit analysis of the cause of the errors at high bit rates. A unique feature in these data is the interlocking of the signal and error data which is accomplished by direct multiplexing of the sample and local error values on digital tape. Thus, the reliable digital computer, rather than separately engineered equipment, is used as the data processing system.

The data reported are the first of a series which will be taken. As a result of this first test, we have improved the calibration procedures and decision circuits. Although we believe all the trends reported here to be true and reliable, the precise numbers will be subject to further verification on the later data. We believe the numbers herein except the number of fades to be within an engineering 10 percent accuracy.

During the dual diversity test (TPO/4), airplane fading was present approximately 28 percent of the time. A precise evaluation of the fading must await the later data.

The single channel distributions were essentially Rayleigh, but departed (were higher) at the low ends. This could be caused by the airplane fading and the selective fading.

Both the fade length data and the error run data indicated a surprisingly high fade rate, or fading bandwidth possibly due to selective fading. The future data will be checked closely to verify this rapid rate, and to assure the absence of partial malfunction of the link during this test.[7] Final conclusions must await the future data.

It should also be remembered that the 1010-modulation used may not reliably measure the intersymbol influence or the effect of different modulation patterns on timing. This will be considered in the future by comparing present data with that which will be taken using a pseudo-random sequence as the modulation.

Finally, it is hoped that the experience with this particular link, as evidenced by these data samples, will be an indication of the problems and issues characteristic of other high bit rate troposcatter links.

---

[7] It has already been learned that spurious errors occur at a rate in the 10^{-7} range, regardless of signal level. These errors are caused by transients from the crystal oven control in the receiver.

APPENDIX A

THE EXPERIMENTAL EQUIPMENT

E. P. Gould

The objective of this appendix is to discuss the experimental data processing system in more detail. This system enables the collection of data on the behavior of the signal simultaneously with the number of errors that occurred. Section A. 1 discusses each of the separate components of the system. Section A. 2 then describes the calibration procedure that should be followed before the equipment is used.

A. 1 THE TEST EQUIPMENT

A block diagram of the entire system was presented in Fig. 4. Referring to this block diagram, we can divide the system into the following:

1) Schmitt trigger circuit
2) Inverter amplifier
3) Pulse standardizer circuit
4) Resettable bit error counter
5) Flip-flop buffer
6) Frame counter
7) Delay units
8) D-A converter unit
9) Analog amplifiers
10) Multiplexer, A-D conversion equipment, and IBM tape deck.

Sections A. 1. 1 to A. 1. 10 provide a detailed discussion of each of these separate parts.

A. 1. 1 Schmitt Trigger Circuit

The Schmitt trigger circuit is a commercial circuit manufactured by the Raytheon Company. The input signal to this circuit was the bit error pulses. The Schmitt circuit has an output of 0 volts whenever the input voltage is below the threshold level and an output of -6 volts whenever the input voltage exceeds the threshold level. This circuit has an adjustable trigger level controlled by a potentiometer. The threshold level was set so that the true bit error pulses could be distinguished from any noise pulses. When properly set, the Schmitt output had an output square pulse corresponding to each bit error and no

output during noise pulses. The 0 to -6 volt output pulses were directly connected into the input of the pulse standardizer.

A. 1. 2 Inverter Amplifier

This circuit was designed and built by the Cooley Electronics Laboratory. The circuit diagram for the inverter amplifier is shown in Fig. 21. The input to this circuit was the positive output pulse from the tropo terminal 288-kc pulse generator. With the input voltage in the ground state, the transistor is saturated and the output voltage is essentially at ground potential. With a positive input pulse, the transistor is driven out of the saturation region into the active region. The output due to the high gain of the transistor would be a very large negative voltage but for the fact that the collector is clamped through a diode to -4 volts which restricts the output to operate between ground and -4 volts. Thus the output is -4 volts with 0 volts input and 0 volts with -4 volts input. The combination of a high gain, high frequency, switching transistor and the clamping action also gives an improvement in the rise time from the input to output pulse. The inverter amplifier is thus a pulse shaper as well as an inverter. The output 0 to -4 volt pulse can be used directly as an input to the pulse standardizer circuit.

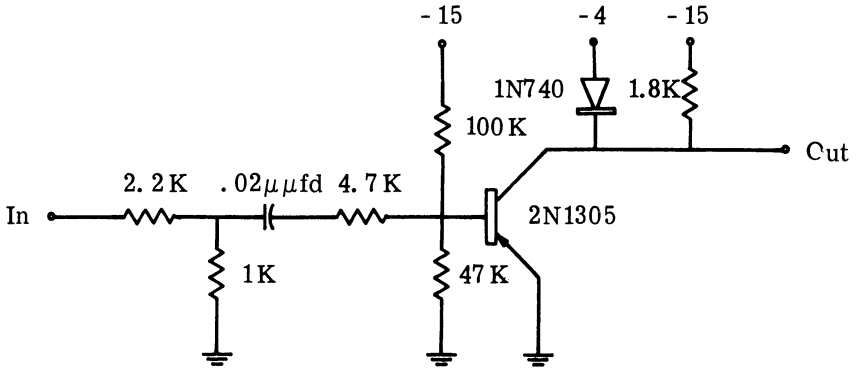

Fig. 21. Circuit diagram for inverter amplifier.

A. 1. 3 Digital Logic

The equipment to be described in this section is built up from Harvey-Wells Digital Data Blocs. These blocs are versatile front, patch-wired units. The diagrams of the circuits shown in Section A. 1. 3 indicate the wiring of the Harvey-Wells packages. This

digital logic requires 0 or -4 volt input and gives a 0 or -4 volt output. A logical "one" is 0 volts and a logical "zero" is -4 volts.

A. 1. 3. 1 Pulse Standardizer Circuit. The pulse standardizer circuits were used as the interface equipment between the tropo terminal equipment and the digital logic used in the data processing equipment. The circuit takes a negative input pulse of any shape and generates a 100 nsec, 0 to -4 volt pulse every time the input waveform passes through -2 volts in a negative direction. The unit will not reset until the input voltage has recovered to at least -1. 2 volts. The pulse standardizer output pulses can be used to operate any of the other Harvey-Wells digital logic blocs. Pulse standardizer circuits were used following the inverter amplifier and the Schmitt trigger circuit. They were also used in conjunction with some delay lines to be described later.

A. 1. 3. 2 Resettable Bit Error Counter. The input to this circuit is the bit error pulses from a pulse standardizer. The output of this counter is a binary representation of the total number of bits in error for each successive frame. A wiring diagram of the resettable bit error counter is shown in Fig. 22. The philosophy of operation is as follows: with each flip-flop initially in the "zero" state, the first pulse from the bit error pulse standardizer is inhibited by the pulse gate but applied to the inverter transistor to change the state of flip-flop 2 to "one." Because of a built-in flip-flop delay, the gate is not enabled until after the first input pulse has decayed. The next bit error pulse passes through the gate and is inhibited by the next stage gate, changing the state of flip-flop 1 to "zero" and flip-flop 2 to "one." The third pulse changes only the first flip-flop and so on until the entire binary count is accomplished. At the end of each frame, the counter is cleared, with all flip-flops reset to the "zero" state by the application of a reset pulse to the inverter gate attached to the "zero" side of each flip-flop. However, just preceding this reset pulse, the output state of each flip-flop is transferred to a flip-flop buffer. The resetting of the counter must follow the transfer of the information by at least 500 nanoseconds to ensure that all previous pulses have completely decayed before another pulse is applied to any flip-flop. The resetting must be finished before the next possible bit error pulse to ensure no counts are lost. A timing diagram of the entire system is shown in Fig. 23.

A. 1. 3. 3 Flip-Flop Buffer. The purpose of the flip-flop buffer is to store the total count of the number of bit errors per frame in a digital form for one complete frame.

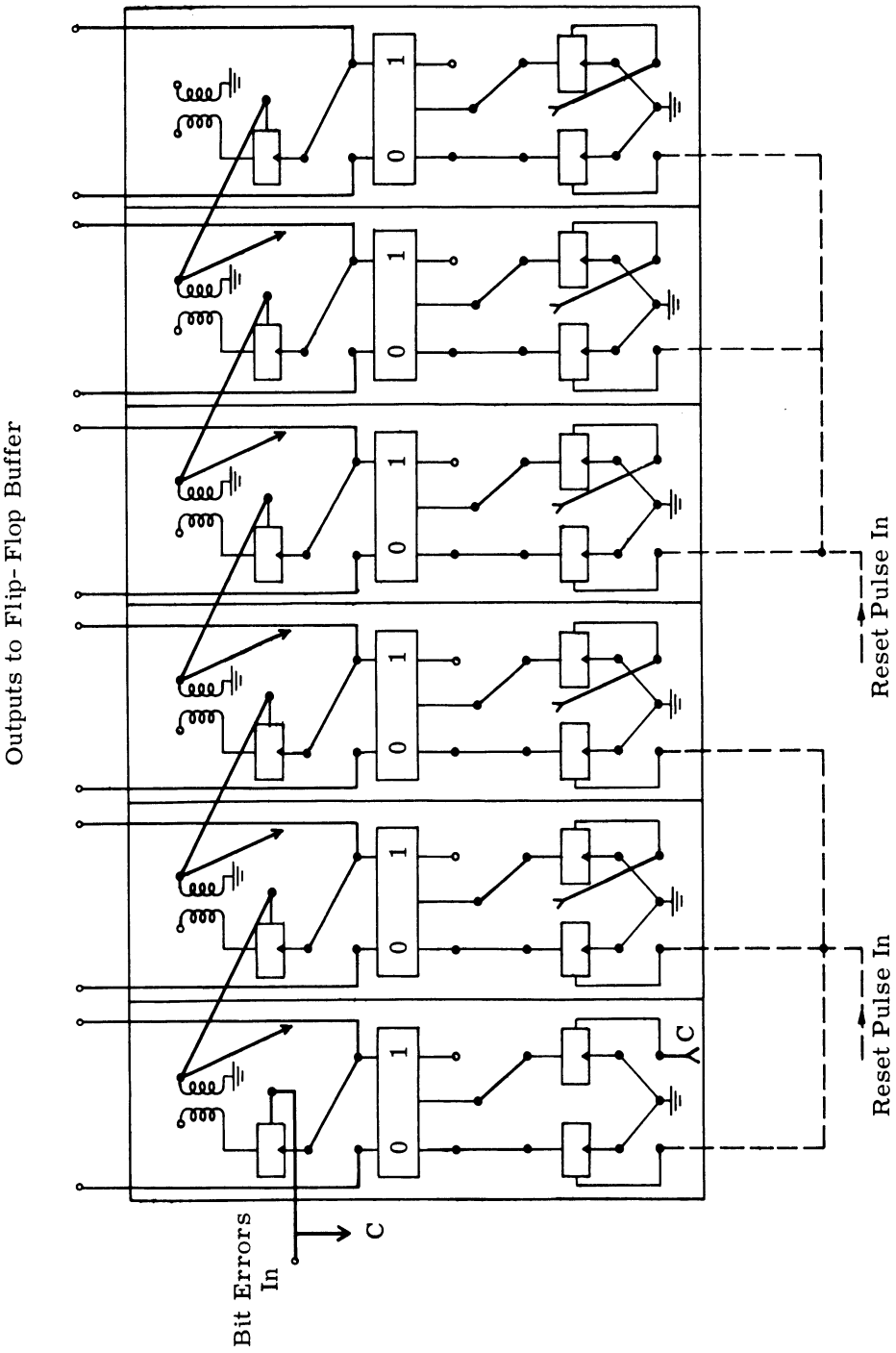

Fig. 22. Diagram of resettable counter.

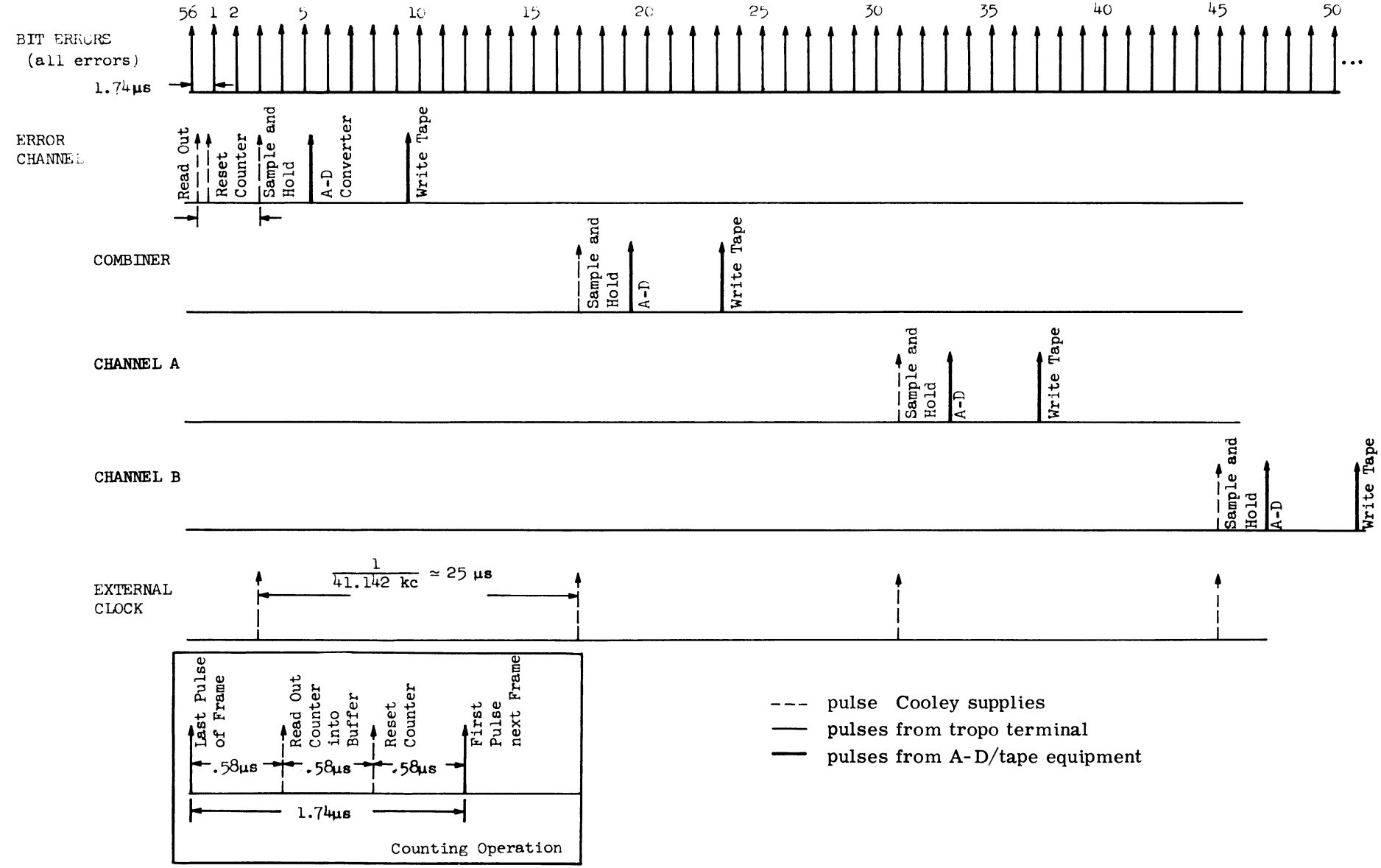

Fig. 23. Timing diagram for data acquisition equipment.

With this storage the count of the errors in the present frame can be started while the remainder of the processing equipment is still operating on the total number of bit errors that occurred in the previous frame. A wiring diagram of this circuit is shown in Fig. 24. The philosophy of operation is as follows: to each flip-flop of the counter there is a corresponding flip-flop of the buffer. The output levels both "zero and one side" from the flip-flops of the bit error counter are applied to the emitters of the inverter transistors of the corresponding flip-flops of the buffer. There is an inverter transistor for each side of each flip-flop. These inverter transistors can be thought of as "pulse steerers"; i. e., a pulse will be passed to change the state of the flip-flop only when the proper logic conditions are met. At the end of each frame, a transfer pulse occurring after the last possible bit error and before the counter is reset is applied to the base of the inverter transistor. The output states of the buffer flip-flops will change to the identical states as contained in the states of the bit error flip-flop counter at the time of the transfer pulse on command of the transfer pulse. The buffer flip-flops will now remain in these states until a new transfer pulse is applied. This is a parallel read-out of data from one set of flip-flops to another at a selected time. In other words, the emitter voltage of the inverter transistors will change at the same rate as the bit error flip-flops but only the states present at the time of the transfer pulse (at the end of each frame) will be switched to the outputs of the buffer flip-flop. Therefore, the buffer outputs change at the frame rate of the transfer pulses; hence the buffer stores the total number of bit errors per frame for one complete frame.

A. 1. 3. 4 Frame Counter. This circuit is used to subdivide the basic 288-kc clock of the tropo system to derive clock pulses at the frame rates of either 41. 142, 20. 571, or 10. 285 kc. These frequencies correspond to frame sizes of 56, 28, and 14 bits per frame. One output of this circuit, the 41. 142-kc clock, is always used to clock the A-D tape unit. This output and the other outputs, depending on the frame size being used, are used to reset the bit error counter and to transfer the data from the bit error counter to the flip-flop buffer at the end of each frame. A wiring diagram of the entire circuit is shown in Fig. 25. This circuit is composed of a three-stage shift register generator and a two-stage binary counter. By some associated digital logic, the three-stage register generator can be used as a divide-by-seven circuit. The first stage of the binary counter can be a divide-by-two circuit, and the output of the second stage of the counter can be a divide-by-four with re-

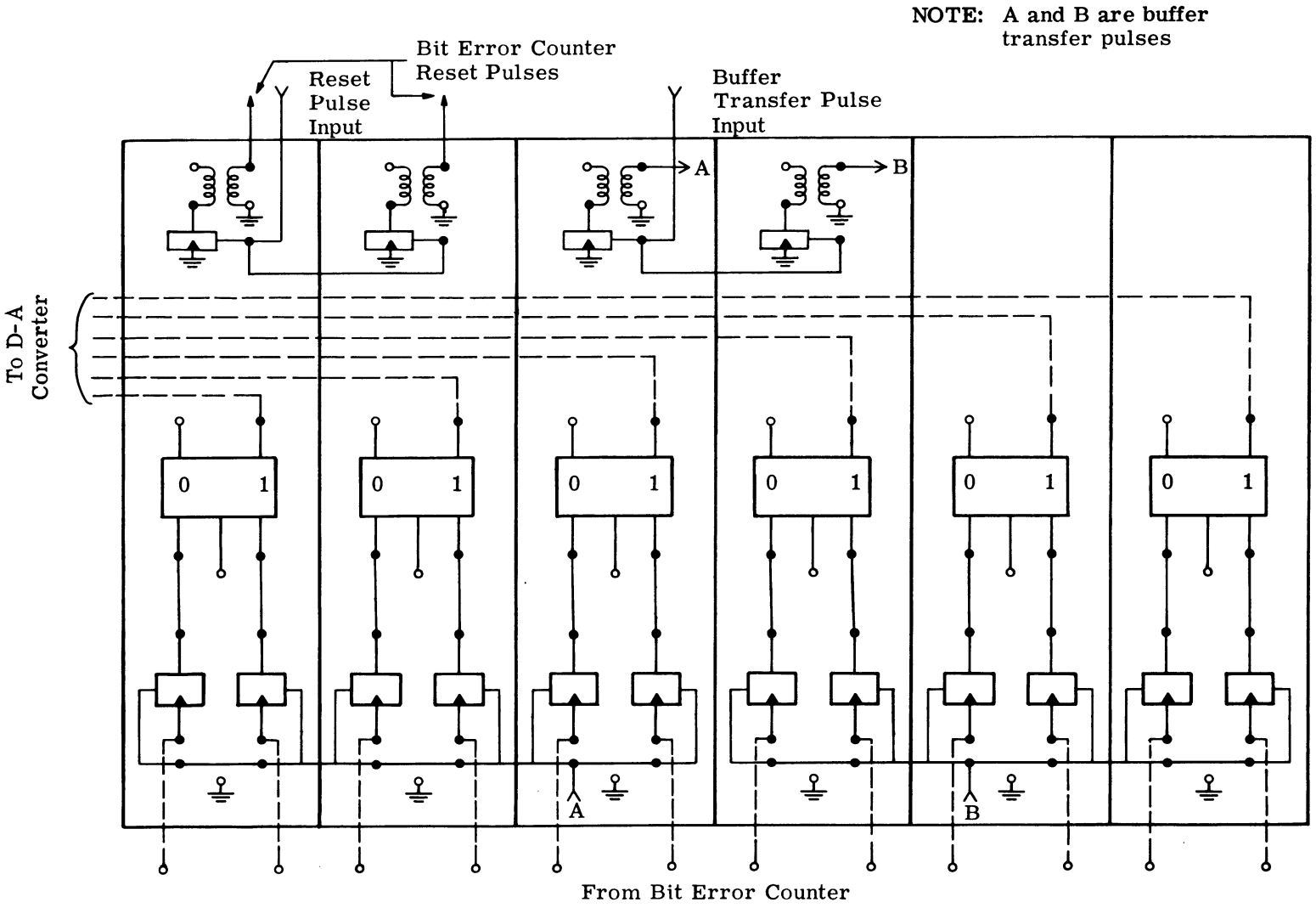

Fig. 24. Diagram of flip-flop buffer.

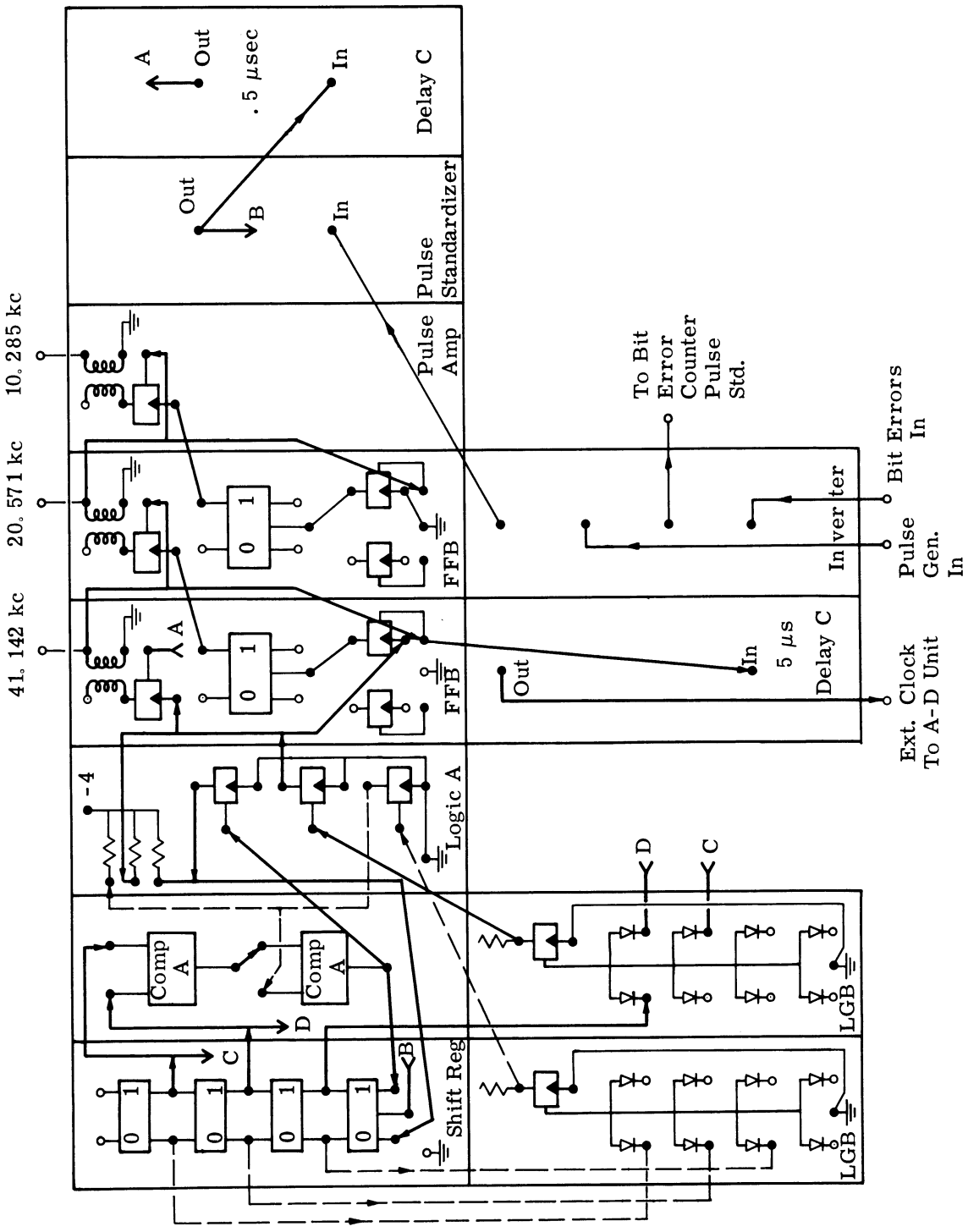

Fig. 25. Diagram of frame counter and interface equipment.

spect to the input clock of the binary counter. Thus, beginning with the 288-kc clock frequency from the tropo terminal equipment, the output of the shift register generator is 288/7 or 41. 142 kc, the output of the first stage of the binary countdown circuit is 41. 142/2 or 20-571 kc and the output of the second stage of the binary countdown circuit is 20. 571/2 or 10. 285 kc. This shift-register generator is of the "fail safe" type in that it will never stop running due to an all-zero state being inadvertently loaded into the register. If an all-zero state is loaded into the register a Logic B AND unit generates a pulse which immediately starts the register running again. The output of the "one side" of each stage of the shift-register generator is added together by a Logic B AND circuit. The combination of three "ones" occurs only once each seven clock pulses. Therefore, the Logic B AND circuit has an output pulse only every seven clock pulses. This pulse is too wide to drive any other pulse logic. For this reason, this pulse is inverted by an inverter Logic A and used to gate the standard clock pulses (slightly delayed) with a pulse gate. The output of the pulse gate is a clock train of standard pulses at a 41. 142-kc rate. These 41. 142-kc clock pulses are then used as the input clock to a two-stage binary counting circuit similar to the one described in Section A. 1. 3. 2. The outputs of the pulse gates of this binary counter are standard pulses of a 20. 571- and 10. 285-kc rate.

A. 1. 3. 5 Delay Units. Delay units are necessary in three distinct places in the data processing equipment: (1) to delay the data transfer pulse behind the last bit error pulse by about 0. 5 μsecond, (2) to delay the reset pulse to the bit error counter by about 0. 5 μsecond behind the data transfer pulse, and (3) to delay the 41. 142-kc clock pulse to the A-D/tape unit by about 10 μseconds behind the bit error reset pulse to allow the system transients to die down before the data is converted to a digital form for placement on the magnetic tape. One of the actual delay units used was manufactured by General Radio Corporation; the other two were Harvey-Wells Data Blocs. Associated with the GR delay lines is some Harvey-Wells Logic to provide drive capabilities for the delay line and to shape the delayed pulse. For item number 1 above, the output of the pulse standardizer with the inverted pulse generator 288-kc output from the tropo terminal equipment as input is delayed by a Harvey-Wells Delay C unit by approximately 0. 5 μsecond. The output of this delay unit is fed directly into the base of a pulse gate where it is gated by the output of the shift-register generator Logic B unit to produce 41. 142-kc clock pulses. These pulses are used as

clock pulses for the remainder of the frame counter. Depending on what frame size is being used, the output of one of these pulse gates of the frame counter is fed into two pulse amplifiers for buffering purposes and the amplifier outputs used as the transfer pulse for the flip-flop buffer. For number 2, the GR delay line is used. One of the outputs depending on the frame size of the pulse gates of the frame counter is inverted by a Logic A unit and fed into an emitter follower bloc. The output of this emitter follower is used to drive the GR delay line. The 0.5 μsecond delayed output of this delay line is fed into a pulse standardizer to reshape the pulse into a standard pulse. The output of this pulse standardizer is fed into two pulse amplifiers for buffering purposes and the amplifier outputs used to reset the bit error counter. For number 3, the 41.142-kc output of the frame counter is delayed by a second Harvey-Wells delay unit for about 5 μseconds. This delay unit creates a pulse whose width is equal to the delay desired. This 5-μsecond wide pulse is used to clock the A-D/tape unit which is clocked off the trailing edge of the pulse.

A. 1. 4 D-A Converter Unit

This unit is a commercial circuit model LP-31 manufactured by the 3-C Corporation. This unit can transform any 6-bit binary number into a corresponding analog voltage. The reference level in this setup was - 10 volts. Therefore, a binary 111111 input gives a - 10-volt output and 000000 a 0-volt output while any binary number in between gives a voltage determined by the formula,

$$\frac{(\text{binary number converted to decimal}) \times (-10)}{64}$$

This unit was used to convert the total number of bit errors in a frame to an analog voltage which could be fed into the A-D/tape unit multiplexer for multiplexing with the other analog inputs. The output of the "one side" of each of the buffer flip-flops was fed directly into the D-A converter. The output of the converter is then placed into one channel of the multiplexer.

A. 1. 5 Analog Amplifiers

The analog amplifiers were operation amplifiers made by Philbrick Corporation. These amplifiers were used as variable gain amplifiers to ensure that each analog signal completely utilized the full 10-volt range of the analog multiplexer and did not go outside

this range. A second reason for their use was to provide a low impedance output into the multiplexer. Their positions in the data processing system are indicated in the system diagram (Fig. 4).

A. 1. 6 Multiplexer, A-D Equipment, and IBM Tape Unit

This data conversion equipment, purchased from the Raytheon Company, allows the sampling and digitizing of analog waveforms with the entry of the digital signals directly on magnetic tape in a format acceptable to the IBM 7090 computer. The multiplexer enables up to four analog signals to be sampled sequentially and their corresponding digital signals to be placed on the magnetic tape. The sampling rate for this equipment was always 41. 142 kc, making the sampling rate per channel either 41. 142 kc, 20. 571 kc, or 10. 285 kc depending on whether 1, 2, or 4 channels are multiplexed together. The accuracy of the digital quantizing of the analog signals was 64 levels for the 10-volt range or 0. 1562 volts per level. The circuitry necessary to provide all the tape movements and special marks needed to ensure the output tapes are directly compatible with the IBM 7090 digital computer are built into this equipment. Other computers using the IBM tape formats also could be used to read these tapes. Appendix B describes in detail the format used on the tape and the programming necessary to analyze the tapes made by this equipment.

A. 2 CALIBRATION PROCEDURE

This section provides a step-by-step description of the calibration procedure which should be followed to ensure satisfactory operation of the data processing equipment.

1) Write test tape of single-channel sine wave $\pm$ 5 volts peak.

2) Play back tape and observe results. Especially look for bit dropouts.

3) Write test tape using four different negative dc voltages through multiplexer.

4) Play back and observe results. Especially watch for multiplexer beginning on the first data signal each tape record.

5) Begin the calibration of the equipment by grounding the system input to the Raytheon equipment and adjusting A-D converter offset potentiometer for all A-D indicator lights out. Do not touch this offset adjustment again.

6) Attach variable dc supply to input to sample and hold circuit and monitor out-

put of sample and hold. Adjust input voltage until output of sample and hold is exactly 1.500 volts using 4-place dc digital voltmeter. This voltage will be used as input to adjust the A-D converter. Attach output of sample and hold with this 1.500 voltage to A-D input. Adjust gain potentiometer A-D until all lights are just barely on. Ground system input again and adjust level potentiometer for all lights just barely out. Put calibrated 1.500 volts on again and check that all lights light. This completes adjustment of AD-10.

7) Begin adjustment of Harvey-Wells digital logic and D-A converter by removing transfer pulse from buffer flip-flop. The FF's can now be set by an external wire from ground to the input of either side of the flip-flop. Attach output of D-A converter through a multiplexer channel into sample and hold. Set a particular FF combination; we suggest 2^5. Adjust D-A reference voltage to approximately -10 volts so that the selected combination of lights on buffer appears on A-D lights. Try other combinations and check lights. Replace reset transfer pulse.

8) Connect Harvey-Wells equipment to tropo terminal by correcting bit error test point to Schmitt Trigger Circuit and Pulse Generator output to inverter circuit.

9) Check output of inverter circuit to see if inverting occurs properly. Check output of pulse standardizer to see if it is functioning correctly. Check Schmitt trigger output and output of attached pulse standardizer for correct operation. Obtain an all-error signal from tropo link.

10) Sink scope on output of bit errors pulse standardizer. Place output of bit errors pulse standardizer on Channel A of oscilloscope and 41.142-kc output of frame counter on Channel B. Adjust Delay C unit until pulses on Channel B lag Channel A by approximately 0.5 μsecond.

11) Sink scope on input to GR delay line. Put input to GR delay line on Channel A. Put output of pulse standardizer attached to output of GR delay line on Channel B. Adjust GR delay line until pulses on Channel B lag pulses on Channel A by about 0.4 - 0.5 μsecond.

12) Check width of clock pulse out of Harvey-Wells Delay C unit which provides clock pulses for A-D/tape unit. Adjust delay unit until these pulses are 5-10 μseconds wide.

13) Put output of 288-kc pulse standardizer directly into input of bit error counter. With reset pulse on 56-bit frame output, buffer output should be a binary 28; with reset pulse on 28-bit frame, buffer output should be a binary 14; and with reset pulse on 14 bit frame, buf-

fer output should be a binary 7. Check A-D lights to ensure number on A-D agrees with buffer number.

14) Now place output of variable clock into bit error counter. Check different frequencies to ensure that lights on flip-flop buffer and A-D unit agree. This completes calibration of Harvey-Wells equipment.

15) Put combined Channel 1 and Channel 2 signal from tropo link into Philbrick amplifiers. Adjust gains individually by attaching to Raytheon equipment and monitoring D-A converter output to see that no clipping occurs. Measure gain of each channel by using a battery input and measuring the input and output of amplifier on a digital voltmeter.

APPENDIX B

DESCRIPTION OF COMPUTER PROGRAMS FOR THE ANALYSIS OF TROPOSPHERIC SCATTER

A. M. Collins

The programs to be described have been written in two languages, MAD (Michigan Algorithm Decoder) and UMAP (University of Michigan Assembly Program), and have been processed on an IBM 7090 digital computer at The University of Michigan with the Michigan Executive System. Some subroutines used in the programs for printing and tape handling are unique to this system. MAD, a compiler language similar to FORTRAN, has been employed for all parts of programs which do not consume extensive computer time. UMAP (an adaptation of the Bell Labs assembly program) has been used where repetition makes optimal programming worth the additional cost in programming and debugging. Tape reading time is minimized by buffering, so that while one record is being unpacked and processed on tape, the next record is being read into core storage.

B. 1 COMPUTER PROGRAMS FOR DATA ANALYSIS TROPOSPHERIC SCATTER

Three different computer programs have been written for the 1-channel, 2-channel, and 4-channel tapes produced. As discussed in Section 4. 1, the single channel is for error data alone; the 2-channel case multiplexed an error count with one signal level; and the 4-channel case multiplexed both signal levels, the combined signal level, and the error count. In each case there is a main program written in MAD language which sets up storage, calls the subroutines to read, unpack, and store the data for each record, and finally sets up and prints out the information. There are two UMAP subroutines, RDTAPE and STORE. RDTAPE merely reads a 4001-word record from tape into core storage. STORE unpacks the data and counts the occurrences needed to compute the distributions printed at the end by the main program.

Each input frame for a channel is in six-bit mode. For the signal channels the voltage level can be one of 2^6 (or 64) different levels coded as 0-63 in the 3 programs. The error channel, as a count of the number of samples in error in each frame, has a maximum of 14 for the 1-channel case, 28 for the 2-channel case, and 56 for the 4-channel case. In the programs the two signal channels are labeled A and B, the combined signal Channel C,

and the error Channel D. In the 1-channel (D) case, each computer word read in from tape contains 6 frames of 6 bits each (or 36 bits). The 2-channel case includes both D and A channels, and each word contains 3 frames arranged D-A|D-A|D-A. The 4-channel case has 3 frames packed into each 2 computer words as follows: 1) D-C-A-B/D-C, 2) A-B/D-C-A-B. In each record the multiplexer must start with the D channel as shown, for the programs assume this in unpacking each record of data.

B. 1. 1 RDTAPE

RDTAPE is a buffered tape routine which reads one record ahead of the record being processed by STORE. RDTAPE reads only fixed length records of 4001 words (the first word is treated as a record header). The record length is based on space limitations in storage for the 4-channel case. The troposcatter tapes have up to 600 records (the exact number to be processed is specified by input data) in one file, with a file mark in front and two at the end. The routine has the following two entries:

1) SETRD sets initial addresses and reads the first record into the lower half of Buffer. If two records in a row at the beginning of tape have parity errors, the program halts.

2) RDTAPE initiates a read into the other half of Buffer after checking that the previous record read correctly. If an end-of-file or a parity error is found in the previous record, the next record is read over the record in error and the program waits until the new record is read in. If there are two end-of-files in succession, the program assumes it is the end of tape and transfers to the print-out section of the main program.

B. 1. 2 STORE

While RDTAPE reads into one-half of Buffer, STORE unpacks and counts the data in the other half. STORE unpacks one frame at a time (finding the values for D; D and A; or D, C, A and B, depending on whether it is a 1-, 2-, or 4-channel tape) and makes appropriate entries in tables, before handling the next frame. A description of the tables for each case follows. Most of the following tables are constructed by increasing a counter for each frame that has a particular value in some channel(s). Hence a linear or two-dimensional array is formed for the entire tape, with each entry containing the count of the number of frames with that value. Tables in b) and c) below, however, are based on runs of frames.

These carry over from record to record, even though some frames are lost during record gaps in preparing the tapes. Figure 26 shows the STORE routine for the 2- and 4-channel cases.

B. 1. 2. 1 One Channel.

a) A distribution of the total number of frames with each error (D) level.

b) A Run-Time Table is formed listing in order each error run and each error-free run and its length. For example, two frames in a row without an error is called an error-free run of length 2. This table has limited storage and is compiled only until that storage is exhausted.

c) Distributions of the total number of error-free runs and error runs of different lengths during the entire tape. For this table the lengths of runs are grouped to show the total number of runs between, for example, 20 and 50 frames in length. (The size of the length groupings is approximately logarithmic.)

B. 1. 2. 2 Two Channel.

a) A distribution of the total number of frames in each entry of an A x D matrix (signal level vs. no. of errors).

b and c) As in the 1-channel case.

d) Distributions of the total number of frames with each signal level (A) both when errors occurred and over-all.

B. 1. 2. 3 Four Channel.

a) As in the 2-channel case but the entries are in a C x D matrix (combined signal level vs. no. of errors).

b and c) As in the 1-channel case.

d) As in the 2-channel case but for the combined signal (C).

e) Distribution of the total number of frames in each entry of an A x B matrix. The A x B distribution when errors occurred is stored in the front portion of the words in this array.

B. 1. 3 Main Program

The main program (see Fig. 27) contains a short loop that reads in and processes each record individually. This loop contains the calls to RDTAPE and STORE. All the

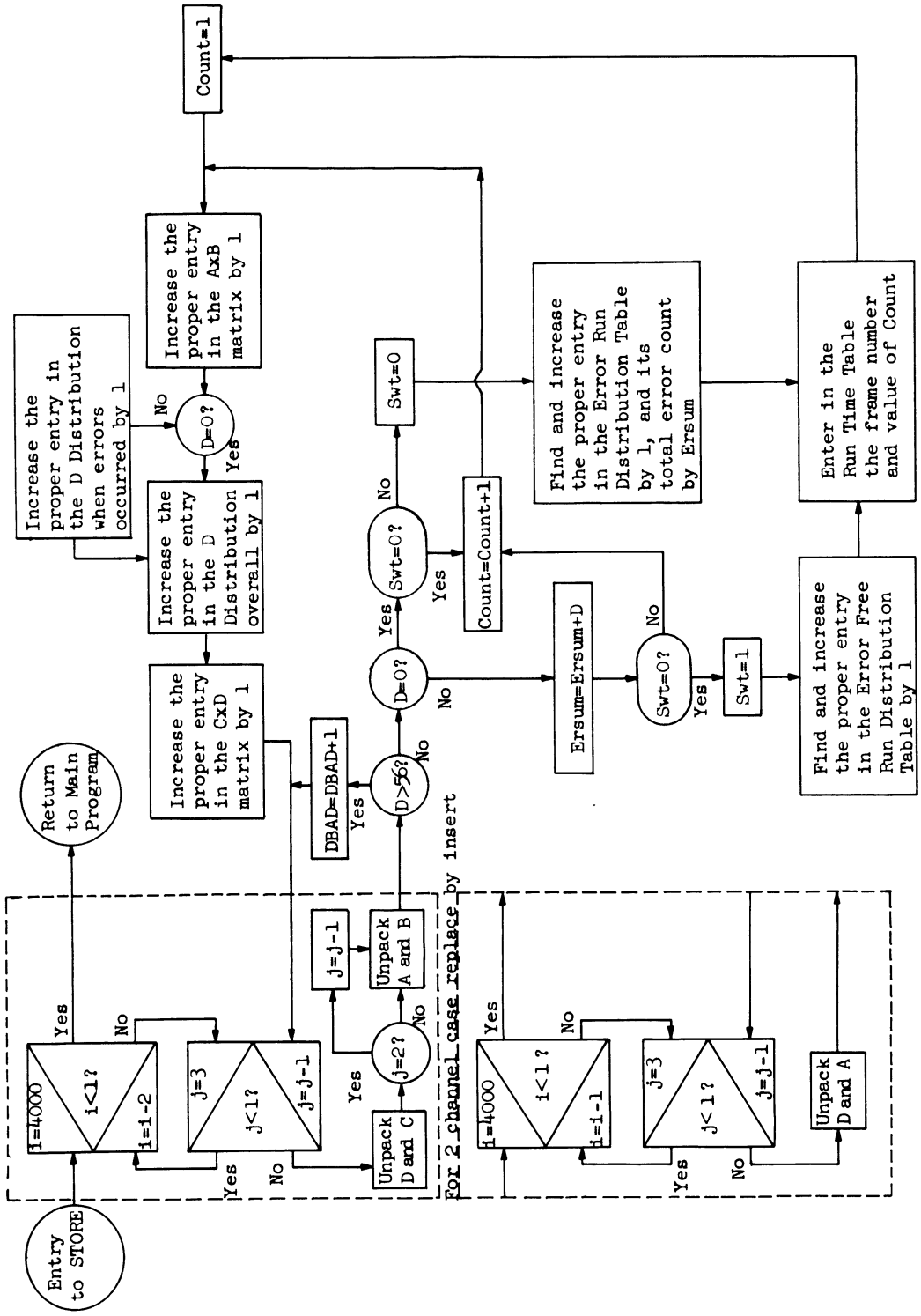

Fig. 26. STORE routine for the 2- and 4-channel cases.

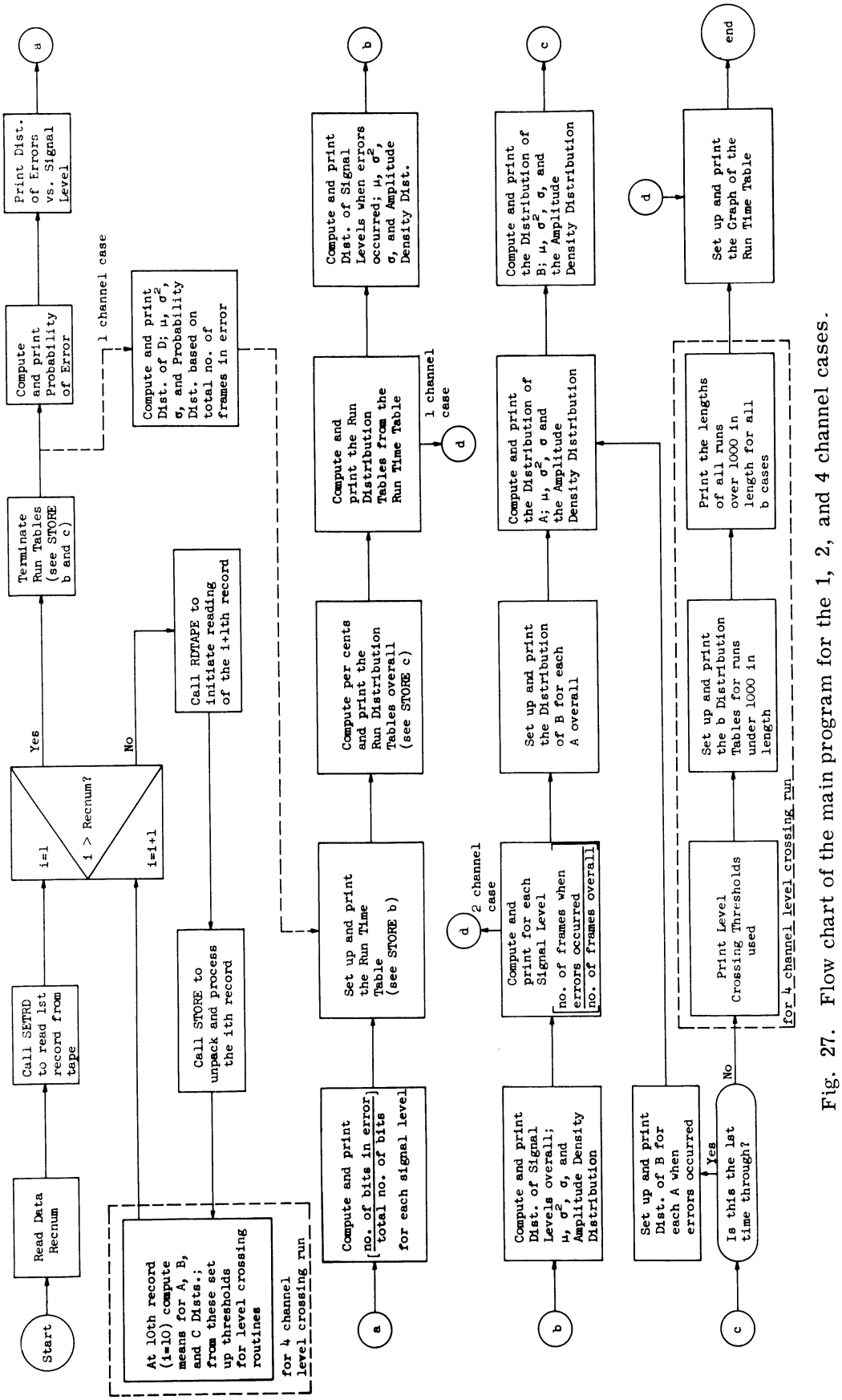

Fig. 27. Flow chart of the main program for the 1, 2, and 4 channel cases.

records are processed before any printing is done. When the loop is completed, the main program terminates the final error and error-free runs in the run tables of b) and c) described in STORE. The remainder of the program for the 2- and 4-channel cases consists of setting up and printing out the following:

(2 & 4)[8]	1) Probability of error computed from the C x D matrix (A x D for the 2-channel case).
(2 & 4)	2) The C x D matrix (A x D for 2 channel) labeled 'Distribution of Errors for Each Signal Level. '
(2 & 4)	3) (No. of bits in error)/(Total no. of bits) for each signal level.
(1, 2 & 4)	4) The run-time table (described in b of the STORE write-up).
(1, 2 & 4)	5) Error and error-free run distribution tables.
(2 & 4)	6) Distribution of the number of frames with each signal level (C for 4 channel and A for 2 channel) when errors occurred; mean, variance, and standard deviation for this distribution; the probability (amplitude density) distribution obtained by dividing this distribution by the total number of frames in error.
(2 & 4)	7) As in 6 but for the entire run rather than when errors occurred.
(2 & 4)	8) The ratio of the distribution in 6 over the one in 7 for each level.

For the 4-channel case only:

(4)	9) The A x B matrix (Distribution of A vs. B).
(4)	10) The distribution of A; the mean, variance, and standard deviation based thereon; the probability distribution based thereon (as was done for C in 7).
(4)	11) As in 10 for B.
(4)	12, 13 & 14) Repeat of 9, 10, and 11 when errors occurred.

For 4-channel case with level crossing only (Section B. 1. 3. 2):

15) Table of thresholds used for each signal channel.

[8]Numbers in parentheses indicate which cases are applicable.

16) Distribution of runs under 1000 in length for each threshold used (these are counted in groups of 8).

17) Listing of runs over 1000 for each threshold.

For all 3 cases:

(1, 2 & 4) 18) Graph of the run-time table (see 4).

For the one-channel case the main program first prints out the distribution of D over-all, the mean, variance, and standard deviation of the distribution, and the probability distribution obtained by dividing each entry by the total number of frames in error. This is followed by items 4, 5, and 18 above.

B. 1. 3. 1 Uncompressed Mean, Variance, and Standard Deviation. As noted, the voltage levels received have been compressed into 64 levels for digital analysis. Items 6, 7, 10, 11, 13 and 14 in the preceding section include values for the uncompressed mean, variance, and standard deviation as well as the compressed values computed directly from the 64-level distribution. The uncompressed figures are obtained from weighting factors read in as input data, which are computed in another program. The weighting factors are derived from calibration data taken on the experimental equipment used to obtain voltages A, B, and C.

B. 1. 3. 2 Level Crossing. A level crossing section has been added to the STORE routine for the 4-channel case. There are two thresholds for each signal channel, and this section counts the length of all runs of consecutive frames below the threshold for that channel. Thus there are six different tables of runs for the different thresholds. All runs less than 1000 in length are counted modulo-8 (except 1 through 7) and those above 1000 listed separately. The thresholds can either be read in initially or computed as a percent of the mean for 10 records. Runs are carried over record gaps.

B. 2 THE DEMULTIPLEXING PROGRAM

This program reads as input a 4-channel tape in six-bit mode and produces 4 tapes each with a single channel on it. To preserve the same time relationships on the output tape as on the input tape, each frame on the output tape is repeated four times. Thus if the first two words of input are of the form, 1) $D_1 - C_1 - A_1 - B_1/D_2 - C_2$ 2) $A_2 - B_2/$

D_3 - C_3 - A_3 - B_3, for the A channel the first two words of output would be 1) A_1 - A_1 - A_1 - A_1/A_2 - A_2 2) A_2 - A_2/A_3 - A_3 - A_3 - A_3. The input records for the program are 4001 words (of which the first is thrown away), and each input record generates two 2000-word records on the 4 output tapes.

Input data allow the user to specify just what records are to be demultiplexed in this way, by listing in a two-entry table the first and last records to be demultiplexed in each section. For the data card [N=4, Record (1) = 2, 4, 6, 6, Recnum = 590*], records 2 through 4 would be demultiplexed as one segment, a file mark inserted on each output tape, and then record 6 would be demultiplexed. N specifies the length of this input table, and the program stops when it has completed the table or when it has read in 590 (Recnum) records. As noted a file mark is inserted between each segment on the output tapes and two marks are placed at the end.

The main program is written in MAD language and handles the tasks of finding which records to demultiplex, and skipping, rewinding, and writing file marks on tape. The RDTAPE routine described previously does the tape reading for the program, and a subroutine called DMULT does the unpacking and writing on tape for each record.

APPENDIX C

SUPPLEMENTARY DATA

C. 1 ADDITIONAL DATA FOR SIGNAL DISTRIBUTION

Additional curves for the signal distribution for the data taken are given in Figs. 28-31. These plots compare the cumulative distribution of the experimental data with the theoretical Rayleigh curve for single-channel plots. (Figures 12 and 13 show corresponding curves for the TPO/3 case.) In the Rayleigh distribution the only independent parameter is the variance σ. The mean $\bar{x}$ of a Rayleigh distribution is $\sqrt{\pi/2}\,\sigma$. In taking measurements, we measure both the mean and variance of the signal strength. If the distribution is Rayleigh, the ratio of the experimental mean to the variance should be 1.25. In some instances the mean-to-variance ratio of the data was not 1.25. For these cases, since it is not known which measurement, $\bar{x}$ or σ, of the data is the closest to the true theoretical values, the data were compared to the theoretical Rayleigh by using the experimental σ as a normalizing factor and also $\bar{x}/1.25$ as a normalizing factor.

It may be noted that the form in which the data were plotted in Fig. 10 is probably the truest form since by plotting the abscissa as db relative to the mean, one reduces those errors which are due to an offset mean.

One source of error in all of these curves (including the ones in Fig. 10) lies in the calibration of the channels. The calibration procedures for all the channels have now been improved for future data. In addition, it must be remembered that theoretical reasons for these curves departing from true Rayleigh are: (1) selective fading, and (2) fading due to airplanes.

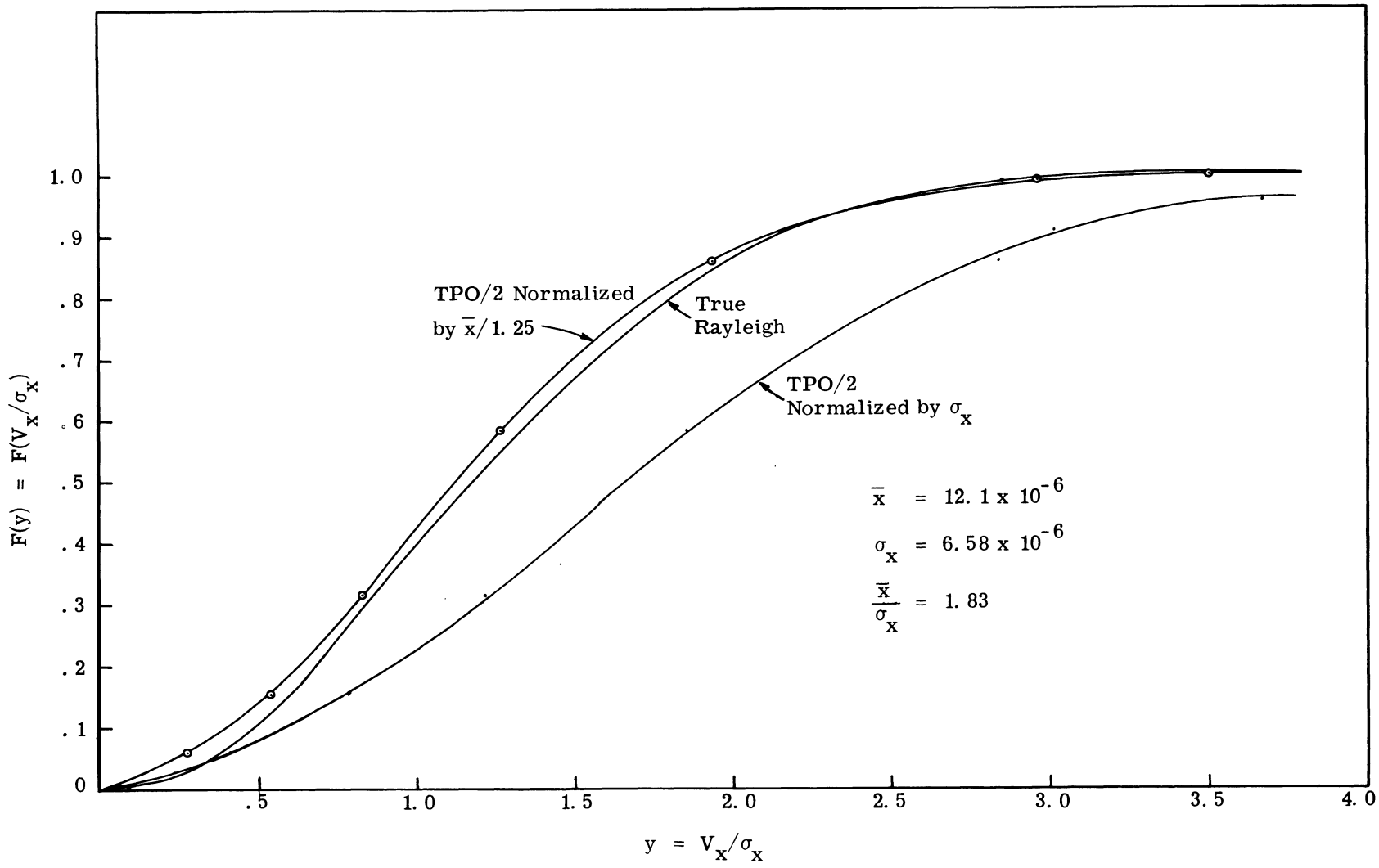

Fig. 28. Comparison of TPO/2 Channel A with Rayleigh distribution.

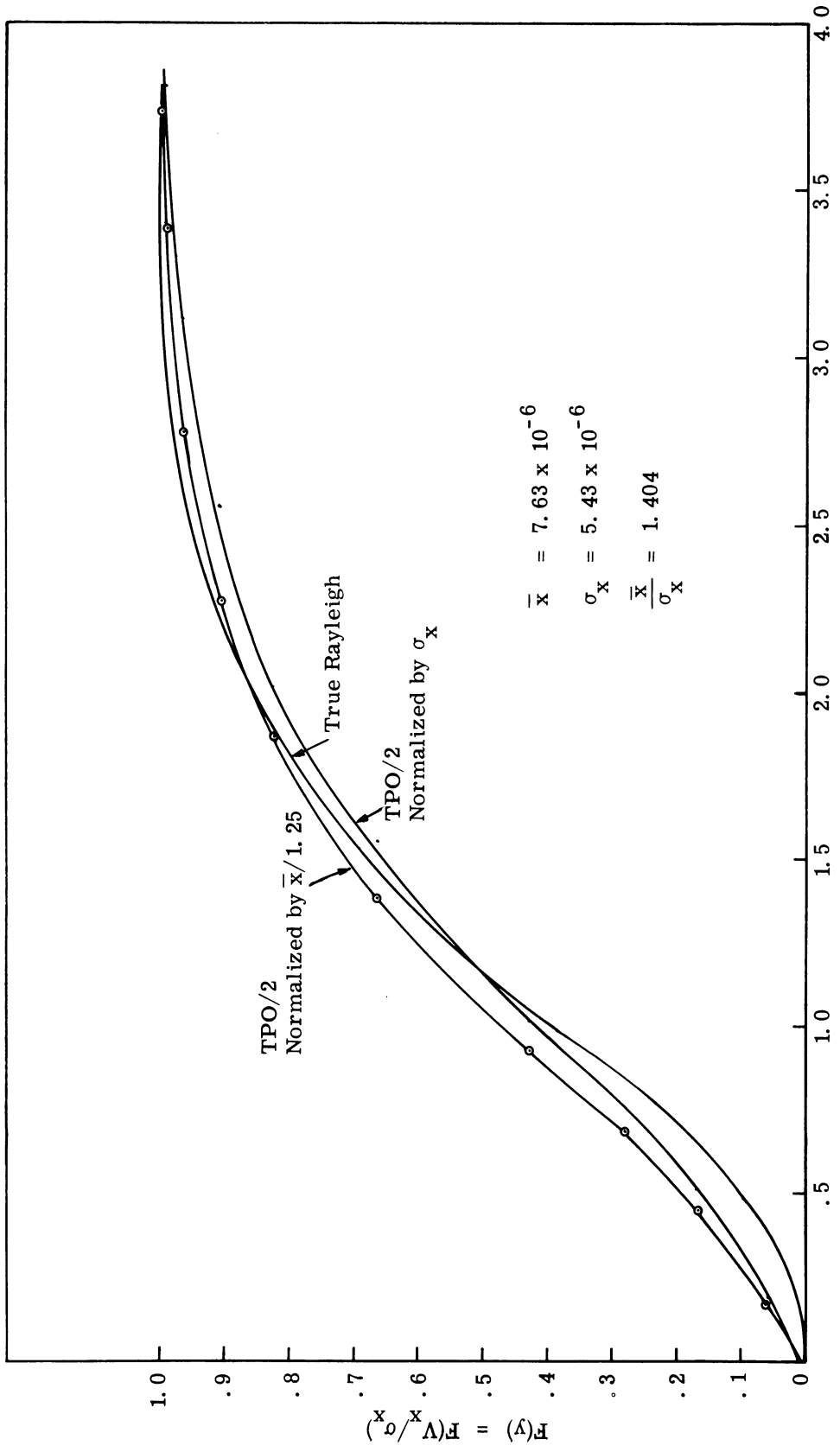

Fig. 29. Comparison of TPO/2 Channel B with Rayleigh distribution.

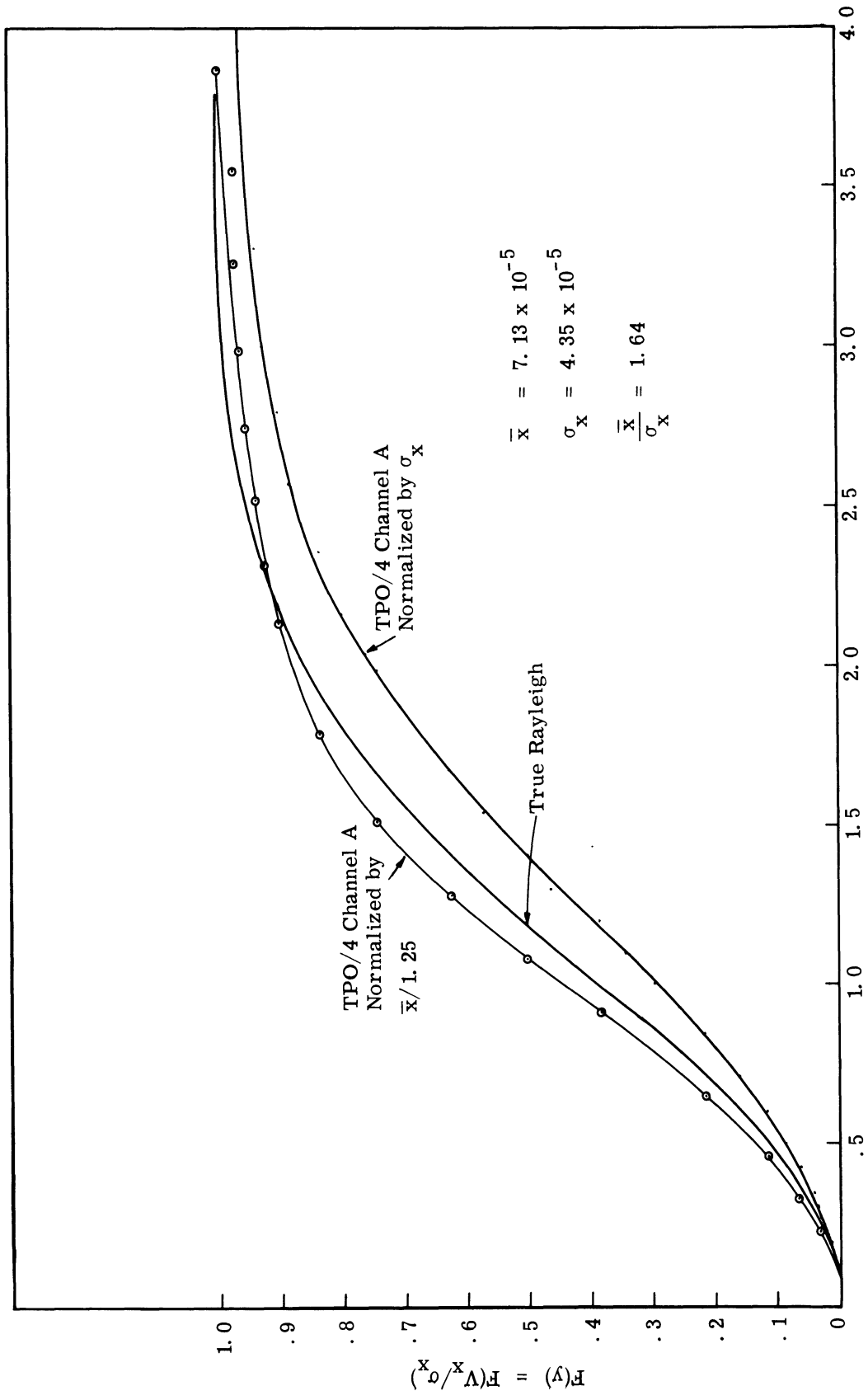

Fig. 30. Comparison of TPO/4 Channel A to Rayleigh distribution.

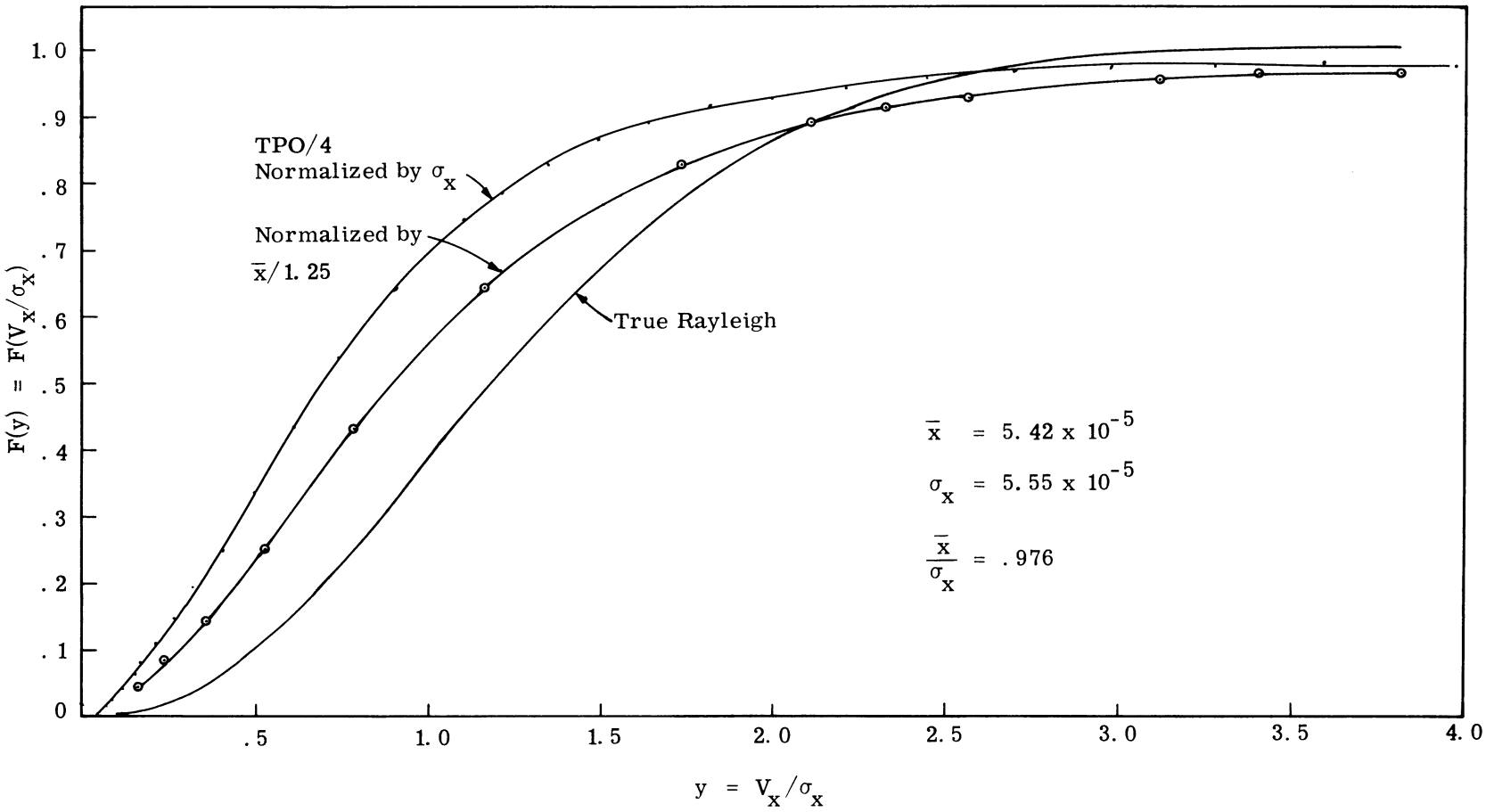

Fig. 31. Comparison of TPO/4 Channel B to Rayleigh distribution.

C. 2 ADDITIONAL DATA ON THE FADING BANDWIDTH

As noted in Ref. 11 the number of crossings at a given signal level can be determined from the theory of random noise if the probability distribution of the signal is known.

For a signal with a Rayleigh distribution and a Gaussian power spectrum with standard deviation σ, the number of one-way crossings per second is given by

$$N(E) = (8\pi \ell n 2)^{\frac{1}{2}} \sigma \left(\frac{E}{E_m}\right) \exp \left[-(\ell n 2) \left(\frac{E}{E_m}\right)^2\right] \qquad (C. 1)$$

where:

E is the signal level in volts

E_m is the mean signal level in volts

σ is the standard deviation of the Gaussian spectrum.

Given the experimental number of one-way crossings at a particular level, Eq. C. 1 can be solved for the standard deviation of the spectrum σ. Reference 12 notes that the bandwidth f_b of a flat power spectrum equivalent to the Gaussian spectrum with standard deviation σ is

$$f_b = \frac{1.25\ \sigma}{2\pi} \qquad (C. 2)$$

where f_b is in cycles per second and σ is in radians per second.

For tapes TPO/2 and TPO/4 the number of one-way crossings were recorded at two levels for both Channel A and Channel B. This results in two separate calculations of f_b for each channel and tape. In Table III, only the results of the lower threshold of tapes TPO/2 and TPO/4 are presented. Table VI gives all eight calculations. As noted earlier, if some of the crossings due to extremely short fades are eliminated by extrapolation of the number of fades versus fade length curve, new calculations of f_b can be made. Using these new experimental values, we obtained the last column of Tables III and VI.

C. 3 ADDITIONAL TABLES AND COMPUTER PRINT-OUT

Additional tables are presented which summarize the error run results. Table VII is a summary of the error-free runs for tape TPO/2 while Table VIII is a summary of error run results for TPO/2. Tables IX and X are summaries of TPO/3 while Tables XI

Table VI. Bandwidth of the fading signal.

Channel	Level Below Mean (db)	N(E)	Experimental Crossings per Second	f_b	f_b'
TPO/2A	-22.6	0.324 σ	23.1	14.2	1.71
TPO/2A	-10.8	1.18 σ	124.5	21.0	1.7
TPO/4A	-21.0	0.361 σ	18.2	10.05	1.32
TPO/4A	- 7.7	1.67 σ	155.5	18.5	1.48
TPO/2B	-24.5	0.260 σ	37.0	28.5	1.92
TPO/2B	-10.2	1.22 σ	139.5	22.9	1.77
TPO/4B	-24.0	0.247 σ	25.2	20.3	2.1
TPO/4B	-10.0	1.21 σ	133.0	21.8	2.43

and XII are summaries of tape TPO/4. Following these six tables are samples of the computer print-out of a time analysis of the error runs. The first sheet gives a table where horizontally the scale is a logarithmic scale of frames and vertically (beginning at the top) is a sequence scale indicating the order in which the runs occurred. Each star (*) represents an error-free run and each x an error run. The distance of the symbols from the left border indicates the length of the error or error-free run. The second computer print-out gives the exact length of the error or error-free run. The first two columns of this print-out correspond to the print-out on the preceding page. Finally, in Table XIII an overall summary of the data is presented. In this table the values are recorded as measured. The quantities were sometimes rounded off in the text because of the inaccuracies in the calibration curves. The starred quantities in Table XIII represent approximate values since the validity of the calibration curves was questioned for the combined signal.

Table VII. Error-free runs over-all for tape TPO/2.

Max. No. in Run	Tally	Percent	Cumulative Tally	Percent
1	273	28. 14	970	100. 00
2	142	14. 64	697	71. 86
5	197	20. 31	555	57. 22
10	117	12. 06	358	36. 91
30	109	11. 24	241	24. 85
100	52	5. 36	132	13. 61
300	13	1. 34	80	8. 25
1000	2	0. 21	67	6. 91
3000	2	0. 21	65	6. 70
10000	14	1. 44	63	6. 49
30000	9	0. 93	49	5. 05
100000	29	2. 99	40	4. 12
300000	11	1. 13	11	1. 13
1000000	0	0. 00	0	0. 00
3000000	0	0. 00	0	0. 00
10000000	0	0. 00	0	0. 00
30000000	0	0. 00	0	0. 00

Table VIII. Error runs over-all for tape TPO/2.

Max. No. in Run	Tally	Percent	Cumulative Tally	Percent	Total Errors	Avg. Error Frame
1	608	62. 75	969	100. 00	1922	3. 16
2	141	14. 55	361	37. 25	1162	4. 12
5	135	13. 93	220	22. 70	2418	5. 12
10	49	5. 06	85	8. 77	2144	5. 85
20	17	1. 75	36	3. 72	1659	6. 50
50	11	1. 14	19	1. 96	3269	8. 48
100	3	0. 31	8	0. 83	1798	8. 00
200	2	0. 21	5	0. 52	3390	11. 30
500	3	0. 31	3	0. 31	11929	11. 37
1000	0	0. 00	0	0. 00	0	---

Table IX. Error-free runs over-all for tape TPO/3.

Max. No. in Run	Tally	Percent	Cumulative Tally	Percent
1	3634	33.38	10887	100.00
2	1628	14.95	7253	66.62
5	2245	20.62	5625	51.67
10	1297	11.91	3380	31.05
30	1074	9.86	2083	19.13
100	368	3.38	1009	9.27
300	108	0.99	641	5.89
1000	147	1.35	533	4.90
3000	92	0.85	386	3.55
10000	93	0.85	294	2.70
30000	126	1.16	201	1.85
100000	73	0.67	75	0.69
300000	2	0.02	2	0.02
1000000	0	0.00	0	0.00
3000000	0	0.00	0	0.00
10000000	0	0.00	0	0.00
30000000	0	0.00	0	0.00

Table X. Error runs over-all for tape TPO/3.

Max. No. in Run	Tally	Percent	Cumulative Tally	Percent
1	4384	40.27	10886	100.00
2	2408	22.12	6502	59.73
5	2140	19.66	4094	37.61
10	841	7.73	1954	17.95
20	443	4.07	1113	10.22
50	316	2.90	670	6.15
100	146	1.34	354	3.25
200	92	0.85	208	1.91
500	77	0.71	116	1.07
1000	39	0.36	39	0.36

Table XI. Error-free runs over-all for tape TPO/4.

Max. No. in Run	Tally	Percent	Cumulative Tally	Percent
1	39	27. 46	142	100. 00
2	21	14. 79	103	72. 54
5	23	16. 20	82	57. 75
10	12	8. 45	59	41. 55
30	10	7. 04	47	33. 10
100	5	3. 52	37	26. 06
300	1	0. 70	32	22. 54
1000	2	1. 41	31	21. 83
3000	1	0. 70	29	20. 42
10000	3	2. 11	28	19. 72
30000	3	2. 11	25	17. 61
100000	10	7. 04	22	15. 49
300000	9	6. 34	12	8. 45
1000000	3	2. 11	3	2. 11
3000000	0	0. 00	0	0. 00
10000000	0	0. 00	0	0. 00
30000000	0	0. 00	0	0. 00

Table XII. Error runs over-all for tape TPO/4.

Max. No. in Run	Tally	Percent	Cumulative Tally	Percent	Total Errors	Avg. Error/ Frame
1	77	54. 61	141	100. 00	402	5. 22
2	34	24. 11	64	45. 39	430	6. 33
5	17	12. 06	30	21. 28	410	6. 9
10	2	1. 42	13	9. 22	144	7. 6
20	7	4. 96	11	7. 80	1450	13. 8
50	2	1. 42	4	2. 84	1274	18. 2
100	1	0. 71	2	1. 42	798	10. 65
200	1	0. 71	1	0. 71	1861	12. 4
500	0	0. 00	0	0. 00	0	---
1000	0	0. 00	0	0. 00	0	---

Table XIII. Over-all summary.

Description	TPO/2 Dual Diversity Parametrics Off	TPO/3 Single Channel Parametrics On	TPO/4 Dual Diversity Parametrics On
Estimated time airplane interference	2 percent	17 percent	28 percent
Mean signal strength above FM threshold	12 db	15 db	20 db
Signal strength Channel A	-80 dbm		-81 dbm
Signal strength Channel B	-84 dbm	-84.4 dbm	-83 dbm
Experimental error count	38,000	1,100,000	7000
Computer error count	29,000	920,000	6788
Probability of bit error	1.5×10^{-4}	4.7×10^{-3}	3.43×10^{-5}
Total frames in error	3,689	121,079	596
Number of fades/sec below threshold level Channel A	-10.8 db -22.6 db 124.5 23.1		-7.7 db -21 db 155.5 18.2
Number of fades/sec below threshold level Channel B	-10.2 db -24.5 db 139.5 37.0		-10 db -24 db 133 25.2
Average length of fade Channel A	-10.8 db -22.6 db 3.0 ms 0.16 ms		-7.7 db -21 db 1.39 ms 0.823 ms
Average length of fade Channel B	-10.2 db -24.5 db 4.92 ms 0.186 ms		-10 db -24 db 1.757 1.09 ms
Total number of error runs	969	10886	147
Average error run length	0.407 ms	1.16 ms	0.426 ms
Approximate fading bandwidth Channel A	17.6 cps		14.2 cps
Approximate fading bandwidth Channel B	21.6 cps		21.1 cps
Fading bandwidth eliminating short fades Channel A	1.7 cps		1.40 cps
Fading bandwidth eliminating short fades Channel B	1.84 cps		2.26 cps

APPENDIX D

THEORETICAL PREDICTION OF FADE LENGTHS FOR AN EQUAL-GAIN DIVERSITY FLAT RAYLEIGH FADING TROPOSCATTER RECEIVER

K. A. Haines

D. 1 INTRODUCTION

In Technical Report No. 143 of this laboratory (Ref. 2, Section 2. 3. 2), fade probabilities for an equal-gain diversity system were calculated. In Section D. 3 of this appendix a more theoretically rigorous approach is presented. This approach results in an equal-gain diversity system which is less susceptible to fade than the switched diversity system. This is not surprising since the signal-to-noise ratio increases by 3 db for the equal-gain system. This result agrees with the situation where loss of synchronization is not a problem (and one considers the errors during a fade), where it is found that equal-gain diversity is slightly better than the switched diversity. It is felt that the curves presented in Figs. 35 and 36 of this appendix are more accurate than Figs. 43 and 44 of Ref. 2.

In order to demonstrate the applicability of this theoretical method, some statistical preliminaries are presented in Section D. 2. Section D. 3 derives the final results presented in Figs. 35 and 36.

D. 2 STATISTICAL PRELIMINARIES

The following analysis is included in order to determine the rate at which independent samples occur in a process which is the sum of two independent Rayleigh processes.

The independence of samples of a Gaussian process is adequately described in several texts, and the basic theoretical steps are outlined in Section D. 2. 1. In Section D. 2. 2, the derivation of the Rayleigh process from a narrowband Gaussian process is given. The rate at which independent samples occur for the Rayleigh is determined using the analysis of Sections D. 2. 1 and D. 2. 2. It is then a simple matter to extend the analysis to the sum of two Rayleigh processes as in Section D. 2. 4.

D. 2. 1 Independent Sample Rate for a Gaussian Process

If two random variables, y_1 and y_2, have a joint distribution function given by (Ref. 13):

$$p(y_1, y_2) = \frac{1}{2\pi \sigma_1 \sigma_2 (1-\rho^2)^{\frac{1}{2}}}$$

$$\exp\left[\frac{-\sigma_2^2(y_1 - m_1)^2 - 2\sigma_1\sigma_2\,\rho(y_1 - m_1)(y_2 - m_2) + \sigma_1^2(y_2 - m_2)^2}{2\sigma_1^2\,\sigma_2^2(1-\rho^2)}\right] \qquad \text{(D. 1)}$$

where:

σ_1 is the standard deviation of y_1,

σ_2 is the standard deviation of y_2,

m_1 is the mean value of y_1,

m_2 is the mean value of y_2, and

ρ is the correlation coefficient defined by

$$\frac{E[(y_1 - m_1)(y_2 - m_2)]}{\sigma_1 \sigma_2} \quad ,$$

they they are said to have a bivariate Gaussian probability density function. In this case, if the correlation coefficient ρ is zero, y_1 is independent of y_2 since $p(y_1 y_2) = p(y_1)\,p(y_2)$. This same description may be applied to an N variable system in which the joint probability density function of the variables y_n is given by (Ref. 13, p. 152):

$$p(y_1, \ldots, y_N) = \frac{1}{(2\pi)^{N/2}\,|\Lambda|^{1/2}}$$

$$\exp\left[-\frac{1}{2|\Lambda|}\sum_{n=1}^{N}\sum_{m=1}^{N}|\Lambda|_{nm}(y_n - m_n)(y_m - m_m)\right] \quad , \qquad \text{(D. 2)}$$

where Λ is the covariance matrix of elements λ_{nm},

where:

$\lambda_{nm} = E[(y_n - m_n)(y_m - m_m)]$,

$|\Lambda|$ is the determinant of Λ, and

m_n and m_m are mean values of y_n and y_m.

Thus, if these N random variables are uncorrelated, they are also independent. We should here note that an often quoted incorrect statement in the case of Gaussian random variables

is, "If N Gaussian random variables are all uncorrelated, they are also statistically independent." In order for this statement to be absolutely true, the additional condition that "the joint probability of these N random variables is multivariate Gaussian (as defined by Eq. D. 2)" must also hold.

A Gaussian random process is defined as a process for which the random variables, $x_{t_1}, \ldots, x_{t_N}$, corresponding to time $t_1, \ldots, t_N$, have a joint Gaussian distribution function which is identical to Eq. D. 2 with $y_1, \ldots, y_N$ replaced by $x_{t_1}, \ldots, x_{t_N}$. It therefore follows that independent samples occur for a Gaussian random process at intervals in which the correlation matrix Λ reduces to the identity matrix times a constant. This occurs when all elements λ_{nm} are zero for all n and m. We will therefore examine the general term $\lambda_{nm} = E[(y_{t_n} - m_{t_n})(y_{t_m} - m_{t_m})]$ where t_n will be redefined as $t_n + \Delta ta$ where $a = 1, 2, 3, \ldots$. If a Δt exists such that this general λ_{nm} goes to zero for all a, then this Δt is the time inter-

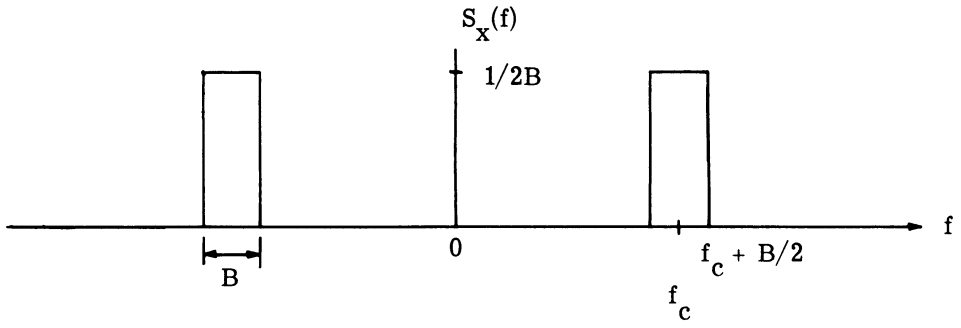

Fig. 32. Spectral density of Gaussian process

val between successive independent samples of the process. We are here considering a Gaussian random process in which the spectral power density S(f) is uniform from -B to B cycles per second as shown in Fig. 32. The correlation function λ_{nm} is

$$R(a\Delta t) = \int_{-\infty}^{\infty} S(f)\, e^{j\omega\tau}\, df \qquad (D.\ 3)$$

$$= \frac{2}{2B} \int_{-B/2}^{B/2} e^{j2\pi f \Delta ta}\, df$$

$$= \frac{\sin \pi B \Delta ta}{2\pi B \Delta ta} \ . \qquad (D.\ 4)$$

This correlation function goes to zero for every a when $\Delta t = 1/B$, and independent samples therefore occur every 1/B seconds for this Gaussian process.

D. 2. 2 Derivation of the Rayleigh

It is well known that the Rayleigh distribution may be derived from a narrowband Gaussian process (Ref. 14). The spectral density for the Gaussian process considered here is shown in Fig. 32.

Denote this narrowband Gaussian process as

$$\mathbf{X}(t) = V(t) \cos [\omega_c t + \phi(t)] , \tag{D. 5}$$

$$= x_c(t) \cos \omega_c(t) - x_s(t) \sin \omega_c t , \tag{D. 6}$$

where:

$$V(t)^2 = x_c(t)^2 + \mathbf{X}_s(t)^2 . \tag{D. 7}$$

Then it may be shown that

$$p(x_c, x_s) = p(x_c)\, p(x_s) = \frac{1}{2\pi\, \sigma_x^{\,2}} \exp \left[- \frac{x_c^{\,2} + x_s^{\,2}}{2\sigma^2} \right] , \tag{D. 8}$$

where:

$$\sigma_x^{\,2} = \langle x_c(t)^2 \rangle = \langle x_s(t)^2 \rangle ,$$

i. e. , $x_c(t)$ and $x_s(t)$ are independent random processes with identical Gaussian distribution functions. By a change of variables,

$$p[V(t), \phi(t)] = \begin{cases} \dfrac{V(t)}{2\pi\sigma_x^{\,2}} \exp \left[- \dfrac{V(t)^2}{\sigma_x^{\,2}} \right] & \text{for } V(t) \geq 0 \\ 0 , \text{ otherwise.} \end{cases} \tag{D. 9}$$

Integrating over ϕ, which is uniformly distributed from 0 to 2π, we get the distribution function for the envelope of x(t) as,

$$p[V(T)] = \begin{cases} \dfrac{V(t)}{\sigma_x^2} \exp\left[-\dfrac{V(t)^2}{2\sigma_x^2}\right] & \text{for } V(t) \geq 0 \\ 0\,, \quad \text{otherwise,} \end{cases} \tag{D. 10}$$

which is the Rayleigh distribution function.

D. 2. 3 Independent Sample Rate of a Rayleigh Distributed Random Process

In this section we wish to find the time interval, τ, between successive independent samples in a Rayleigh process. We thus wish to find τ for which

$$p[x_s(t),\ x_s(t+\tau),\ x_c(t),\ x_c(t+\tau)] = p[x_s(t)]\ p[x_s(t+\tau)]\ p[x_c(t)]\ p[x_c(t+\tau)]\ . \tag{D. 11}$$

The process $x_s(t)$ is a Gaussian process and thus $p[x_s(t),\ x_s(t+\tau)]$ is a bivariate distribution. This is also true for $p[x_c(t),\ x_c(t+\tau)]$, and since $x_c(t)$ is independent of $x_s(t)$, one then gets the following four-dimensional multivariable distribution:

$$p[x_c(t),\ x_s(t),\ x_c(t+\tau),\ x_s(t+\tau)]$$

$$= \frac{1}{4\pi^2\,|\Lambda|^{\frac{1}{2}}} \exp\left\{-\frac{1}{2|\Lambda|}\sum_{n=1}^{2}\sum_{m=1}^{2}|\Lambda|_{nm}\,x_n\,x_m\right\}\ , \tag{D. 12}$$

where the covariance matrix is

$$\Lambda = \begin{Vmatrix} \sigma_x^2 & 0 & R_c(\tau) & R_{cs}(\tau) \\ 0 & \sigma_x^2 & -R_{cs}(\tau) & R_c(\tau) \\ R_c(\tau) & -R_{cs}(\tau) & \sigma_x^2 & 0 \\ R_{cs}(\tau) & R_c(\tau) & 0 & \sigma_x^2 \end{Vmatrix}\ . \tag{D. 13}$$

$R_s(\tau) = R_c(\tau) = E[x_c(t),\ x_c(t+\tau)]$ reduces after some algebra (Ref. 13, p. 162) to

$$R_c(\tau) = 2\int_0^\infty s_x(f)\cos 2\pi(f-f_c)\tau\ df\ ,$$

$$= 0 \text{ when } \tau = \frac{1}{B}\,,\ \frac{2}{B}\,,\ \ldots \text{ etc. for the} \tag{D. 14}$$

spectral density of Fig. 32.

Similarly,

$$R_{cs}(\tau) = 2\int_0^\infty s_x(f)\sin 2\pi(f-f_c)\tau \; df$$

$$= 0 \text{ for any } \tau \text{ and for the spectral density of Fig. 32.} \qquad \text{(D. 15)}$$

Equation D. 12 may be rewritten as:

$$p[x_c(t),\, x_s(t),\, x_c(t+\tau),\, x_s(t+\tau)] = \frac{1}{4\pi^2\,|\Lambda|^{\frac{1}{2}}}$$

$$\exp\left\{-\frac{1}{2|\Lambda|^{\frac{1}{2}}}\begin{vmatrix} \sigma_x^2[x_c(t)^2 + x_s(t)^2 + x_c(t+\tau)^2 + x_s(t+\tau)^2] \\ -2R_c(\tau)\,[x_c(t)\,x_c(t+\tau) + x_s(t)\,x_s(t+\tau)] \\ -2R_{cs}(\tau)\,[x_c(t)\,x_s(t+\tau) - x_s(t)\,x_c(t+\tau)] \end{vmatrix}\right\} . \qquad \text{(D. 16)}$$

By changing variables to V(t), $\phi(t)$, V(t+τ), and $\phi(t+\tau)$, and integrating over $\phi(t)$ and $\phi(t+\tau)$, both of which are uniformly distributed from 0 to 2π, we obtain (Ref. 13, p. 163)

$$p(V_1,V_2) = \begin{cases} \dfrac{V_1V_2}{|\Lambda|^{\frac{1}{2}}}\; I_o\left\{\dfrac{V_1V_2[R_c^{\,2}(\tau) + R_{cs}^{\,2}(\tau)]^{\frac{1}{2}}}{|\Lambda|^{\frac{1}{2}}}\right\} \exp\left[-\dfrac{\sigma_x^{\,2}(V_1^{\,2}+V_2^{\,2})}{2|\Lambda|^{\frac{1}{2}}}\right] \\ \qquad\qquad \text{when } V_1, V_2 \geqq 0\ , \\ 0\ , \text{ otherwise}\ . \end{cases} \qquad \text{(D. 17)}$$

From this equation, it is obvious that using the spectral density of Fig. 32 for the random process from which the Rayleigh was derived, $p(V_1,V_2)$ for $\tau = 0, \frac{1}{B}, \frac{2}{B}, \ldots$ etc., is given by:

$$p(V_1,V_2) = p(V_1)\,p(V_2) = \frac{V_1V_2}{|\Lambda|^{\frac{1}{2}}}\exp\left[-\frac{\sigma_x^{\,2}(V_1^{\,2}+V_2^{\,2})}{2|\Lambda|^{\frac{1}{2}}}\right] , \qquad \text{(D. 18)}$$

and thus independent Rayleigh samples occur at intervals separated by $\frac{1}{B}$ in time. It has therefore been shown that independent samples occur at exactly the same rate as for the limiting Gaussian random process from which the Rayleigh was derived.

D. 2. 4 Independent Sample Rate for the Sum of Two Independent Rayleigh Processes

We wish to investigate here those values of τ for which

$$p\left\{[V_1(t) + V_2(t)],\ [V_1(t+\tau) + V_2(t+\tau)]\right\} = p[V_1(t) + V_2(t)]\ p[V_1(t+\tau) + V_2(t+\tau)] .$$

We may write

$$p\left\{[V_1(t) + V_2(t)],\ [V_1(t+\tau) + V_2(t+\tau)]\right\} = p[V_1(t) + V_2(t)]\ p_{V_1(t)+V_2(t)}$$

$$[V_1(t+\tau) + V_2(t+\tau)] . \qquad \text{(D. 19)}$$

From Section D. 2. 3, we know that for $\tau = \frac{1}{B}, \frac{2}{B}, \ldots$ etc., $V_1(t)$ is independent of $V_1(t+\tau)$ and $V_2(t)$ is independent of $V_2(t+\tau)$. Also, $V_1(t)$ and $V_2(t)$ are independent processes. Therefore, $p_{V_1(t)+V_2(t)}[V_1(t+\tau) + V_2(t+\tau)] = p[V_1(t+\tau) + V_2(t+\tau)]$ for $\tau = \frac{1}{B}, \frac{2}{B}, \ldots$ etc., and the sum of two independent Rayleigh processes have independent samples at intervals spaced $\frac{1}{B}$ apart in time, when the spectral density of the random process from which the Rayleighs are derived is uniform as shown in Fig. 32.

D. 2. 5 Spectral Density of the Rayleigh Process

We will assume here that the Rayleigh process is derived from a narrowband Gaussian process. If such a Gaussian process is applied to the input of a half-wave linear rectifier in tandem with a lowpass filter, the filter output will be the envelope of the Gaussian process, i. e. , the Rayleigh process. The correlation function of the output of the linear rectifier is (Ref. 13, p. 270):

$$R_y(\tau) = \frac{\sigma_x^2}{2\pi} + \frac{1}{4} R_x(\tau) + \frac{1}{4\pi\sigma_x^2} R_x^2(\tau) + \frac{1}{48\pi\sigma_x^4} R_x^4(\tau) \qquad \text{(D. 20)}$$

$$+ \text{ (other less significant terms)} .$$

The spectral density of this rectifier output is then,

$$S_y(f) = \frac{\sigma_x^2}{2\pi}\,\delta(f) + \frac{1S_x(f)}{4} + \frac{1}{4\pi\,\sigma_x^2}\,{}_2S_x(f)$$

$$+ \frac{1}{48\pi\,\sigma_x^4}\int_{-\infty}^{\infty} {}_2S_x(f')\,{}_2S_x(f-f')\,dx \qquad \text{(D. 21)}$$

$$+ \text{(insignificant terms)}\ ,$$

where $S_x(f)$ is the spectral density of the input noise, and

$${}_2S_x(f) = \int_{-\infty}^{\infty} S_x(f')\,S_x(f-f')\,df' \ . \qquad \text{(D. 22)}$$

If $S_x(f)$ is as indicated in Fig. 32, the lower frequency portions of ${}_2S_x(f)$ are shown in Fig. 33(a).

The resulting lower frequency spectrum of $\int_{-\infty}^{\infty} {}_2S_x(f')\,{}_2S_x(f-f')\,df'$ is shown in Fig. 33(b). Note that $\sigma_x^2 = 1$ for the spectrum of Fig. 32. The resulting spectral density of the lowpass filter output is then the central peak of the spectral density of Fig. 33(a), plus the central peak of Fig. 33(b), plus the impulse at dc whose area $= \frac{1}{2\pi}$.

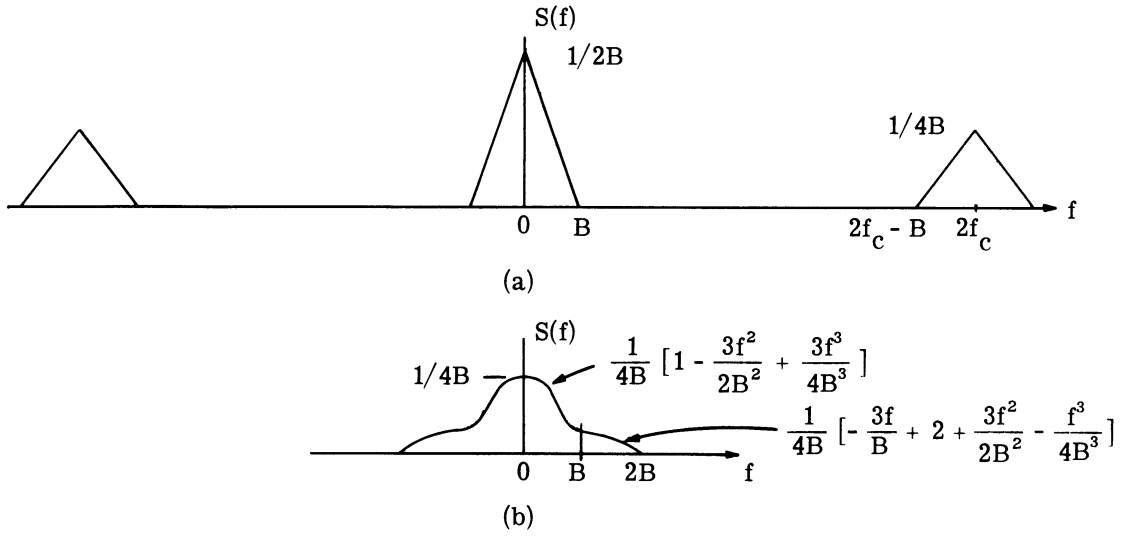

Fig. 33. Spectral components of Rayleigh process.

If this spectral density is accurate enough [i. e., if cutting off the series for $R_y(\tau)$ at the fourth term was accurate enough], the ratio of the ac power to the dc power should be approximately equivalent to the ratio of the ac power to the dc power in a Rayleigh

process. This ratio for the Rayleigh process is

$$\frac{P_{ac}}{P_{dc}} = \frac{\overline{R^2} - \overline{R}^2}{\overline{R}^2} = \frac{2\sigma^2 - \frac{\pi}{2}\sigma^2}{\frac{\pi}{2}\sigma^2} = 0.274 \ . \tag{D. 23}$$

Now we will calculate this ratio for the system output. The integral of the central peak of $S_x(f)$ in Fig. 33(a) is $\frac{1}{2}$. The integral of the central peak of ${}_2S_x(f)$ in Fig. 33(b) is $\frac{3}{8}$. Thus, the total ac power is

$$P_{ac} = \frac{1}{4\pi} R^2{}_x(0) + \frac{1}{48\pi} R^4{}_x(0) = \frac{1}{4\pi}\left(\frac{1}{2}\right) + \frac{1}{48\pi}\left(\frac{3}{8}\right) = \frac{1}{2\pi}(0.2656) \ . \tag{D. 24}$$

The dc power is, of course, the area of the impulse at zero frequency, and is given by

$$P_{dc} = \frac{1}{2\pi} \ . \tag{D. 25}$$

Thus the ratio of the ac to dc power is

$$\frac{P_{ac}}{P_{dc}} = 0.266 \ . \tag{D. 26}$$

This ratio is within 3 percent of the correct value of 0. 274. Hence, the combined spectral densities of Figs. 33(a, b), and the impulse function at zero frequency is deemed adequate to represent the process.

D. 3 METHOD OF ANALYSIS

Assume that the Rayleigh process, which describes the fading for a troposcatter link, has a spectral density not too different from that discussed above. It then has independent samples spaced at intervals of $\frac{1}{B}$ seconds, based on the analysis of Section D. 2. 3. For the equal-gain receiver then, independent samples also occur at intervals of $\frac{1}{B}$ as shown in Section D. 2. 4.

Let $P'_{1,2}(0)$ be the probability of a critical fade in an independent sample time of $\frac{1}{B}$. If this probability is small, then the probability of one or more critical fades in a time T is given by (Ref. 2, p. 72)

$$P(BT, Bt_0, k) \cong 1 - e^{-P'_{1,2}(0)\,BT} \ , \tag{D. 27}$$

where:

k = fading level (threshold), expressed as a fraction of voltage mean,

t_0 = the duration of a critical fade.

The next step in the analysis is to find an expression for $P'_{1,2}(0)$ in terms of t_0 and k. Consider the following:

Define $P_1\ B \cdot \frac{1}{B},\ Bt,\ k_1$ = probability of one or more fades of length $\geq$ t below the level k_1 in an observation time $\frac{1}{B}$ ($\approx$ probability of 1 fade).

Define $\left.\frac{\partial P_1\ B \cdot \frac{1}{B},\ Bt,\ k_1}{\partial t}\right|_{t_1}$ = probability of one fade of length = t_1 below the level k_1 in an observation time $\frac{1}{B}$ on channel 1, i. e., the occurrence of an event such as in Fig. 34(a).

Define $\left.\frac{\partial P_2(Bt_1,\ Bt,\ k_2)}{\partial t}\right|_{t_0}$ = probability of one fade of length = t_0 below the level k_2 in an observation time t_1 on Channel 2 [i. e., the occurrence of an event such as in Fig. 34(b) in which the observation time is the fade time of Channel 1],

where $k_2 = k - k_1$.

$\left.\frac{\partial P_1(1,\ Bt,\ k_1)}{\partial t}\right|_{t_1} \cdot \left.\frac{\partial P_2(Bt_1,\ Bt,\ k_2)}{\partial t}\right|_{t_0}$ = probability of one fade of length = t_0 for the equal-gain diversity system in an observation time $\frac{1}{B}$, when Channel 2 has a fade of length = t_0 below level k_2.

If we integrate the above expression over k_2, we will have accounted for all cases in which the fade on Channel 2 just causes a system fade. Integrating over k_2 is identical to integrating over k_1 if k is fixed at the system threshold fade level. Next we must integrate over t_1 in order to account for all states of Channel 1 which lead to fades. Thus,

$P'_{1,2}(0)$ = the probability of a fade in observation time $\frac{1}{B}$

$$= \int_{t_1=t_0}^{1/B} \int_{k_2=0}^{k} \left.\frac{\partial P_1(1,\ Bt,\ k_1)}{\partial t}\right|_{t_1} \cdot \left.\frac{\partial P_2(Bt_1,\ Bt,\ k_2)}{\partial t}\right|_{t_0} dk_2\ dt_1 \qquad \text{(D. 28)}$$

$$= \int_{t_1=t_0}^{1/B} \int_{k_1=k}^{0} \left.\frac{\partial P_1(1,\ Bt,\ k_1)}{\partial t}\right|_{t_1} \cdot \left.\frac{\partial P_2(Bt_1,\ Bt,\ k_2)}{\partial t}\right|_{t_0} dk_1\ dt_1 \ .$$

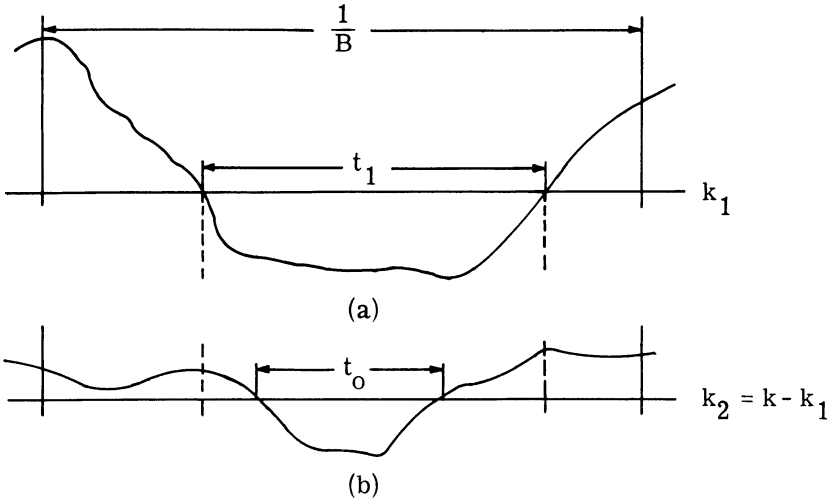

Fig. 34. Signal amplitudes, (a) on channel 1, (b) on channel 2.

Based on Favreau (Ref. 15), we may extract the following four equations for a single channel:

$$P'(0,\ k,\ t_0) = I(k)\ e^{-\frac{t_0 B}{r(k)}} \qquad \text{(D. 29)}$$

$$\log I(k) = 1 \cdot 263 \log k + .361 \qquad \text{(D. 30)}$$

$$r(k) = .0407 + .21\,k \qquad \text{(D. 31)}$$

$$P(BT,\ Bt_0,\ k) = 1 - e^{-P'(0,\ k,\ t_0)\,BT} \qquad \text{(D. 32)}$$

Thus, we may evaluate the double integral in the following manner:

$$\left.\frac{\partial P(1, Bt, k_1)}{\partial t}\right|_{t_1} = \left.\frac{\partial\left[1 - e^{-P'(0, k_1, t)}\right]}{\partial t}\right|_{t_1} , \qquad \text{(D. 33)}$$

$$= -e^{-P'(0,k_1,t_1)} \frac{I(k_1)B}{r(k_1)} e^{-t_1 B/r(k_1)} ,$$

$$\approx \frac{-I(k_1)B}{r(k_1)} e^{-t_1 B/r(k_1)} \quad \text{for small } P'(0,k,t_0) . \tag{D. 34}$$

$$\left.\frac{\partial P_2(Bt_1, Bt, k_2)}{\partial t}\right|_{t_0} = \left.\frac{\partial\left[1 - e^{-Bt_1 P'(0,k_2,t)}\right]}{\partial t}\right|_{t_0} ,$$

$$= -e^{-Bt_1 P'(0,k_2,t_0)} Bt_1 I(k_2) e^{-t_0 B/r(k_2)} \frac{1B}{r(k_2)} , \tag{D. 35}$$

$$\approx \frac{-t_1 I(k_2)}{r(k_2)} B^2 e^{-t_0 B/r(k_2)} \quad \text{for small } P'(0,k,t_0) . \tag{D. 36}$$

$$\int_{t_1=t_0}^{1/B} \int_{k_1=k}^{0} \left.\frac{\partial P_1(1, Bt, k_1)}{\partial t}\right|_{t_1} \cdot \left.\frac{\partial P_2(Bt_1, Bt, k_2)}{\partial t}\right|_{t_0} dk_1\, dt_1$$

$$= B^3 \int_{k_1=1}^{0} \int_{t_1=t_0}^{1/B} \frac{I(k_1) I(k_2)}{r(k_1) r(k_2)} t_1 e^{-t_1 B/r(k_1)} e^{-t_0 B/r(k_2)} dt_1\, dk_1 ,$$

$$= B \int_{k_1=k}^{0} \frac{I(k_1) I(k_2)}{r(k_2)} e^{-t_0 B/r(k_2)} r(k_1)$$

$$\left\{ e^{\frac{1}{r(k_1)}} \left[\frac{1}{r(k_1)} + 1\right] - e^{-t_0 B/r(k_1)} \left[\frac{t_0 B}{r(k_1)} + 1\right] \right\} dk_1 . \tag{D. 37}$$

$$P'_{1,2}(0) = \int_{k_1=k}^{0} \left[\frac{I(k_1)\, I(k-k_1)}{r(k-k_1)} e^{-t_0 B/r(k-k_1)} Br(k_1) \right]$$

$$\left\{ e^{-\frac{1}{r(k_1)}} \left[\frac{1}{r(k_1)} + 1\right] - e^{-t_0 B/r(k-k_1)} \left[\frac{t_0 B}{r(k_1)} + 1\right] \right\} dk_1 . \tag{D. 38}$$

By substituting equations for r(k) and I(k) into the above expressions, we may obtain a computer solution for $P'_{1,2}(0)$. It is then a simple matter to use this resultant $P'_{1,2}(0)$ in Eq. D. 27 to get the fade probability in an observation time T.

The system fade probabilities were evaluated by the above method, for values of $k = 0.05/\sqrt{2}$, and $0.1/\sqrt{2}$, and for $t_0 = .3 \times 10^{-3}$ sec, 2×10^{-3} sec, and 3.75×10^{-3} sec, as a function of T. An equal-gain system k corresponds to a single channel threshold of $k_1/\sqrt{2}$, as explained in Ref. 2, Part 2, Section 2.3. These new curves for the equal-gain diversity system are presented in Figs. 35 and 36. They can be compared to those of Figs. 43 and 44 of Ref. 2. As noted in the introduction, the curves now indicate that the equal-gain diversity system is less susceptible to fade than the switched diversity system.

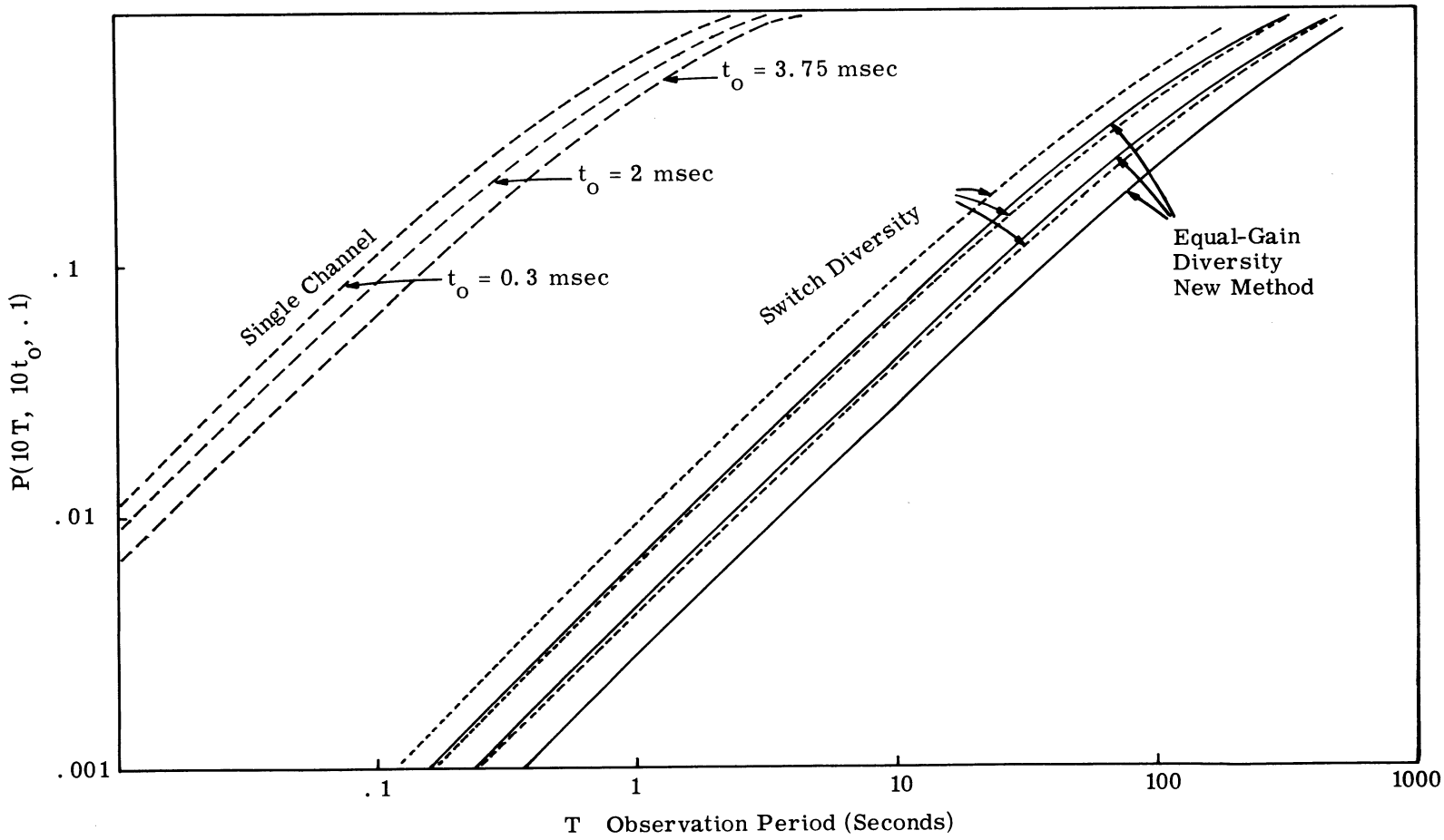

Fig. 35. Fade probability versus observation period.
Threshold ratio k_1 = 0.1

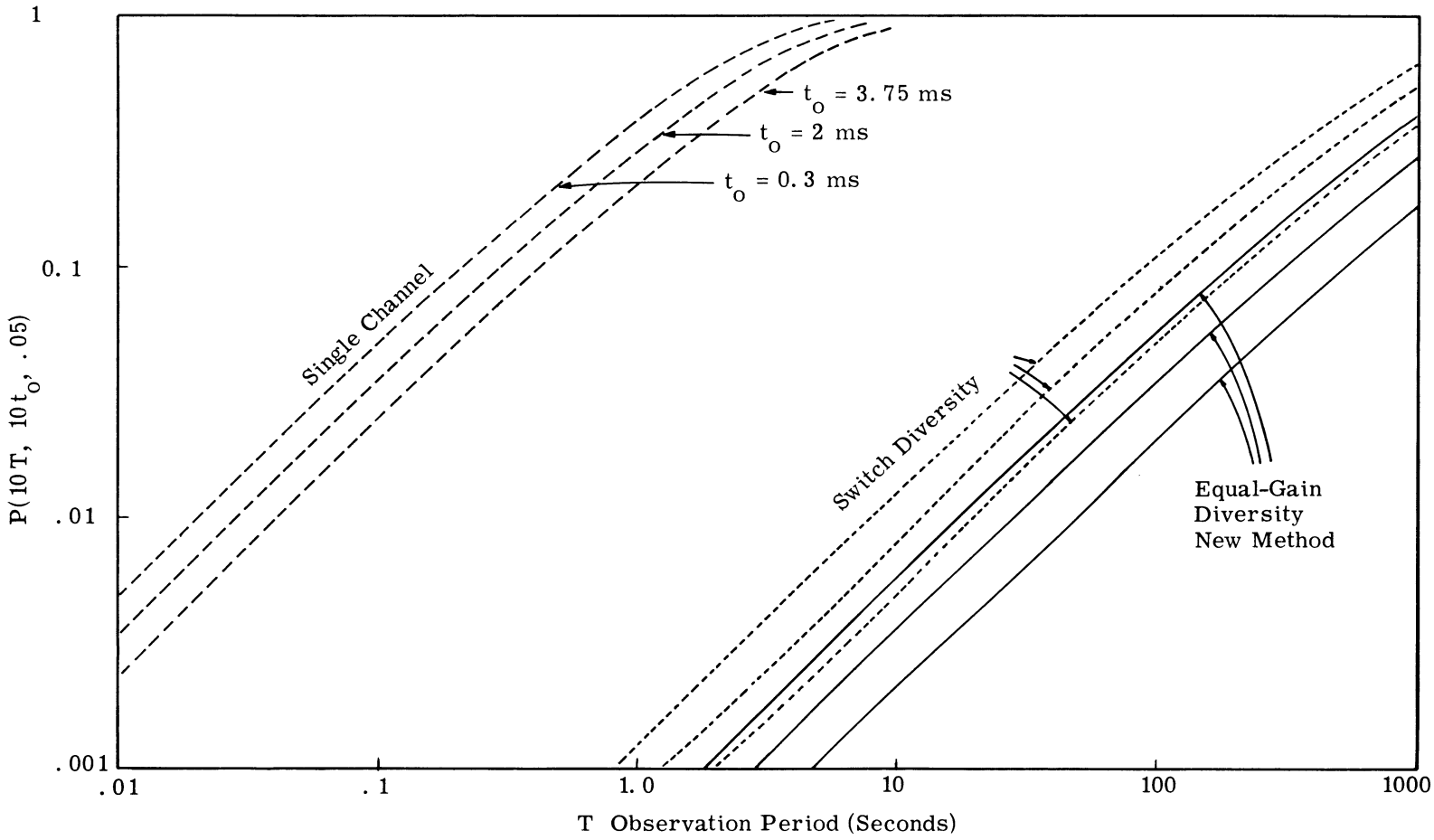

Fig. 36. Fade probability versus observation period.
Threshold ratio $k_1 = .05$

REFERENCES

1. JTAC Report, "Long Range Tropospheric Transmission," Proc. IRE, January 1960, pp. 30-44.

2. M. P. Ristenbatt and K. A. Haines, Digital Communication Studies, Cooley Electronics Laboratory Technical Report No. 143, The University of Michigan, Ann Arbor, Michigan, August 1963.

3. Ground Telecommunication Performance Standards, Tropospheric Systems, NBS Report 6767, June 15, 1961.

4. A. B. Crawford, et al., "Studies in Tropospheric Propagation beyond the Horizon," BSTJ, September 1959, p. 1067.

5. E. D. Sunde, "Digital Troposcatter Transmission and Modulation Theory," BSTJ, No. 1, Part 1, January 1964, p. 143.

6. Private communication with I. Kullback of Radio Relay Branch, Communications Dept., USAEL.

7. A. Tepfer, PCM Troposcatter Error Instrumentation System, RCA Report No. CR-61-419-11, April 28, 1961.

8. Tropospheric Scatter, Principles and Applications, Collins Radio Company, Task Report No. 45-56-0024, March 1960.

9. R. R. Favreau, "Evaluation of Complex Statistical Functions by an Analog Computer," 1956 IRE National Convention Record, Computers.

10. S. W. Rice, "Distribution of the Duration of Fades in Radio Transmission: Gaussian Noise Model," BSTJ, No. 3, May 1958, pp. 581-635.

11. A. B. Crawford, D. C. Hogg and W. H. Kummer, "Studies in Tropospheric Propagation beyond the Horizon," BSTJ, Vol. XXXVIII, No. 5, September 1959.

12. E. D. Sunde, "Digital Troposcatter Transmission and Modulation Theory," BSTJ, Vol. XLIII, No. 1, January 1964.

13. W. B. Davenport, Jr. and W. L. Root, Random Signals and Noise, McGraw-Hill, New York, 1958.

14. J. S. Bendat, Principles and Applications of Random Noise Theory, John Wiley and Sons, New York, 1958.

15. R. R. Favreau, H. Low and I. Pfeffer, "Evaluation of Complex Statistical Functions by an Analog Computer," IRE National Convention Record, Computers, 1956, pp. 31-37.

DISTRIBUTION LIST

	No. Copies
Office of the Assistant Secretary of Defense (Research and Engineering), The Pentagon ATTN: Technical Library, Room 3E1065 Washington 25, D. C.	1
Office of Chief of Research and Development Department of the Army ATTN: CRD/M Washington 25, D. C.	1
Commanding General U. S. Army Materiel Command ATTN: R and D Directorate Washington 25, D. C.	1
Commanding General U. S. Army Electronics Command ATTN: AMSEL-AD Fort Monmouth, New Jersey	1
Commander Defense Documentation Center Cameron Station Alexandria, Virginia	3
Commanding General USA Combat Developments Command ATTN: CDCMR-E Fort Belvoir, Virginia	1
Commanding Officer U. S. Army Combat Developments Command Fort Huachuca, Arizona	1
Commanding General U. S. Army Electronics R and D Activity ATTN: Technical Library Fort Huachuca, Arizona	1
Chief U. S. Army Security Agency Arlington Hall Station Arlington 12, Virginia	1
Deputy President U. S. Army Security Agency Board Arlington Hall Station Arlington 12, Virginia	1
Director, U. S. Naval Research Laboratory ATTN: Code 2027 Washington 25, D. C.	1
Air Force Cambridge Research Laboratories ATTN: CRZC L. G. Hanscom Field Bedford, Massachusetts	1

DISTRIBUTION LIST (Cont.)

	No. Copies
Rome Air Development Center ATTN: RAALD Griffiss Air Force Base, New York	1
U. S. National Bureau of Standards Boulder Laboratories ATTN: Library Boulder, Colorado	1
AFSC Scientific/Technical Liaison Office U. S. Army Electronic Laboratories ATTN: AMSEL-RD-LNA Fort Monmouth, New Jersey	1
Commanding Officer U. S. Army Electronics Laboratories ATTN: Logistics Division (Mr. A. Boniello, AMSEL-RD/ND-4) Fort Monmouth, New Jersey	8
Commanding Officer U. S. Army Electronics Laboratories ATTN: Director of Engineering Fort Monmouth, New Jersey	1
Commanding Officer U. S. Army Electronics Laboratories ATTN: AMSEL-RD/ND-4 Fort Monmouth, New Jersey	1
Commanding Officer U. S. Army Electronics Laboratories ATTN: Technical Documents Center Fort Monmouth, New Jersey	1
Director National Security Agency ATTN: R12 (M. Klein) Fort George Meade, Maryland	1
Commanding General U. S. Army Electronics Command ATTN: AMSEL-IO-P, Information Office Fort Monmouth, New Jersey	1
Director Cooley Electronics Laboratory The University of Michigan Ann Arbor, Michigan	1
File Cooley Electronics Laboratory The University of Michigan Ann Arbor, Michigan	69